Dissecting the role of Nup35 and Nup107 in nuclear pore complex assembly and mitosis in *Caenorhabditis elegans*

EDUARDO RÓDENAS MARTÍNEZ

Tesis Doctoral

Universidad Pablo de Olavide

2011

Dissecting the role of Nup35 and Nup107 in nuclear pore complex assembly and mitosis in *Caenorhabditis elegans*

PhD thesis completed at Centro Andaluz de Biología del Desarrollo (CABD), Universidad Pablo de Olavide

Sevilla, July 2011

PhD Student Eduardo Ródenas Martínez

PhD Director Peter Askjaer

PhD Tutor Manuel Muñoz

Caminante, son tus huellas
el camino y nada más;
Caminante, no hay camino,
se hace camino al andar.
Al andar se hace el camino,
y al volver la vista atrás
se ve la senda que nunca
se ha de volver a pisar.
Caminante no hay camino
sino estelas en la mar.

Antonio Machado

Esta tesis no hubiese sido posible sin el apoyo recibido durante estos años por toda la gente que he tenido a mi alrededor. En primer lugar me gustaría agradecer a Peter por su apoyo incondicional en este proyecto. No solo has sido un magnífico director de tesis sino que además has sabido crear en todo momento un ambiente en el laboratorio en el que todos nos hemos sentido apoyados y reconfortados. Gracias por todo y seguro que te echaré de menos durante mi postdoc. También quiero agradecer a todos los miembros del laboratorio por el buen ambiente hemos creado entre todos nosotros. A Adela por su capacidad de entender a la gente, ha sido un placer compartir estos momentos contigo y espero que nuestra amistad no cambie nunca. A Cristina Ayuso, por su paciencia y buena voluntad, eres una gran mujer! A Cristina González, por su pasión científica y las discusiones que hemos tenido y tendremos. A Aga, que a pesar de venir de la "fría" Polonia, es una de las personas mas dulces y cálidas que he tenido el placer de conocer. Y por supuesto a Machupi, que has sido una de las personas que más me ha hecho reír durante este tiempo.

No puedo dejar de agradecer a toda la gente del CABD, niñas de Micro incluidas, por la rica interacción que hemos tenido durante estos años. A Antonio Miranda, por ser tan buen amigo y por ser un gran apoyo en todo lo que respecta al mundo "gusanil". A toda la gente del laboratorio de Antonio, especialmente a Bri y a Nando, habéis sido muy buenos amigos. También me gustaría agradecer a todo el laboratorio de Genética, en especial a Rafa y María por su amistad y los buenos momentos que hemos pasado juntos. A Ramón, por su personalidad y por las buenas charlas que nos hemos pegado en los pasillos del CABD.

De igual forma me gustaría agradecer a toda la comunidad portuguesa del CABD, en especial a Carla, Pedro, Renata y Ana Sara ya que nos habéis hecho sentir como en casa a Ana y a mí.

De la misma manera me gustaría agradecer a todo la gente de los laboratorios de Skarmeta y Juan Ramón, en especial a Jose Luis, Juan y Silvia, Ana y JR y a Ze. Hemos pasado muy buenos momentos juntos y habéis sido un gran apoyo para Ana también.

De manera especial me gustaría agradecer a Ozren y a Miriam. Nos hemos convertido en muy buenos amigos, y en un futuro espero que podamos seguir compartiendo tan buenos momentos.
Obviamente también quiero agradecer a mi ahora ya mujer, Ana. Todo esto no hubiese sido posible sin tu apoyo y tu gran humanidad. Siempre has sabido darme tu punto de vista crítico, es un placer contar contigo como compañera de viaje (todavía nos quedan muchas cosas por hacer juntos!).
Por último me gustaría agradecer por supuesto a toda mi familia, por su apoyo incondicional durante toda mi vida en los proyectos en que me he embarcado. A Josué, que aparte de buen hermano, has sido un gran amigo y consejero en infinidad de momentos. Y finalmente a mis padres por apoyarme y por haberse convertido en unos magníficos modelos a seguir.

INDEX

Abreviations

aa	amino acid
ALPS	ArfGAP1 Lipid Packing Sensor
APC/C	Anaphase Promoting Complex/Cyclosome
ChIP	Chromatin Immunoprecipitation
CPC	Chromosome Passenger Complex
CSF	Cytostatic Factor
DSB	Double Strand Break
ER	Endoplasmic Reticulum
GFP	Green Fluorescent Protein
INM	Inner Nuclear Membrane
Kap	Karyopherin
KD	KiloDalton
KMN	Kinetochore Microtubule Network
LAD	Lamin Associated Domain
MW	Molecular Weight
NE	Nuclear Envelope
NEBD	Nuclear Envelepe Break Down
NES	Nuclear Export Signal
NGM	Nematode Growth Medium
NLS	Nuclear Localization Signal
NPC	Nuclear Pore Complex
NPP	Nucleoporin (*C. elegans* nomenclature)
NTF	Nuclear Transport Factor
Nup	Nucleoporin (Vertebrate and yeast nomenclature)
ONM	Outer Nuclear Membrane
ORF	Open Reading Frame
PBS	Phosphate Buffered Saline
PCR	Polymerase Chain Reaction
PNM	Pronuclei Meeting
Pom	Pore Membrane Protein
PTC	Premature Termination Codon
rER	rough Endoplasmic Reticulum
RNAi	RNA interference
RT-PCR	Reverse transcription polymerase chain reaction
Rtn	Reticulon
SAC	Spindle Assembly Checkpoint
SDS	Sodium Dodecyl Sulfate
SDS-PAGE	Sodium Dodecyl Sulfate Polyacrylamide Gel Electrophoresis
siRNA	small interference RNA
TEM	Transmission Electron Microscopy
unc	uncoordinated
WT	Wild-type
Y2H	Yeast Two Hybrid
γ-TuRC	γ-Tubulin Ring Complex

1. Resumen

La membrana o envoltura nuclear (NE) es la estructura que separa el núcleo del citoplasma en las células eucariotas. Las principales funciones de la NE son el anclaje de la cromatina en el núcleo, el proporcionar estabilidad al núcleo y el correcto posicionamiento del núcleo dentro de la célula. La formacion de la NE es esencial para la supervivencia celular, y mutaciones en genes implicados en la formación de la NE causan diferentes enfermedades genéticas humanas. Estas enfermedades constituyen un grupo en expansión de alteraciones, siendo todas ellas clínicamente diferentes y severas.

A pesar del papel esencial de la NE y de la severidad de las enfermedades asociadas a defectos de la misma, nuestros conocimientos sobre la composición, dinámica y función de la NE presentan aún numerosas incógnitas. Hasta el momento, se han descrito en detalle menos de una docena de proteínas esenciales de la NE, lo que ha permitido vislumbrar tan sólo una pequeña porción de la compleja biología de la misma.

La NE está compuesta por una membrana nuclear interna (INM), una membrana nuclear externa (ONM) y por debajo de la INM se puede encontrar la lámina nuclear, que es el principal sitio de anclaje de la cromatina a la NE. En el punto de fusión de la INM y la ONM se encuentran los complejos de poros nucleares (NPCs). El NPC es una macroestructura que presenta una simetría radial de 8 ejes, compuesto por múltiples copias de 30 proteínas diferentes, también llamadas nucleoporinas. Estas nucleoporinas normalmente se asocian entre si formando subcomplejos, siendo el subcomplejo Nup107-160 uno de los componentes estructurales mas importantes del NPC.

La principal función de los NPCs es el transporte de macromoléculas entre el núcleo y el citoplasma. Cada NPC presenta un canal central compuesto por nucleoporinas ricas en repeticiones de FG y todas las macromoléculas que quieran entrar en el núcleo, tendrán que interactuar con estas nucleoporinas para su apropiado transporte nuclear. Aunque la principal función de los NPCs es el transporte de macromoléculas a través de la NE, se ha demostrado en los últimos años que los NPCs también juegan un papel esencial en la regulación de la expresión génica (Akhtar and Gasser, 2007; Brown and Silver, 2007), en la organización nuclear de la cromatina (Kalverda et al., 2008) y en funciones

relacionadas con los cinetocoros durante mitosis (Loiodice et al., 2004; Mishra et al., 2010; Orjalo et al., 2006; Zuccolo et al., 2007).

Durante esta tesis, hemos profundizado en la caracterización de dos nucleoporinas: Nup35 y Nup107, esta última perteneciente al subcomplejo Nup107-160.

La primera parte de esta tesis ha estado enfocada en la caracterización de la nucleoporina Nup35. Hemos realizado el primer análisis mutacional de esta proteína durante el desarrollo embrionario en *C. elegans* y partiendo de una estirpe mutante para el gen *npp-19*, que codifica la proteína Nup35 en *C. elegans*, y utilizando técnicas de RNAi hemos sido capaces de demostrar que Nup35 es una proteína esencial para la correcta formación de los NPCs. El proceso de ensamblaje postmitótico del NPC consta de cuatro pasos esenciales (Hetzer and Wente, 2009). Primero Mel-28, una proteina que presenta un dominio de interacción de ADN, se asocia a la cromatina en los sitios donde se van a originar los NPCs (Galy et al., 2006; Rasala et al., 2006; Rasala et al., 2008). En segundo lugar Mel-28 recluta el complejo Nup107-160, formando una estructura conocida como "preporo"(Franz et al., 2007; Gillespie et al., 2007). Una vez que el "preporo" se ha formado, componentes de membrana del NPC como NDC1 y Pom121 se asocian al complejo Nup107-160 (Mitchell et al., 2010; Rasala et al., 2008). En cuarto y último lugar una serie de nucleoporinas solubles como Nup35 y Nup155 terminan el trabajo de ensamblaje postmitótico de los NPCs (Franz et al., 2005; Hawryluk-Gara et al., 2008; Mitchell et al., 2010; Rodenas et al., 2009). Durante esta tesis hemos sido capaces de determinar que en la ausencia de Nup35, los primeros tres pasos de la biogenesis del NPC ocurren correctamente, pero es en el cuarto paso del ensamblaje donde observamos que Nup35 juega un papel esencial.

La segunda parte de esta tesis está enfocada en la caracterización de otra nucleoporina que pertenece al complejo Nup107-160 del NPC llamada Nup107. Una de las principales características de las proteínas que pertenecen al complejo Nup107-160 es que se localizan en los NPCs durante interfase y durante mitosis, cuando la envoltura nuclear se rompe, estas proteínas se localizan en los cinetocoros (Belgareh et al., 2001; Loiodice et al., 2004; Orjalo et

al., 2006; Zuccolo et al., 2007). Hemos realizado el análisis de las estirpes mutantes para el gen *npp-5*, que codifica la proteina Nup107 en *C. elegans*, *npp5(tm3039)* y *npp-5(ok1966)*. Hemos demostrado mediante ensayos de inmunofluorescencia, RT-PCR y Western blot que ambas estirpes son mutantes nulos para la proteina Nup107.

Previamente en diferentes estudios se había observado que la ausencia de Nup107 causaba una inestabilidad en el subcomplejo Nup107-160 en células humanas y en extractos de *Xenopus* (Boehmer et al., 2003; Harel et al., 2003b; Walther et al., 2003a). Una de las primeras e importantes conclusiones de este estudio es que en la ausencia de Nup107, el subcomplejo Nup107-160 permanece estable en *C. elegans,* lo que permite el análisis individual de las nucleoporinas que componen el subcomplejo Nup107-160 en *C. elegans*.

Usando una amplia variedad de estirpes reporteras, hemos investigado como la ausencia de Nup107 afecta a la función de los cinetocoros, a la segregación de ADN durante mitosis, al transporte nucleoplasmico y a la respuesta al estrés celular durante diversos estadíos del desarrollo en *C. elegans*.

Observamos que tanto la estructura del NPC como el transporte de macromoléculas entre el núcleo y el citoplasma no se ven afectados en mutantes *npp5(tm3039).* Por otro lado, hemos sido capaces de demostrar que los embriones mutantes *npp5(tm3039)* presentan un defecto en la estructura de los cinetocoros, lo que presumiblemente causa problemas en la segregación del ADN durante mitosis. También hemos observado que los embriones *npp5(tm3039)* son hipersensibles a condiciones de anoxia, lo que sugiere que el spindle assembly checkpoint (SAC) podría estar activado en estos mutantes. Siguiendo esta observación hemos demostrado que ciertamente el SAC esta activado en los embriones *npp5(tm3039)*, y que existe una interacción física entre Nup107 y Mad1/MDF-1, un miembro del SAC.

En conclusión, hemos demostrado que la proteina Nup107 en *C. elegans* es esencial para el ensamblaje correcto de los cinetocoros durante mitosis, y que la ausencia de Nup107 provoca la activación del SAC. Hemos demostrado también que existe una interacción física entre Nup107 y Mad1, lo que sugeriría que quizás Nup107 puede jugar un papel en la activación directa del SAC.

2. Introduction

1. The nuclear envelope (NE)

The nuclear membrane, also known as the nuclear envelope (NE), is the physical barrier between the nucleus and the cytoplasm of eukaryotic cells. It was shown more than 60 years ago that the NE of amphibian oocytes consist of a double lipid bilayer (Callan and Tomlin, 1950). The NE serves as a physical barrier to separate the DNA in the nucleus from the cytosolic material and it has been reported to have an important function in the organization and transcription of chromatin (Akhtar and Gasser, 2007; Mekhail and Moazed, 2010). Two membranes, the outer (ONM) and the inner (INM) membranes compose the NE. The ONM is continuous with the rough endoplasmic reticulum (rER) while the INM is connected to the nuclear lamina, which acts as a site of attachment for chromatin and provides structural stability to the nucleus (Hetzer, 2010a). Both the ONM and the INM are fused where nuclear pore complexes (NPCs) span the NE. It is thought that a nuclear periphery–INM–ONM–cytoskeleton connection is created that is responsible for nuclear positioning and nuclear movement (Malone et al., 2003; Padmakumar et al., 2004; Starr and Han, 2002; Starr et al., 2001).

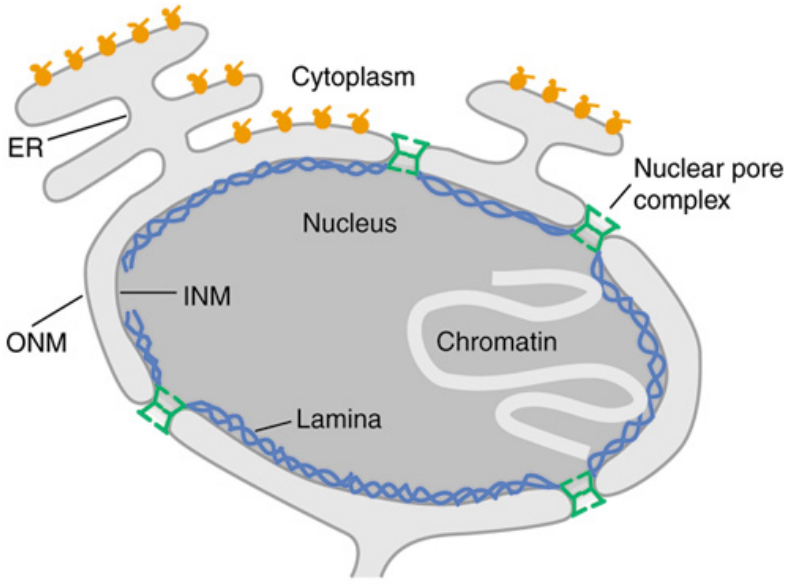

Figure 1. Schematic representation of the NE. The NE is composed of the INM and the ONM, which separate the nucleus from the cytoplasm. The nuclear lamina is connected to the INM and links chromatin to the NE. NPCs span the NE at the sites where the INM and the ONM fused together. Adapted from (Schirmer and Gerace, 2002)

1.1 <u>Nuclear envelope breakdown (NEBD)</u>: In higher eukaryotes the NE disassembles during mitosis in a process known as nuclear envelope break down (NEBD). NEBD starts at the onset of mitosis, during the prophase-prometaphase transition (Burke and Ellenberg, 2002), and the components of the nucleoplasm and the cytoplasm are mixed. Two different models have been proposed for NEBD. The first model proposes that the NE membrane breaks down into vesicles that are distinct from the mitotic ER, based on experiments where membrane vesicles enriched in NE proteins can be isolated from embryonic extracts (Collas and Courvalin, 2000; Sasagawa et al., 1999; Vigers and Lohka, 1991). According to the second model for NEBD the NE proteins are absorbed into the ER during mitosis. This model is based on studies that show that INM and ER proteins interact and localize to the same mitotic tubular network during mitosis (Collas and Courvalin, 2000; Daigle et al., 2001; Ellenberg et al., 1997; Yang et al., 1997). The current view of NEBD based on more recent technologies favors this second model over the first one.

Proteins that compose the NPC are called nucleoporins or nups and although most nucleoporins are dispersed during mitosis to the cytoplasm or to the ER, there are also a few interesting exceptions, such as the members of the Nup107-160 subcomplex . Components of the Nup107 subcomplex localize to the kinetochores during mitosis (Belgareh et al., 2001; Loiodice et al., 2004) and previous studies have shown that they play a role in the proper assembly of the mitotic spindle *in vitro* (Orjalo et al., 2006). Just after NEBD the mitotic spindle starts to be established in order to capture and later segregate properly all the duplicated chromosomes.

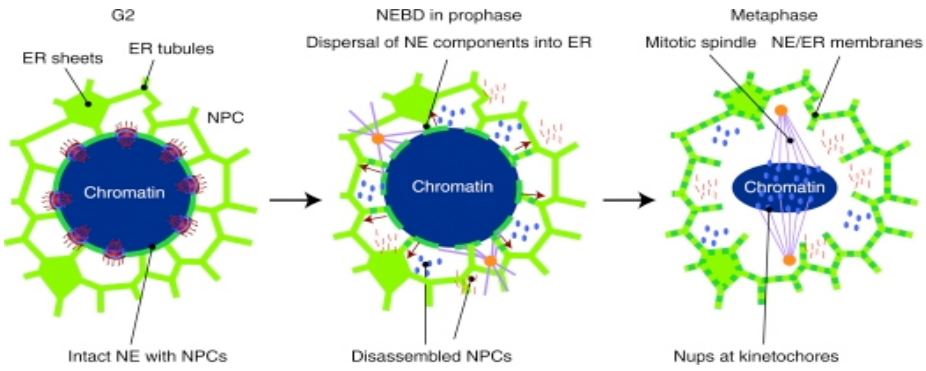

Figure 2. Illustration of NEBD. At the entry into mitosis the NPCs disassemble and the NE is reabsorbed by the ER. During prometaphase, a group of nucleoporins localizes to kinetochores and the spindle is constituted. In metaphase chromosomes are membrane free. Adapted from (Hetzer, 2010a)

1.2 <u>NE reformation after mitosis</u>: shortly after anaphase onset, during late anaphase and telophase, the NE reassembles. The process of NE reformation starts by recruitment of INM proteins from the mitotic ER to the surface of decondensing chromatin (Pyrpasopoulou et al., 1996; Wilson and Newport, 1988). In *C. elegans* BAF-1, a highly conserved DNA binding protein, plays a role in NE reassembly by presumably recruiting INM proteins that have a LEM domain to the surface of chromatin (Gorjanacz et al., 2007b). The second step of NE reassembly is the binding of the ER tubules to chromatin (Anderson and Hetzer, 2007), leading to flattened double membrane patches on chromatin. The final step of NE reassembly is the fusion of membrane patches into a closed envelope, which occurs concomitant with NPC assembly.

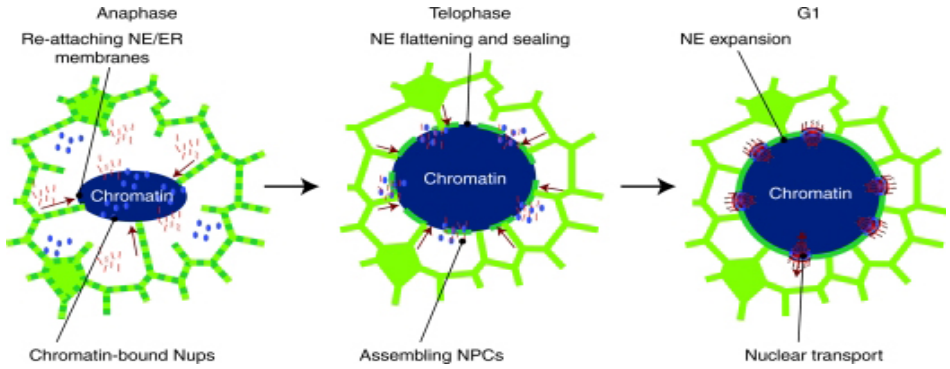

Figure 3. NE reformation around segregated chromosomes. During anaphase, both ER membranes (red arrows) and a subset of nucleoporins associate with chromatin. NE proteins still present in the ER are recruited to chromatin and mediate NE flattening. During early telophase, the NE closes and NPCs assemble in a step-wise manner. As soon as the NPCs are transport competent, the NE enlarges and cells enters G1 phase. Adapted from (Hetzer, 2010a)

2. <u>The nuclear pore complex</u>

The NPC is an eight-fold symmetrical structure composed of multiple copies of ~30 different nucleoporins (Alber et al., 2007b; Cronshaw et al., 2002; Rout et al., 2000). The NPC structure and composition is evolutionary conserved (**Table 1**) from yeasts to mammals (Suntharalingam and Wente, 2003; Yang et al., 1998), although estimates of its molecular mass range from 60-125 KDa in mammals to ~40-60 KDa in yeasts.

The main function of the NPC is to mediate bidirectional transport between the nucleus and the cytoplasm (Lim and Fahrenkrog, 2006). Besides, the NPC and

nucleoporins have been implicated in different cellular processes like chromatin organization (Kalverda et al., 2008) and regulation of gene expression (Akhtar and Gasser, 2007; Brown and Silver, 2007) as well as kinetochore functions during mitosis (Loiodice et al., 2004; Mishra et al., 2010; Orjalo et al., 2006; Zuccolo et al., 2007).

Mammalian	S. cerevisiae	C. elegans
Nup35	Nup53p	NPP-19
Nup37	-	-
Nup43	-	C09G9.2
Nup50	Nup2p	NPP-16
Nup54	Nup57p	NPP-1
Nup58/45	Nup49p	NPP-4
Nup62	Nsp1p	NPP-11
Nup75	Nup85p	NPP-2
Nup88	Nup82p	-
Nup93	Nic96p	NPP-13
Nup96	Nup145Cp	NPP-10C
Nup98	Nup145Np Nup100p Nup116p	NPP-10N
Nup107	Nup84p	NPP-5
Nup133	Nup133p	NPP-15
Nup153	Nup1p Nup2p Nup60p	NPP-7
Nup155	Nup157p Nup170p	NPP-8
Nup160	Nup120p	NPP-6
Nup188	Nup188p	-

Mammalian	S. cerevisiae	C. elegans
Nup205	Nup192p	NPP-3
Nup214	Nup159p	NPP-14
Nup358/RanBP2	-	NPP-9
Sec13R	Sec13p	NPP-20
Seh1	Sehp	NPP-18
Pom121	-	-
Gp210	-	NPP-12
Ndc1	Ndc1p	NPP-22
Tpr	Mlp1p Mlp2p	NPP-21
RAE1	Gle2p	NPP-17
ALADIN	-	-
NLP1/hCG1	Nup42p	-
-	Nup59p	-
-	Nup116p	-
-	Nup100p	-
-	Pom134p	-
-	Pom152p	-
-	Pom33	-

Table 1. Mammalian, *S. cerevisiae* and *C. elegans* nucleoporins. Adapted from (D'Angelo and Hetzer, 2008)

2.1 <u>NPC structure</u>: the earliest description of the NPC structure was presented more than 40 years ago (Gall, 1967), and from then on a great effort has been put in determining the three-dimensional structure of the NPC using a variety of techniques, such as field-emission in-lens scanning electron microscopy (FEISEM) and cryo-electron tomography (Beck et al., 2004; Beck et al., 2007).

The NPC spans the NE at sites where the INM and the ONM are fused (D'Angelo and Hetzer, 2006). The NPC is composed of a scaffold component that encircles a central transport channel and two rings, the nuclear and the cytoplasmic rings. The scaffold is composed of the Nup107-160 and the Nup93-205 subcomplexes and the central channel is filled with nucleoporins rich in FG repeats. Eight filaments are attached to the nuclear and to the cytoplasmic rings. Whereas the

nuclear filaments are joined together forming the nuclear basket, the cytoplasmic filaments have loose ends that interact with cargoes in the cytoplasm controlling their transport to the nucleus (D'Angelo and Hetzer, 2008).

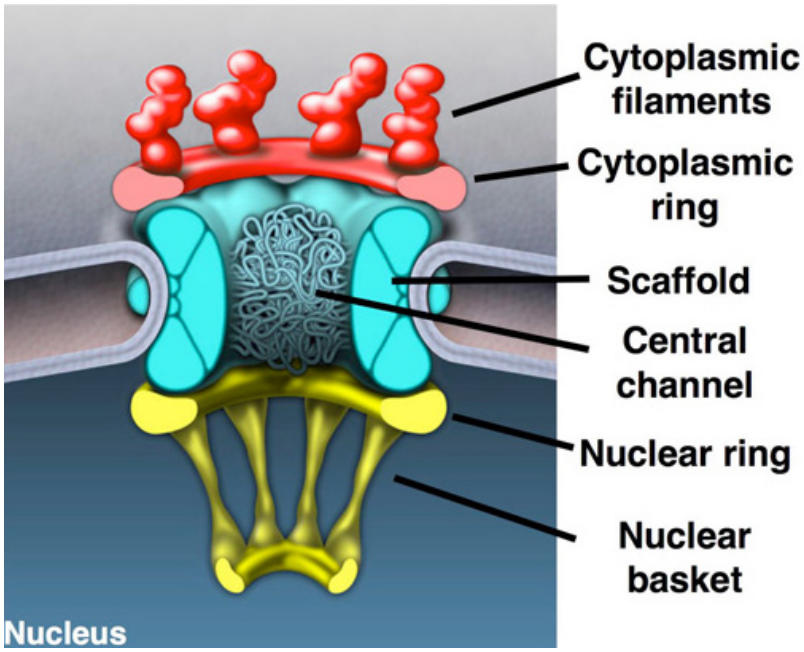

Figure 4. Schematic illustration of the NPC. Adapted from (D'Angelo and Hetzer, 2008).

Experimental evidence indicates that the NPC and the vesicle coats originated from a common ancestor in evolution (Brohawn and Schwartz, 2009) . Brohawn and Schwartz propose that the NPC structural scaffold, like the vesicle coats, is a polygonal network embedded in membranes and composed of vertex and edge elements that forms a molecular lattice upon which additional nucleoporins assemble.

2.2 <u>NPC composition</u>: Despite its enormous size and complexity, the NPC is built by approximately only 30 different nucleoporins. These nucleoporins are believed to be present in 8, 16 or 32 copies due to the eight-fold symmetry of the NPC. We can distinguish between three main groups of nucleoporins based on their function and composition. The first group would be compose by the nucleoporins rich in phenylalanine-glycine (FG) repeats, which are thought to constitute the permeability barrier of the NPC and they localize in the central

channel and the cytoplasmic filaments (Frey and Gorlich, 2009; Frey et al., 2006; Wu et al., 1995). It has also been reported that Pom121, a transmembrane protein responsible for the anchorage of the NPC to the NE in vertebrates, also is a FG repeat nucleoporin (Antonin et al., 2005). Molecules bigger than 30-40 KDa rely on active transport mechanisms to interact with FG repeat nucleoporins in order to pass through the NPC. The second group of nucleoporins that build the NPC are nucleoporins that lack FG repeats. These nucleoporins are also called structural nucleoporins and they form the backbone of the overall architecture of the NPC.

Nucleoporins usually interact between each other to form subcomplexes, which are thought to act as the building blocks of the NPC (Alber et al., 2007a; Schwartz, 2005). Three main subcomplexes have been identified so far in vertebrates, which are the Nup107-160, Nup93 and Nup62 subcomplexes. The Nup107-160 and the Nup 93 subcomplexes are structural subcomplexes and they are stably bound to the NPC, whereas more peripheral nucleoporins show a more dynamic behaviour (Rabut et al., 2004). The Nup62 subcomplex is composed of nucleoporins rich in FG repeats and it localizes to the central channel of the NPC.

Finally, there is a third group of nucleoporins that anchor the NPC to the NE, the pore membrane proteins (Poms). Only three Poms have been identified so far in vertebrates: Pom121, Ndc1 and gp210 (Antonin et al., 2005; Cohen et al., 2003; Mansfeld et al., 2006; Mitchell et al., 2010). Poms in general are less well conserved than other nucleoporins, and in *C. elegans* only two transmembrane nucleoporins have been found so far, NDC1/NPP-22 (Mansfeld et al., 2006) and gp210/NPP-12 (Cohen et al., 2003). A novel Pom, called Pom33, has been recently discovered in yeast (Chadrin et al., 2010), which resembles the function of the vertebrate gp210.

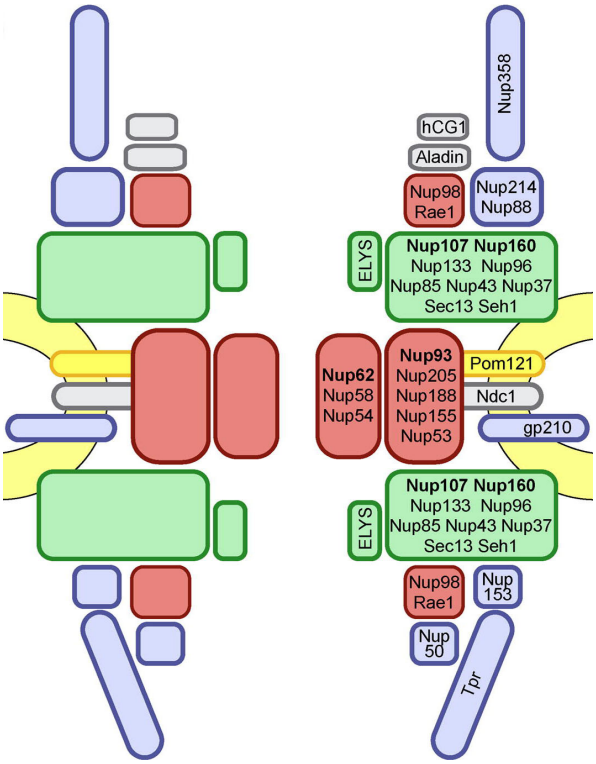

Figure 5. Diagram of the modular structure of the metazoan NPC. Schematic view of how the different subcomplexes interact with each other to build the NPC. Nucleoporins and complexes recruited during the first, second, third and forth step of postmitotic NPC assembly as described below are colored in green, yellow, red and blue, respectively. Adapted from (Antonin et al., 2008).

2.3 <u>NPC biogenesis</u>: The biogenesis of NPCs is an essential requirement for cell survival and proliferation. There are two stages where biogenesis of NPCs occurs: one at the end of mitosis when the NE starts reforming around the segregated chromosomes (postmitoitc assembly) and the other one during interphase as the NE surface enlarges (interphase assembly). The mechanisms by which NPC assembly occurs differ from one to another.

2.3.1 NPC postmitotic assembly: The current view of postmitotic NPC biogenesis in higher eukaryotes involves four essential steps (Hetzer and Wente, 2009). First, the binding of MEL-28/ELYS to chromatin via a conserved AT-hook motif marks the sites of nuclear pore assembly (Galy et al., 2006; Rasala et al., 2006; Rasala et al., 2008). Second, chromatin-bound MEL-28/ELYS recruits the Nup107-160 subcomplex to nuclear pore initiation sites (Franz et al., 2007; Gillespie et al., 2007), to constitute what is known as the "prepore". Depletion of

MEL-28/ELYS prevents recruitment of Nup96 and Nup107 (Galy et al., 2006) but the molecular details of this interaction are still unknown. Third, NPC membrane components, such as NDC1 and POM121 are engaged via interactions with the Nup107-160 subcomplex (Mitchell et al., 2010; Rasala et al., 2008). And fourth, incorporation of soluble nucleoporins including Nup35 and Nup155 is required to complete NPC assembly (Franz et al., 2005; Hawryluk-Gara et al., 2008; Mitchell et al., 2010; Rodenas et al., 2009).

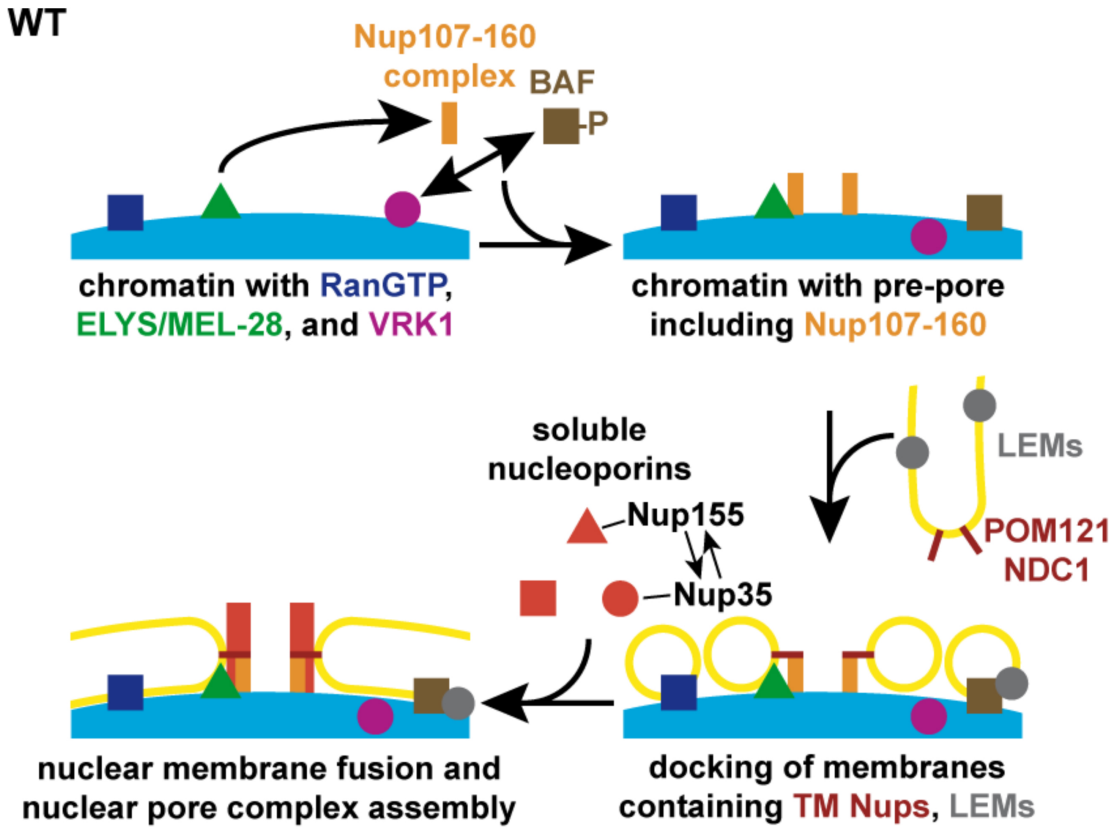

Figure 6. Scheme of the postmitotic assembly of NPC. The GTPase Ran and the nucleoporin ELYS/MEL-28 are essential to initiate NPC assembly through recruitment of the Nup107-160 subcomplex while the protein kinase VRK is required to release BAF from chromatin during mitosis. Once on the chromatin, the Nup107-containing pre-pore will recruit transmembrane nucleoporins such as POM121 and NDC1 whereas BAF will interact with integral nuclear membrane proteins such as emerin and LEM2. Finally, soluble nucleoporins including Nup35 and Nup155 are recruited concomitantly with sealing of the nuclear membranes

A previous model based on in vitro assays in Xenopus eggs suggested that postmitotic NPC assembly did not require an initial "prepore" formation (Macaulay and Forbes, 1996). According to this model, NPC assembly starts with the fusion of the ONM and INM, allowing for membrane hole formation where

the NPC will be assembled. However, recent studies cited above strongly suggest that the correct model for postmitotic NPC biogenesis is the "prepore" model and the earlier model would fit better with the assembly of NPCs during interphase. According to this "prepore" model, NPC assembly has to be regulated in space (NPC assembly occurs at chromatin) and time (NPC assembly occurs when chromosomes are segregated and the NE starts to reform). How is this spatial and temporal regulation on NPC assembly achieved? The spatial regulation is at least partially achieved by the activity of RanGTP and its counterplayer importin β. The members of the Nup107-160 subcomplex and other nucleoporins bind to importin β during mitosis, which prevents their assembly into NPCs (Harel et al., 2003a; Walther et al., 2003b). On chromatin, where RanGTP is produced by its guanine nucleotide exchange factor RCC1, nucleoporins will be released from importin β by RanGTP and they will be able to start the assembly of NPCs (Li and Zheng, 2004). On the other hand, the temporal regulation of postmitotic NPC assembly is achieved by means of phosphorylation. Several nucleoporins are phosphorylated during mitosis, which may correlate with chromatin association (Favreau et al., 1996; Glavy et al., 2007; Macaulay et al., 1995). When the spindle assembly checkpoint (SAC) is satisfied, anaphase onset is triggered by activation of the anaphase promoting complex (APC). Activation of the APC provokes the inactivation of the kinase Cdk1 (van Zon and Wolthuis, 2010). As Cdk1 gets inactivated, phosphatases eliminate many mitosis specific protein phosphorylations. The dephosphorylation of nucleoporins at anaphase onset is thought to temporally regulate their ability to bind chromatin and start NPC assembly (Onischenko et al., 2005).

2.3.2 NPC assembly during interphase: compared to the postmitotic NPC assembly, little is known about NPC assembly during interphase, although it is an essential process since as the NE enlarges new NPCs need to be incorporated into it. Moreover, species with a so-called closed mitosis (i.e. the NE remains intact during mitosis) rely strictly on NPC assembly into existing nuclear membranes. Recent studies suggest that postmitotic and interphase NPC assembly occurs by distinct mechanisms (Doucet et al., 2010). It has been suggested that the density of NPCs in the NE remains constant

throughout interphase (Dultz and Ellenberg, 2010), indicating that NPC assembly is tightly linked to NE expansion. Maul et al. already had observed in 1972 that HeLa cells double their number of NPCs through the cell cycle, going from 2000 NPCs in G1 to 4000 NPCs in G2 (Maul et al., 1972). In contrast, Dultz and Ellenberg in 2010 observed that normal rat kidney (NRK) cells only increase the number of NPCs from G1 to G2 in around 44%, going from 1960 NPCs in G1 to 2830 NPCs in G2.A plausible explanation for this controversy could be that experiments were done in different cell types with different cell cycle lengths and metabolic rates and/or that the techniques used to measure the number of NPCs were different.

NE expansion requires an intact ER, suggesting that the ER provides the membranes needed for NE growth (Anderson and Hetzer, 2007). The expression levels of ER and INM interacting proteins probably coordinate NE expansion. NPCs that are inserted into the NE during interphase are formed by a de novo process (D'Angelo et al., 2006), instead of duplications of preexistent NPCs in the NE. The insertion of the de novo NPCs into an intact NE requires a fusion of the INM and the ONM, which provokes a membrane curvature. Recent evidence suggests that the fusion of the INM and the ONM is mediated by the transmembrane nucleoporin Pom121 (Doucet et al., 2010). The fusion process generates membrane curvature, which is stabilized by a family of proteins called Reticulons (Rtn) (Dawson et al., 2009). Once the INM and the ONM are fused, the Nup107-160 subcomplex is recruited to the NE to constitute the NPC scaffold structure. The recruitment of the Nup107-160 subcomplex to the NE occurs via its member Nup133, which presents an ArfGAP1 Lipid Packing Sensor (ALPS) motif that senses the membrane curvature of the fused INM and ONM. This ALPS motif has been shown to be essential for NPC assembly during interphase (Doucet et al., 2010).

As it happens with the postmitotic NPC assembly, RanGTP interaction with importin β is essential in this step for the release of Nup107-160 subcomplex to allow its targeting with the membrane curvature (D'Angelo et al., 2006; Harel et al., 2003a; Ryan et al., 2003; Walther et al., 2003b). The subsequent steps on how NPC assembly occurs during interphase are not well understood yet, leaving open several exciting questions for future research.

Two main differences can be drawn when we compare the postmitotic and the interphase NPC assembly mechanisms. First, the binding of Mel28/ELYS to chromatin is critical for postmitotic NPC assembly but seems to be dispensable for interphase assembly and second, the ALPS motif of the Nup133 nucleoporin is essential for interphase NPC assembly while it appears to be dispensable for postmitotic assembly (Doucet et al., 2010).
All the studies cited above clearly suggest that NPC assembly occurs via two distinct mechanisms in organisms that undergo open mitosis, the postmitotic and the interphase NPC assembly mechanisms. On the other hand, in organisms that undergo closed mitosis, such as yeast, NPCs will be assembled only following the interphase mechanism.

2.4 <u>NPC disassembly</u>: NPC disassembly has been only observed during mitosis and there is no evidence that NPC are dismantled during interphase. The mechanisms underlying NPC disassembly are not well understood yet, but there is some evidence that the trigger of NPC disassembly during mitosis could be the phosphorylation of different nucleoporins by Cdk1 (Lenart et al., 2003; Lusk et al., 2007; Macaulay et al., 1995; Onischenko et al., 2005). It is still unclear how mitotic phosphorylation of nucleoporins could cause NPC disassembly, but one possibility could be that phosphorylation of the different nucleoporins would prevent their association into subcomplexes, which are believed to be the building blocks of the NPC. Supporting this idea, it has been previously demonstrated that nucleoporins need to be dephosphorylated right after anaphase onset in order to initiate NPC assembly (Walther et al., 2003b).

2.5 <u>NPC maintenance</u>: several nucleoporins present a dynamic behavior during interphase, coming on and off the NPC. By contrast, nucleoporins that build the scaffold NPC are very stable and they are only exchanged once per cell cycle, when the NE breaks down (D'Angelo et al., 2009). How these scaffold nucleoporins are maintained in the NPC during interphase is currently unknown and there has not been reported a mechanism of disassembly of NPCs during interphase. In consequence cells that have stopped dividing (e. g. after differentiation) will have the same NPCs throughout their entire life span, which

means that NPCs would be subject to age-dependent damage affecting their function and nuclear integrity (D'Angelo et al., 2009). D'Angelo et al. demonstrated that NPCs deteriorate with time, and that nucleoporins responsible for maintaining the pore diffuse barrier are lost over time, leading to an increased nuclear permeability.
In support of this idea, there have been also different studies that relate alterations of the nuclear structure with the aging phenomenon (Haithcock et al., 2005; Herndon et al., 2002), in which they showed a correlation between the aging process and the deterioration of the nuclear lamina.

2.6 NPC function: The NPC functions as the key regulator of macromolecular traffic between the nucleus and the cytoplasm (Kohler and Hurt, 2007; Stewart, 2007). Although the primary function of the NPC is transport, other functions have been associated to the NPC such as gene regulation, DNA repair and chromatin organization (Ahmed et al., 2010; Kalverda et al., 2008; Palancade et al., 2007; Tan-Wong et al., 2009; Vaquerizas et al., 2010).

2.6.1 NPC and transport: As mentioned above the main function of the NPC is to regulate the transport of macromolecules between the nucleus and the cytoplasm. The transport of the majority of macromolecules into and out of the nucleus shares a common active mechanism. This mechanism consists on the binding of nuclear transport factors (NTFs) to the transport signals present in the cargoes. The majority of NTFs belong to the karyopherin (Kap) family of proteins, and they are also known as importins or exportins. Importins specialize in the transport of macromolecules into the nucleus, while exportins regulate the transport of cargoes to the cytoplasm.
The transport signals present in the cargoes consist of short amino acid sequences named nuclear localization signal (NLS) for import and nuclear export signal (NES) for export (Lange et al., 2007; Xu et al., 2010).
Nuclear transport of macromolecules consists in three main steps (Akey and Goldfarb, 1989). First the NTF (importin or exportin) needs to recognize and bind the transport signal (NLS or NES) of the cargo. Second, the NTF-cargo complex interacts with the nucleoporins rich on FG repeats present in the central

channel of the NPC, allowing the crossing of the NPC (Lim et al., 2007; Lim et al., 2006). How exactly FG nucleoporins carry out this gating function in molecular terms is still unclear. Third, when the NTF-cargo complex reaches its designated compartment (nucleoplasm or cytoplasm) it needs to be dissociated. In the case of import, the dissociation of the NTF-cargo complex inside the nucleus is mediated by RanGTP. RanGTP is found predominantly in the nucleus, where it associates with the NTF causing the release of the cargo in the nuclear compartment. In the case of export, RanGTP inside the nucleus induces the association of NTFs and NES present in the cargoes to be exported. Once in the cytoplasm, GTP hydrolysis will disassociate the NTF-cargo complex, releasing the cargo in the cytoplasm. The resulting NFT and RanGDP are recycled back into the transport pathway (Kuersten et al., 2001; Nachury and Weis, 1999).

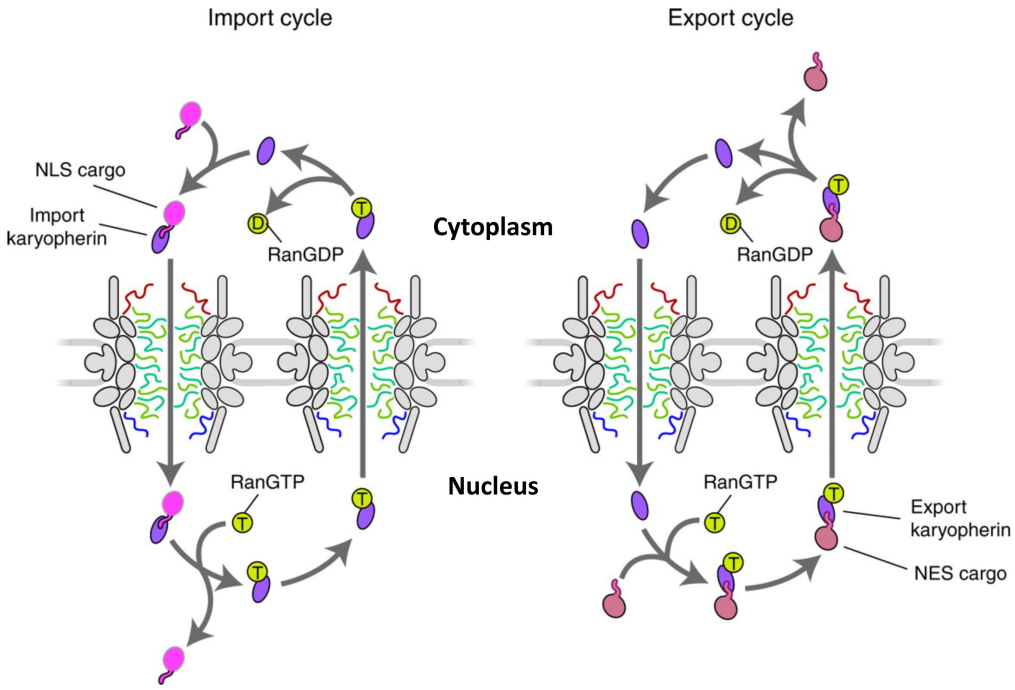

Figure 7. The nuclear transport cycle for karyopherins and their cargos. See text for details. Adapted from (Wente and Rout, 2010)

2.6.2 NPC and gene expression: chromatin is highly organized within the nucleus and depending on its degree of compactness (among other factors) it can be actively transcribed or silenced. The highly compacted chromatin, known as heterochromatin, is found both at the nuclear interior and

the nuclear periphery, although in many cell types it is preferentially bound to the nuclear periphery. Additionally, transcriptionally inactive regions such as centromeres and telomeres are frequently associated to the nuclear periphery (Hediger et al., 2002). This would suggest that gene expression is promoted in the nucleoplasm, whereas the nuclear periphery tends to promote gene silencing (Finlan et al., 2008; Kumaran and Spector, 2008; Reddy et al., 2008; Towbin et al., 2009). The nuclear lamina, a mesh-like network that lies just beneath the NE, has been proposed to be the key regulator of gene expression at the nuclear periphery in multicellular organisms (Andres and Gonzalez, 2009). The nuclear lamina interacts with heterochromatin through binding with histones or specific DNA sequences called lamina-associated domains (LADs) (Guelen et al., 2008; van Steensel, 2011). One exception to the assumption that peripheral chromatin is silenced occurs at the NPC in yeast. Over the last decade it has became evident that highly transcribed genes are associated with the NPCs in *S. cerevisiae*. Chromatin immunoprecipitation (ChIP) assays have demonstrated that nucleoporins that belong to the NPC such as yNup116, yNup60 and yNup2 associate with genes that are actively transcribed (Casolari et al., 2004). Moreover, some highly transcribed genes appear to be associated to the NPC even after transcriptional repression in yeast (Brickner et al., 2007), and this retention at the NPC after repression is believed to serve as a memory of previously transcriptional activity to generate a faster transcriptional response following reactivation (Brickner, 2009). The observation that highly transcribed genes associate to the NPC has not been firmly demonstrated in higher eukaryotes, and some recent studies in *Drosophila* suggest that some nucleoporins, such as Nup98, regulate gene expression away from the NPC by their association with chromatin within the nucleoplasm (Capelson et al., 2010; Kalverda et al., 2010)

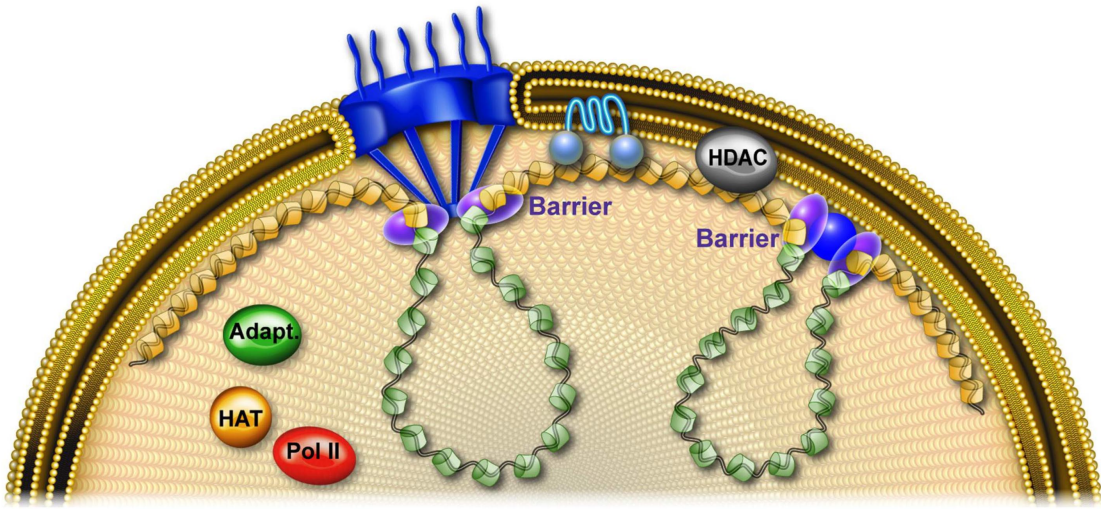

Figure 8. Model for the function of NPCs as barriers between heterochromatin and euchromatin in yeast. Hypothetical model shows partitioning of the chromatin fiber into distinct heterochromatic (yellow) and euchromatic regions (green) in *S. cerevisiae*. NPCs and other tethering stations at the NE (dark blue) organize the chromatin fiber into distinct topological domains by gene loop formation and by establishing various forms of chromatin barriers to prevent the spread of heterochromatin factors. Adapted from (Kohler and Hurt, 2010).

In conclusion, individual NPCs seem to be zones of transition between transcriptionally repressed zones at the nuclear periphery, and the gene-NPC interactions may promote both transcription and the definition of heterochromatin-euchromatin boundaries (Kohler and Hurt, 2010) in yeast. Also the role of NPCs in gene regulation could be a possible explanation for the implication of nucleoporins in cancer development (Kraemer et al., 1994; Xu and Powers, 2009).

2.6.3 NPC and DNA repair: the NPC has been also implicated in the DNA repair pathway, either in the stabilization or in the repair of the DNA ends like those found at double stranded DNA breaks (DSBs) or at telomeres (Towbin et al., 2009). Recent studies in yeast have revealed that DSBs that failed to be repaired are recruited to the NPC basket causing the activation of alternative DNA damage repair pathways in a final attempt to repair the lesions (Khadaroo et al., 2009; Oza et al., 2009; Oza and Peterson, 2010). It is important to consider that actively transcribed loci are highly exposed to DNA damage, and it has been shown that NPCs helps to recruit the damaged DNA to the nuclear

periphery where the repair machineries are (Khadaroo et al., 2009). It has also been demonstrated recently that NPCs seem to induce the recruitment of the DNA repair machinery, including Yku70 to the nuclear periphery (Nagai et al., 2008; Palancade et al., 2007).

2.6.4 NPC and the cell cycle: upon entry in mitosis the NE breaks down and the NPCs are disassembled. Certain nucleoporins, in particular the members of the Nup107-160 complex, localize to the kinetochores and to the mitotic spindle during mitosis (Joseph et al., 2002; Loiodice et al., 2004; Salina et al., 2003; Zuccolo et al., 2007) and they have been implicated in a variety of mitotic processes including assembly of the mitotic spindle (Orjalo et al., 2006), spindle assembly checkpoint (SAC) activity (Katsani et al., 2008), kinetochore functions (Zuccolo et al., 2007), chromosome passenger complex (CPC) localization (Platani et al., 2009), nucleation of microtubules at kinetochores during mitosis (Mishra et al., 2010) and also they have been implicated in the progression of cytokinesis (Rasala et al., 2006).
These nucleoporins, through their relocalization during mitosis, contribute essentially to the spatio-temporal coordination of mitosis.

3. The Nup107-160 subcomplex

The Nup107-160 subcomplex (Nup107 complex from now on) is the major structural subunit of the NPC both in size and complexity and when the NE breaks down at the onset of mitosis, proteins from the Nup107 complex localize to the mitotic spindle and to the kinetochores (Belgareh et al., 2001; Loiodice et al., 2004; Orjalo et al., 2006). The *S. cerevisiae* equivalent of the Nup107 complex is the Nup84 subcomplex, which has a molecular weight of around 500 KDa and is present in 16 copies per NPC (Alber et al., 2007b). Members of the Nup107 complex are localized on both sides of the NPC in yeast (Rout et al., 2000) and vertebrates (Belgareh et al., 2001; Enninga et al., 2003).
The Nup107 complex has been shown to play critical roles in mRNA export (Doye et al., 1994; Heath et al., 1995), NPC assembly (Harel et al., 2003b; Walther et al., 2003a) and in various events during mitosis (see references above).

3.1 <u>Composition of the Nup107 complex</u>: the vertebrate Nup107 complex is composed of 9 nucleoporins: Nup160, Nup133, Nup107, Nup96, Nup85, Nup43, Nup37, Sec13 and Seh1. The yeast Nup84 subcomplex is nearly identical to the Nup107 complex in vertebrates, only that it is composed of 7 nucleoporins lacking the vertebrate Nup43 and Nup37 subunits. Eight different members have been found in *C. elegans* for the Nup107 complex, lacking the vertebrate Nup37 subunit so far.

Vertebrate	*S. cerevisiae*	*C. elegans*
Nup160	Nup120	NPP-6
Nup133	Nup133	NPP-15
Nup107	Nup84	NPP-5
Nup96	Nup145-C	NPP-10C
Nup85	Nup85	NPP-2
Nup43	----	C09G9.2
Nup37	----	----
Sec13	Sec13	NPP-20
Seh1	Seh1	NPP-18

Table 2. Different homologs of the Nup107 complex. Terminology of the different homologs of the Nup107 complex in vertebrates, *S. cerevisiae* and *C. elegans*

The difference on the number of subunits in each organism could be due to the fact that the Nup43 and Nup37 subunits for *S. cerevisiae* and the Nup37 subunit for *C. elegans* have not yet been discovered. Alternatively, these nucleoporins may play species-specific functions within the Nup107 complex rather than structural roles.

The yeast heptameric Nup84 subcomplex can be reconstituted from proteins expressed in *Escherichia coli* and it has been reported to have a Y-shaped structure by electron microscopy (Lutzmann et al., 2002). Also several crystal structures of subunits of the complex have been isolated, showing the interaction between the different subunits (Boehmer et al., 2008; Brohawn et al., 2008; Debler et al., 2008; Hsia et al., 2007).

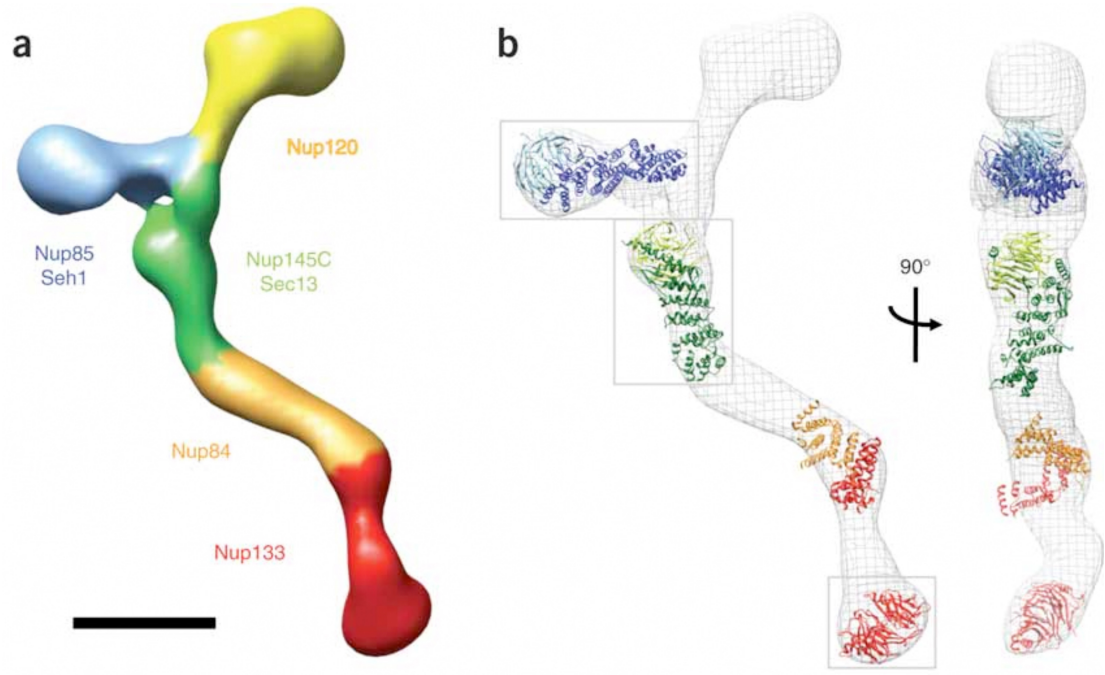

Figure 9. The Nup84 subcomplex conformation in yeast. (A) Nup84 subcomplex conformation based on mapped nucleoporin localization and biochemical interactions. Scale bar, 100 Å. (B) Docking of the available crystal structures. Two different views are shown. Adapted from (Kampmann and Blobel, 2009).

3.2 <u>Role in mitotic spindle assembly</u>: the Nup107 complex has been proposed to play an essential role in the mitotic spindle assembly (Orjalo et al., 2006). Using *in vitro* assays with *Xenopus* egg extracts (CSF extracts), Orjalo et al. showed that CSF extracts depleted for the Nup107 complex when incubated with sperm chromatin were defective in the assembly of the mitotic spindle. Also they confirmed that the role of the Nup107 complex in spindle assembly occurs upstream or independent of the initial Ran-mediated microtubule assembly pathway. Addition of RanGTP to mitotic CSF extracts causes the assembly of microtubules in a chromosome independent manner. Orjalo et al. confirmed in this study that mitotic *Xenopus* CSF extracts depleted of the Nup107 complex were also capable of assembling microtubules upon addition of RanGTP. Contrary to the idea that the Nup107 complex is essential for proper mitotic spindle assembly, there has been two recent studies where they showed that the morphology of the mitotic spindle was not affected upon depletion of the Nup107 complex in HeLa cells (Platani et al., 2009; Zuccolo et al., 2007). This controversy could be explained by the fact that the Nup107 complex broadly localizes to spindle and Ran-induced asters in *Xenopus* extracts (Orjalo et al.,

2006), whereas it localizes mainly at kinetochores and can only be transiently observed at spindle poles and proximal spindle fibers in HeLa cells (Loiodice et al., 2004; Orjalo et al., 2006), suggesting that the mechanism by which the spindle assembles in HeLa cells and *Xenopus* egg extracts might be different.

3.3 <u>Role in kinetochore functions</u>: it was not until 2001 when Belgareh et al. first reported the localization of subunits of the Nup107 complex to kinetochores in mammalian cells. Since then, different studies have focused on the possible role of the complex during mitosis at the kinetochores, although it is still unclear what is exactly its function there.

3.3.1 Kinetochore: kinetochores are complex proteinaceous assemblies that attach chromosomes to microtubules during mitosis. A proper kinetochore assembly is essential for correct segregation of chromosomes during cell division and more than 80 proteins have been described so far in the human kinetochore (Cheeseman and Desai, 2008). The kinetochore structure and composition have been extensively studied using different approaches such as cryoelectron microscopy, mass spectrometry, electron tomography and X-ray crystallography (Brinkley and Stubblefield, 1966; Dong et al., 2007; McEwen et al., 2007). These studies revealed that the kinetochore have a trilaminar morphology composed of the inner, the central and the outer kinetochore.

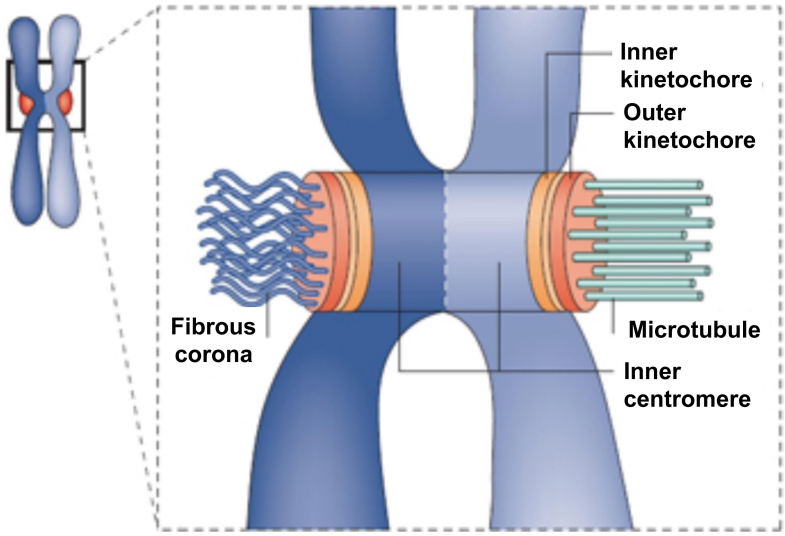

Figure 10. Vertebrate kinetochore ultrastructure. A schematic of a mitotic chromosome with paired sister chromatids — the chromatid on the right is attached to microtubules and the chromatid on the left is unattached. Adapted from (Cheeseman and Desai, 2008).

The inner kinetochore is the region that interacts with centromeric chromatin. The principal subunit of the inner kinetochore is the histone H3 variant CENP-A and it was one of the first kinetochore proteins to be identified (Earnshaw and Migeon, 1985; Palmer et al., 1991; Sullivan et al., 1994). CENP-A deposition at centromeric regions is mediated by Mis18 and KNL2 (Fujita et al., 2007; Hayashi et al., 2004; Maddox et al., 2007). The central kinetochore is the region between the inner and the outer kinetochore and it has a less dense appearance when observed by electron microscopy. Finally, the outer kinetochore is the region that interacts with spindle microtubules. Two major components of the outer kinetochore plate are the Ndc80 complex and the protein CENP-F. The Ndc80 complex is composed of four different subunits: Ndc80, Nuf2, Spc24 and Spc25. The Ndc80 complex has been extensively studied and X-ray crystallography structures from the individual members have been isolated (Wei et al., 2007; Wei et al., 2006). The Ndc80 complex together with the Mis12 complex and KNL1 composes the kinetochore-microtubule network (KMN), which comprises the principal kinetochore-microtubule attachment site in chromosomes. Functional assays of the KMN network have revealed that KNL1 and the Ndc80 complex are indispensable for the interaction between kinetochores and microtubules (Cheeseman et al., 2006; DeLuca et al., 2002; McCleland et al., 2003).

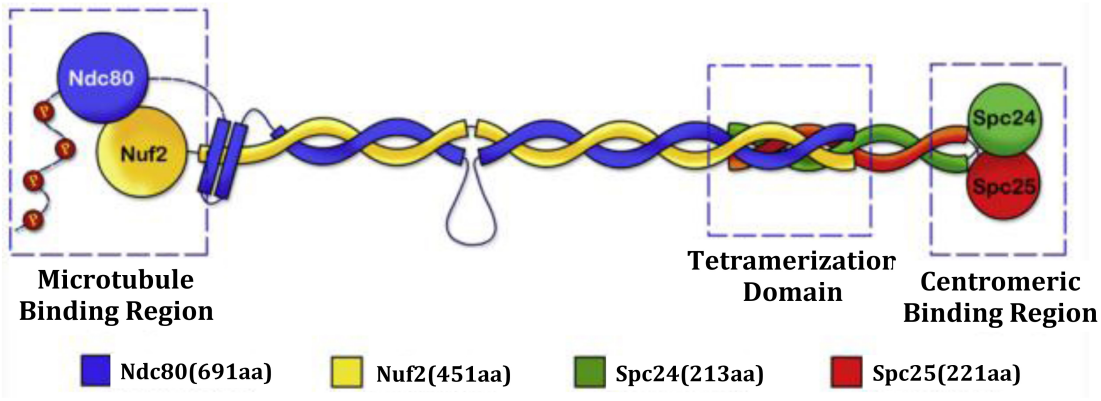

Figure 11. Representation of the Ndc80 complex. The tetrameric NDC80 complex composed of Ndc80, Nuf2, Spc25 and Spc24. The heterodimer Ndc80-Nuf2 conforms the region of interaction with microtubules within the complex. Adapted from (Wang et al., 2008).

Functional analysis of the Nup107 complex in HeLa cells demonstrated that the Ndc80 complex mediates its localization to the kinetochore (Zuccolo et al., 2007). Cells depleted of Nuf2 or Ndc80 by siRNA showed a reduction in the recruitment of the Nup107 complex to the kinetochore. Moreover, it was shown by immunofluorescence assays that Nup133 (a member of the Nup107 complex) colocalizes with Ndc80 at the kinetochores. In the same study, Zuccolo et al. showed an interaction between Nup133 and CENP-F (another outer kinetochore subunit) in a yeast two hybrid assay. However, depletion of CENP-F by siRNA in HeLa cells only partially affected the targeting of Nup133 to kinetochores, suggesting that CENP-F is only responsible for the targeting of a minor fraction of the Nup107 complex to the kinetochores. Overall, the Nup107 complex recruitment to the kinetochores seems to be mediated mainly by the Ndc80 complex and partially by CENP-F, and its function could be related with the proper attachment of microtubules to the kinetochores.

3.3.2 Spindle Assembly Checkpoint (SAC): The spindle assembly checkpoint (SAC) is a mitotic control mechanism that ensures that chromosomes do not segregate until they are properly bi-oriented and attached to microtubules (Tanaka, 2010). The best-characterized components of the SAC are Mad1, Mad2, Mad3 (also known as BubR1), Bub1, Bub3 and Mps1, which were first identified in yeast (Hoyt et al., 1991; Li and Murray, 1991). During interphase Mad1 and Mad2 localize to the NPCs in yeast via Mlp1 and Mlp2 (Iouk et al., 2002; Scott et al., 2005). In *Drosophila* cells the interaction of Mad1 and

Mad2 with the NPC is mediated by Mtor, the *Drosophila* ortholog of vertebrate Tpr (Katsani et al., 2008), while in *Xenopus* and human cells the interaction is mediated by Tpr (Campbell et al., 2001; Lee et al., 2008). The role of Mad1 and Mad2 at the NPC during interphase is still unclear today, leaving open interesting questions for future research.

During mitosis in somatic mammalian cells if a single kinetochore is not properly attached to spindle microtubles, the SAC is turned on and delays the onset of anaphase by sequestering Cdc20, an activator of the Anaphase Promoting Complex/Cyclosome (APC/C) (Fang et al., 1998; Hwang et al., 1998). The APC/C is an E3 ubiquitin ligase that targets key mitotic substrates for degradation, such as cyclin B and securin. Degradation of securin leads to activation of separase that has a cohesin-cleaving activity, leading to anaphase onset (Stemmann et al., 2001). The SAC is also turned on by lack of stretch-induced tension between kinetochores on sister chromatids (Maresca and Salmon, 2009; Uchida et al., 2009; Wan et al., 2009).

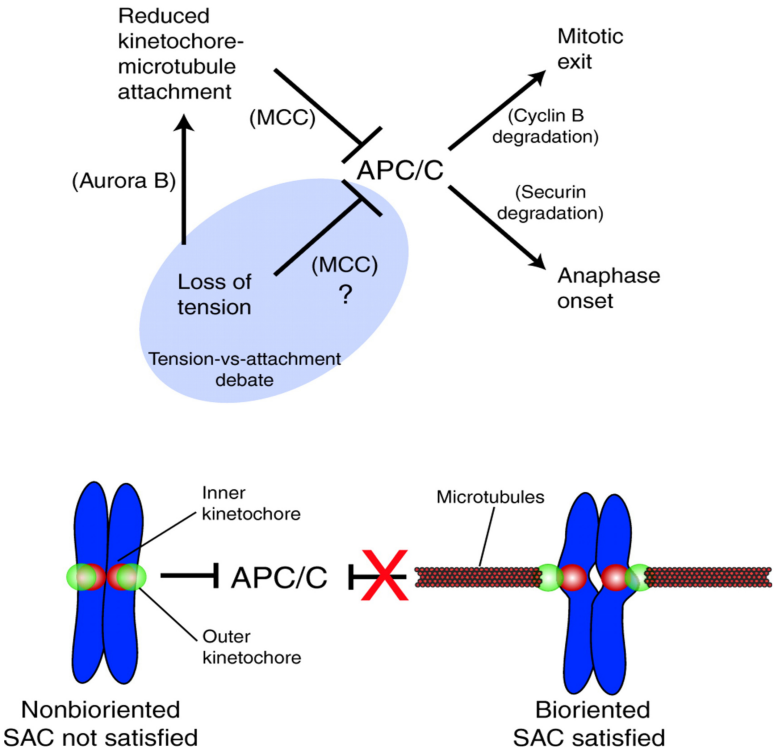

Figure 12. Schematic representation of the SAC pathway. Activation of the SAC by reduced kinetochore-microtubule attachment inhibits the APC by sequestering the APC subunit Cdc20. Lack of tension between sister chromatids also seems to generate an activation of the SAC. Adapted from (Maresca and Salmon, 2010).

In vitro studies in *Xenopus* extracts have shown that there is an enrichment of the Nup107 complex to kinetochores when they are not properly attached to spindle microtubules (Orjalo et al., 2006). In the same study, they showed that the recruitment of SAC proteins to kinetochores in *Xenopus* extracts treated with nocodazole (a microtubule depolymerizing reagent that causes activation of the SAC) seems to be independent of the Nup107 complex.

3.4 <u>Role in CPC localization</u>: the chromosome passenger complex (CPC) is composed of the protein kinase Aurora B and its regulatory subunits survivin, borealin and INCENP (Earnshaw and Bernat, 1991). The CPC localizes to the chomosome arms during prophase controlling chromosome structure and organization. During prometaphase the CPC localizes at centromeres and its function is to sense and regulate proper kinetochore-microtubule attachments. When improper kinetochore-microtubule interactions occur, Aurora B will disrupt these interactions by phosphorylating the Ndc80 complex resulting in an Ndc80 complex that is less affine to microtubules. The result of this will be a "free" kinetochore, which in turn will activate the SAC (Biggins et al., 1999; Cheeseman et al., 2002; Hauf et al., 2003; Lampson et al., 2004; Pinsky et al., 2006). Also it has been proposed that the CPC could play a more direct role in the regulation of the SAC by properly localizing BubR1 and Mad2 to kinetochores (Ditchfield et al., 2003; Vader et al., 2007). Furthermore, it has been suggested that the CPC could play a role in directly inhibiting the APC (Vader et al., 2007; Vader et al., 2008).

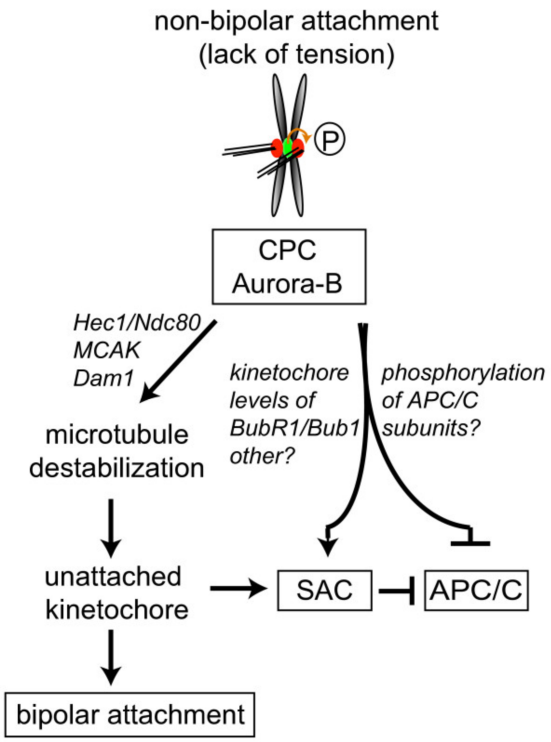

Figure 13. Possible functions of the CPC in the generation of the "wait anaphase" signal. In response to inappropriate attached kinetochores, the CPC not only destabilizes the kinetochore-microtubule attachment, but it could also directly control the SAC and/or the inhibition of the APC. Adapted from (Vader et al., 2008).

During cytokinesis, the CPC localizes to the spindle midzone suggesting that it also plays a role in the last step of cell division (Carmena et al., 2009; Ruchaud et al., 2007).

The Nup107 complex has been shown to be critical for the localization of the CPC to centromeres during prometaphase (Platani et al., 2009). Depletion of the Nup107 complex by siRNA against Seh1 in HeLa cells caused a mislocalization of Aurora B at centromeres. This observation suggests that the Nup107 complex is involved, by regulation of Aurora B localization, in the error-connection mechanism that eliminates kinetochore-microtubule mis-attachments. Platani et al. also suggested that depletion of Seh1 by siRNA in HeLa cells caused a mislocalization of Aurora B from the spindle midzone during cytokinesis, suggesting that the Nup107 complex could be also playing a role in cytokinesis.

3.5 <u>Role in microtubule nucleation</u>: The γ-tubulin ring complex (γ-TuRC) is an essential and conserved microtubule nucleator (Luders and Stearns, 2007; Wiese and Zheng, 2006) and it has been recently associated to the Nup107

complex (Mishra et al., 2010). Mishra et al. demonstrated that the γ-TuRC complex interacts biochemically and *in vivo* with the Nup107 complex using HeLa cells and *Xenopus* extracts. The γ-TuRC complex localizes to kinetochores during mitosis and this localization is mediated by the Nup107 complex. Moreover, both the Nup107 and the γ-TuRC complexes were shown in this study to be indispensable for nucleation of microtubules at kinetochores in a RanGTP-dependent manner.

4. <u>Objectives</u>: The main objectives proposed in this thesis are the following:

1. To determine the role of Nup35 and Nup107 in the nuclear pore complex (NPC) assembly, nuclear envelope (NE) morphology and nuclear transport.

2. To analyze the relationship between members of the Nup107-160 subcomplex during interphase and mitosis.

3. To understand the role of Nup107 at the kinetochores during mitosis.

4. To analyze the involvement of Nup107 in the spindle assembly checkpoint (SAC).

5. To study the role of Nup107 in development, including physiological aging.

3. Results

1. Dissection of a conserved nuclear pore subcomplex reveals a novel role of Nup107 in mitosis

1.1 Nup107/NPP-5 is required for proper development: To evaluate the implication of Nup107 in animal development we characterized two mutant alleles of the *C. elegans* homolog of Nup107, encoded by the *npp-5* gene. Allele *tm3039* is a 524 bp deletion from the 1st intron to the 4th exon whereas 1291 bp from the 4th exon to the 6th exon are deleted in allele *ok1966* (**Fig. 14**). Reverse transcription PCR revealed the activation of a cryptic 3' splice site in *tm3039*, causing a premature termination codon (PTC) after 35 amino acid residues. The deletion in *ok1966* similarly induces a PTC downstream of the mutation, but in this case approximately one third of the ORF is intact.

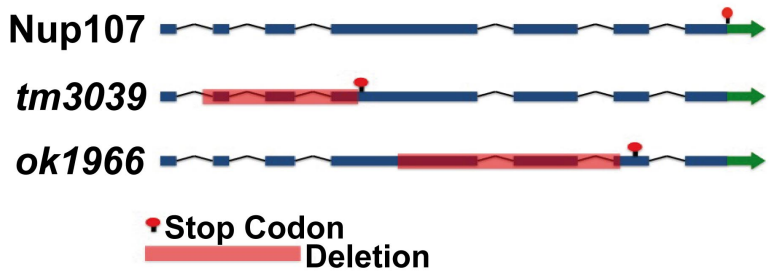

Figure 14. Schematic representation of *C. elegans* Nup107 and deletion alleles *npp-5(ok196)* and *npp-5(tm3039)*. Exons and introns are indicated by boxes and lines, respectively.

We raised an antibody against a peptide from the N-terminus of Nup107. As expected from the molecular lesion, neither Western blotting (**Fig. 15A**) nor immunofluorescence analysis (**Fig. 15B**) revealed a specific signal in *tm3039* mutants. The absence of signal in *ok1966* mutants suggested that the PTC renders the mRNA unstable.

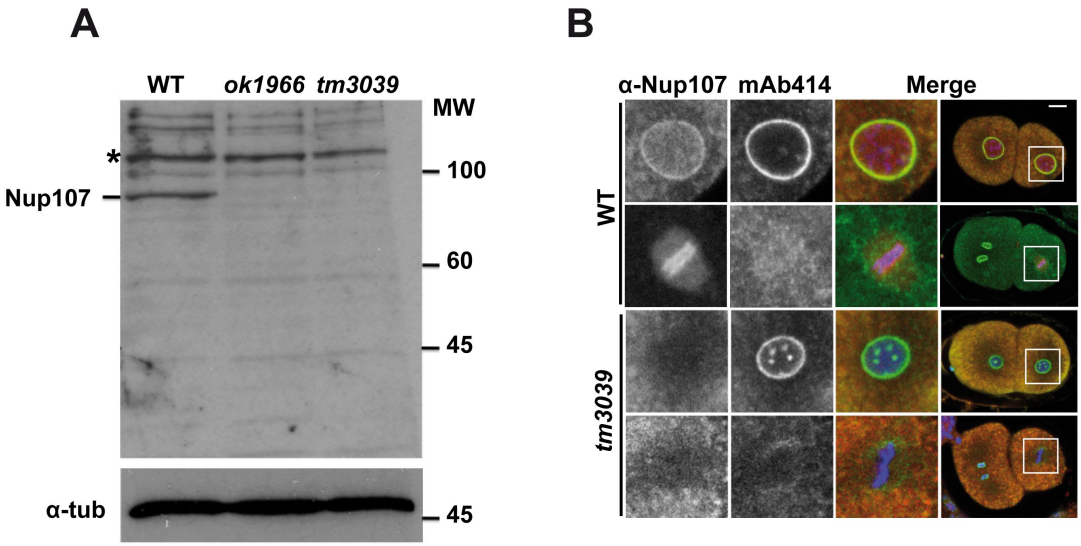

Figure 15. *npp-5(tm3039)* and *npp-5(ok1966)* are null mutations of Nup107. (A) Western blot analysis of approximately 1500 *ok1966* and *tm3039* embryos compared to 1500 wild type embryos. Upper and lower panels show probing with α-Nup107 and α-alpha-tubulin antibodies respectively. In wild type embryos, Nup107 appeared with a molecular weight of ~92 KDa, while in mutant *npp-5(ok1966)* and *npp-5(tm3039)* embryos this band disappears. (B) Wild type and *tm3039* embryos were fixed and stained with α-Nup107 antiserum (red) and monoclonal antibody mAb414 (green). Chromatin was detected using Hoechst 33258 (blue). Boxed regions in the merge panels are shown at higher magnification to the left, illustrating Nup107 and mAb414 staining individually. Scale bars, 10 μm

Both mutants can be propagated as homozygous strains, however, we introduced a balancer chromosome into each strain to avoid selection for suppressor mutations or epigenetic changes. Adult offspring from heterozygous animals consisted in 26.2-26.7% homozygous mutants (*ok1966*, *n*=806; *tm3039*, *n*=757), indicating that maternal contribution of Nup107 enables mutants to complete embryonic and larval development. Analyzing brood size of F1 homozygous mutants revealed a decrease of 21.9% in *ok1966* and 33.4% in *tm3039* (**Table 3**; p<0.005). For both alleles we observed a low but statistically significant increase in the frequency of lethality among F2 embryos produced by F1 homozygous mutants (**Table 3**; 5.3-7.3%). F2 larval development was severely compromised in both mutants with only 8.9-12.0% of the offspring developing into adults at 20°C (**Fig. 16**). At 25°C no offspring developed into fertile adults, suggesting a higher requirement for Nup107 when developmental pace is increased (**Table 3**). Importantly, ectopic expression of GFP-Nup107 fully restored embryonic and larval development of *ok1966* and *tm3039* mutants (**Table 3; Fig. 16**). Together with the identical behavior of the two mutant alleles

this confirmed that the observed phenotypes could be attributed to the *npp-5* gene. We therefore concluded that Nup107 plays a critical role in *C. elegans* development.

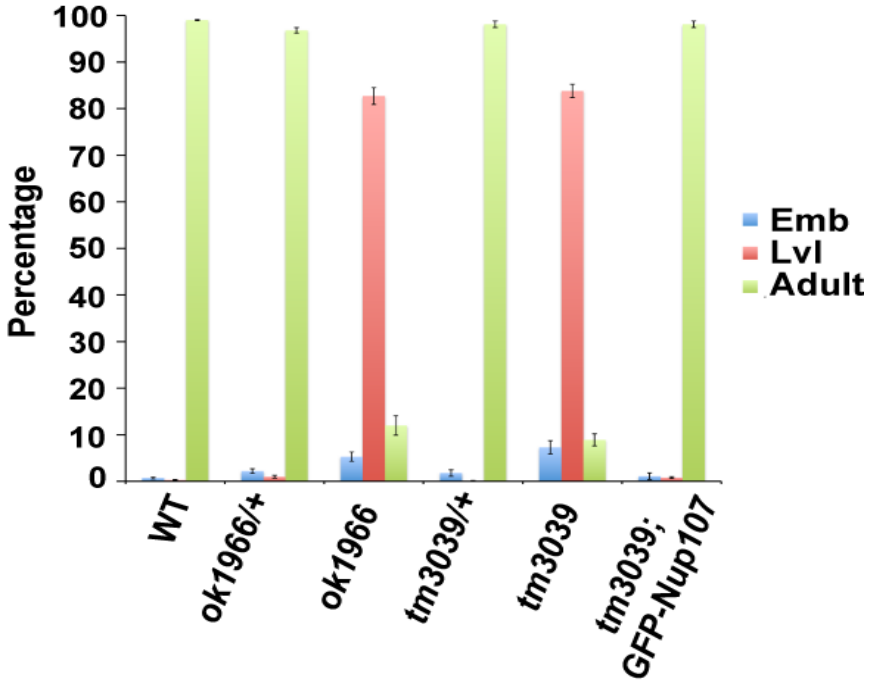

Figure 16. *ok1966* and *tm3039* generic phenotypes. Percentage of wild type, *ok1966* and *tm3039* offspring dying during embryogenesis (Emb) or larval development (Lvl) or reaching adulthood (Adult). Error bars indicate the standard error of the mean.

Strain	*n*[a]	Brood size[b] (average ±S.E.M.[f])	Embryonic lethality[c] (average ±S.E.M.)	Larval lethality[d] (average ±S.E.M.)	Adults[e] (average ±S.E.M.)
Wild type, 20°C	6	319±6	0.7±0.2%	0.3±0.1%	99.0±0.1%
Wild type, 25°C	3	217±25	1.8±1.0%	0.2±0.2%	98.0±1.1%
ok1966/+, 20°C	5	273±10†	2.2±0.5%	1.0±0.3%	96.8±0.6%
ok1966, 20°C	6	249±15†	5.3±1.0%*	82.7±1.8%*	12.0±2.1%*
tm3039/+, 20°C	5	257±11†	1.8±0.7%	0.1±0.1%	98.1±0.7%
tm3039, 20°C	10	212±14†	7.3±1.4%*	83.8±1.4%*	8.9±1.3%*
tm3039; GFP-Nup107, 20°C	9	259±19	1.1±0.7%	0.8±0.2%	98.1±0.7%
tm3039, 25°C	4	145±14†	18.2±4.1%*	81.8±4.1%*	0.0±0.0%*

Table 3. Development of *ok1966* and *tm3039* mutants. Heterozygous or first-generation homozygous mutant L4 hermaphrodites were incubated on NGM plates at indicated temperatures and moved to fresh plates every 8-16h. Wild type N2 strain was used as control. [a] number of founders. For each founder, brood sizes[b] and the percentages of embryonic lethality[c], arrested or dead larvae[d] and adults[e] were determined after 0h, 24h and 96h. [f] Standard error of the means. Significant differences by two-tailed t-test: † different from the wild type at same temperature ($p<0.005$). Significant differences by Chi-square test: * different from the wild type at same temperature ($p<0.001$).

1.2 <u>Nup107 is dispensable for nuclear protein import</u>: The developmental arrest could potentially reflect defects in NE function, including nucleocytoplasmic transport. To test this, we monitored the growth rate of P1 cell nuclei following the first mitosis in embryos expressing green fluorescent protein (GFP) fused to histone H2B (**Fig. 17**). While nuclei in embryos produced by heterozygous siblings (which for simplicity are referred to as control embryos hereafter) grew by 0.56±0.02 μm^3/sec (time interval 152-696 sec after anaphase

onset; *n*=12) the rate was reduced to 0.42±0.02 μm³/sec in F2 mutant embryos (*n*=13) (25.6% decrease, $p<2*10^{-5}$). The final size of P1 nuclei was reduced by 12.8% ($p<0.05$). In both control and *tm3039* embryos P1 nuclei kept growing until entry into mitosis, which occurred after ~832 sec in control and ~880 sec in mutant embryos. Thus, absence of Nup107 reduced nuclear growth and delayed entry into mitosis.

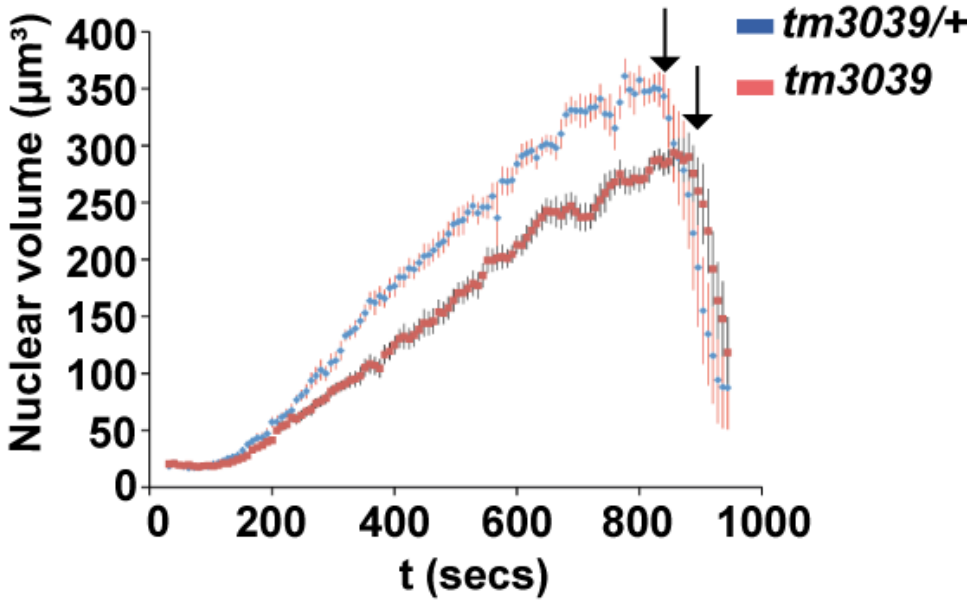

Figure 17. Nuclear growth over time of P1 nucleus in *tm3039/+* and in *tm3039*. Size of P1 nuclei was determined by time-lapse microscopy, revealing a significant slower nuclear growth rate in *tm3039* embryos (*n*=13) compared to *tm3039/+* embryos (*n*=12). Time is relative to P0 anaphase onset.

Structural changes in NPCs can affect NE permeability. Inert molecules larger that ~45 kD are normally unable to cross the NE, but depletion of nucleoporins can increase this permeability barrier. We investigated whether this was also the case in *tm3039* embryos by injecting the gonad arms of hermaphrodites with mixtures of fluorescent dextrans (Galy et al., 2003). However, 70 kD and 155 kD dextrans were effectively excluded from nuclei from both control and *tm3039* embryos, indicating that the permeability barrier was not grossly affected in the absence of Nup107 (**Fig. 18**).

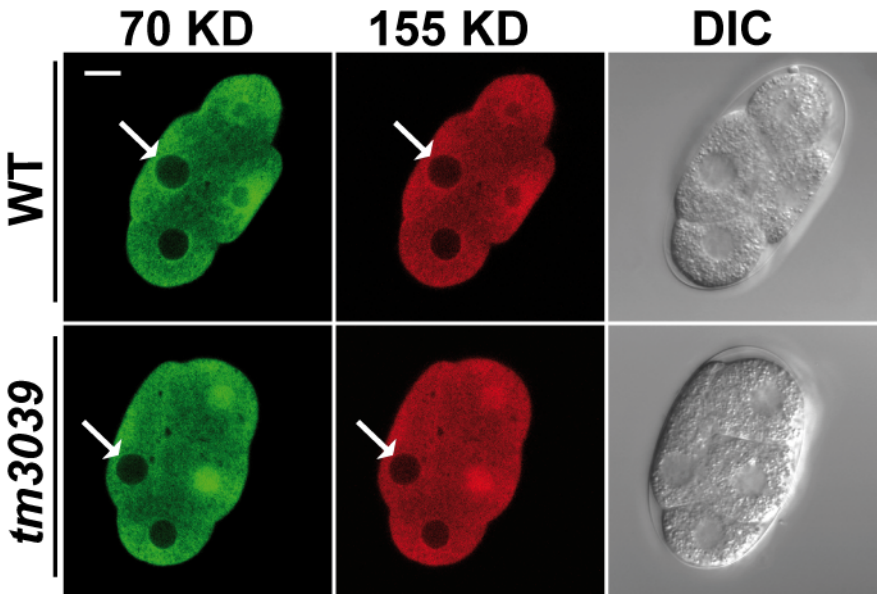

Figure 18. Dextran injections into WT and *tm3039* gonads. Gonads of wild type (*n*=14) and *tm3039* (*n*=16) animals were injected with a mixture of 70 kD (green) and 155 kD (red) dextrans. Exclusion of the dextrans from embryonic nuclei (arrows) was observed by live confocal microscopy. Scale bars, 10 µm. Note that nuclei at the right of the embryo are in mitosis and thus do not show exclusion.

Next, we monitored nuclear accumulation of several protein substrates fused to GFP. PIE-1 is a transcriptional regulator found specifically in germline blastomeres where it is imported into the nucleus by an unknown transport pathway (Reese et al., 2000). In both control and *tm3039* 4-cell stage embryos robust nuclear accumulation of GFP-PIE-1 was observed in the P2 cell, although time-course analysis indicated a trend for slower import in the absence of Nup107 (**Fig. 19A**; p=0.40). Similarly, stress-induced nuclear import of the transcription factor DAF-16 fused to GFP as well as constitutive nuclear import of lacZ-GFP coupled to the SV40 T-antigen Nuclear Localization Signal (NLS) in intestine and vulva cells was normal in Nup107 mutants (**Fig. 19B; C**). We therefore concluded that Nup107 is dispensable for importin α/β-mediated nuclear protein import, but we cannot rule out that nucleocytoplasmic transport of other substrates may be Nup107-dependent.

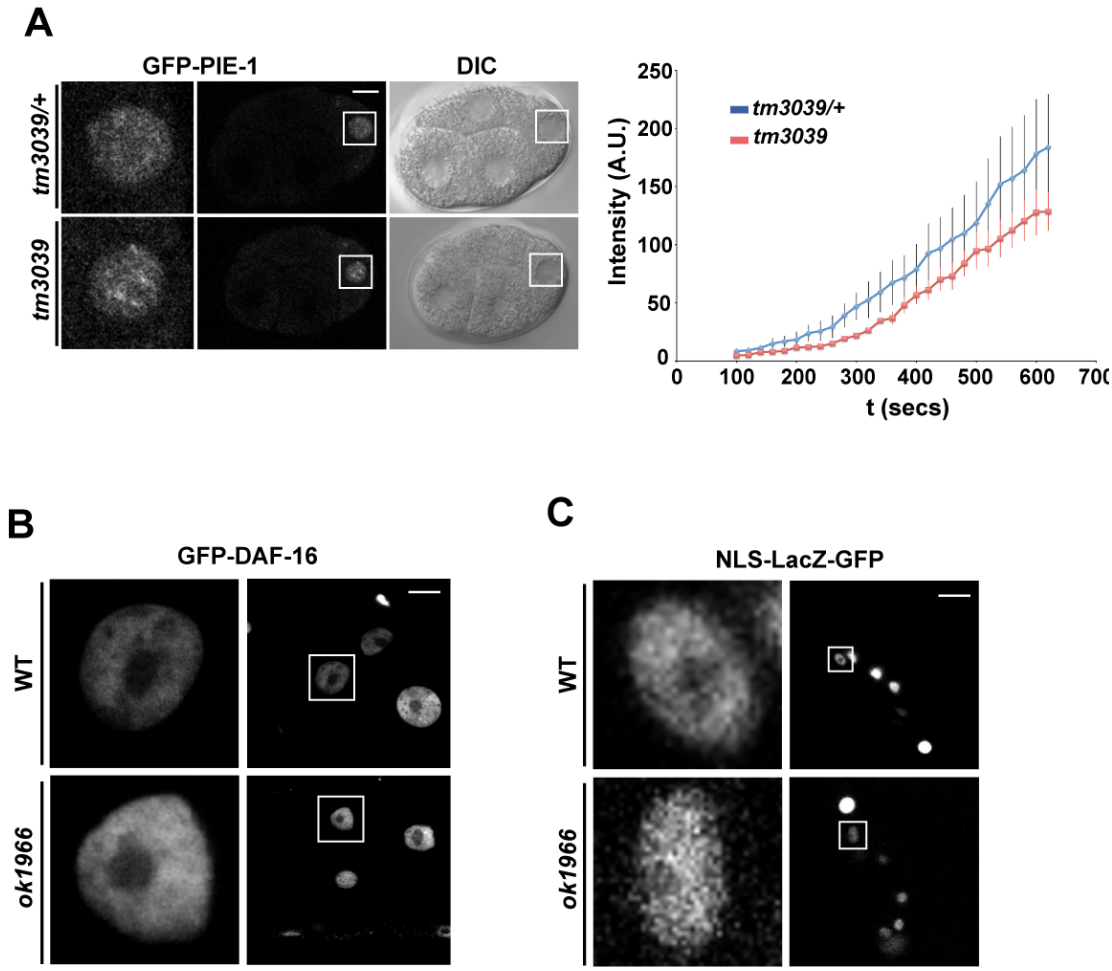

Figure 19. Import of proteins occurs normally in *tm3039* and *ok1966* mutants.
(A) Nuclear import of GFP-PIE-1 into P2 nuclei was analyzed by time-lapse microscopy. Import in *tm3039* embryos (*n*=10) was comparable to control embryos (*n*=10). Time is relative to P1 anaphase onset. Error bars indicate the standard error of the mean. (B) Import of GFP-DAF-16 in *ok1966* compared to wild type. (C) Import of NLS-LacZ-GFP in *ok1966* compared to wild type. Scale bars, 10 µm.

1.3 <u>NPC assembly can occur in the absence of Nup107</u>: The Nup107 complex is essential for post-mitotic and interphase NPC assembly (D'Angelo et al., 2006; Harel et al., 2003b; Walther et al., 2003a) but the relative contribution of each member of the subcomplex has remained largely unknown, partly because siRNA approaches in vertebrate cells leads to a general down regulation of most or all components. To address the issue of co-regulation, embryonic extracts from wild type and *tm3039* animals were analyzed by Western blotting using antibodies against Nup96 and Nup133 from the Nup107 complex as well as Nup35, Nup98, and Nup153. Except for Nup133, all these nucleoporins were present at normal levels in *tm3039* embryos (**Fig. 20**). Moreover, it was

previously shown that knockdown of Nup107 does not affect expression of MEL-28/ELYS in *C. elegans* (Galy et al., 2006). Conversely, RNAi against Nup35 (Rodenas et al., 2009), Nup155 (Franz et al., 2005) or MEL-28/ELYS (Galy et al., 2006) was shown not to affect on expression of Nup107. The independent expression of individual nucleoporins tested so far underlines the usefulness of *C. elegans* as genetic system to dissect the function of NPC components (Gorjanacz et al., 2007a). Affinity purified antibodies against Nup133 gave rise to two bands of the expected size (~128 kD) in wild type extracts but, intriguingly, only a single band in *tm3039* (**Fig. 20**).

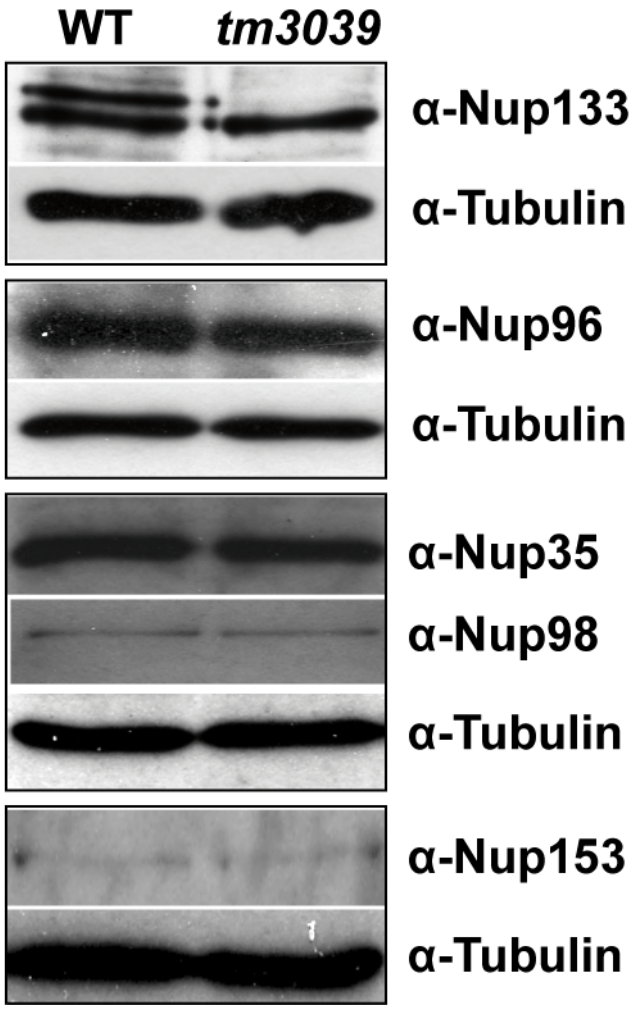

Figure 20. Expression and localization of most Nups are Nup107-independent. Western blot analysis of embryonic extracts showed similar expression levels of Nup96, Nup35, Nup98 and Nup153 in *tm3039* embryos compared to the wild type. In contrast, Nup133 appeared as a duplet in the wild type but not in the mutant.

Comparing extracts from wild type embryos to extracts from embryos produced by animals heterozygous for a Nup133 deletion allele (*ok1954*) showed that both bands correspond to Nup133 protein (**Fig. 21**).

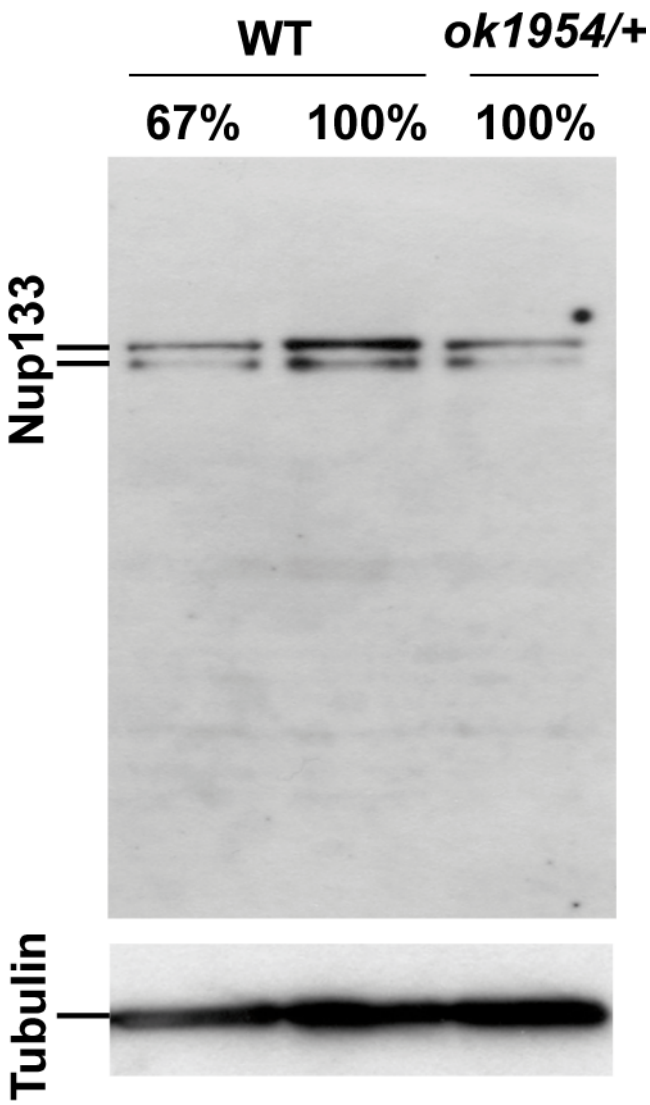

Figure 21. WB in *ok1954/+* compared to WT using Nup133 Abs. Both bands seem to correspond to Nup133 since they are less abundant in extracts from heterozygous mutants.

We next analyzed whether the lack of Nup107 prevented proper localization of components of the Nup107 complex. MEL-28/ELYS and Nup96 localized at the nuclear periphery in interphase and to kinetochores during mitosis in both wild type and *tm3039* embryos (**Fig. 22**). Moreover, the monoclonal antibody mAb414, a general NPC marker, showed normal staining in the absence of Nup107.

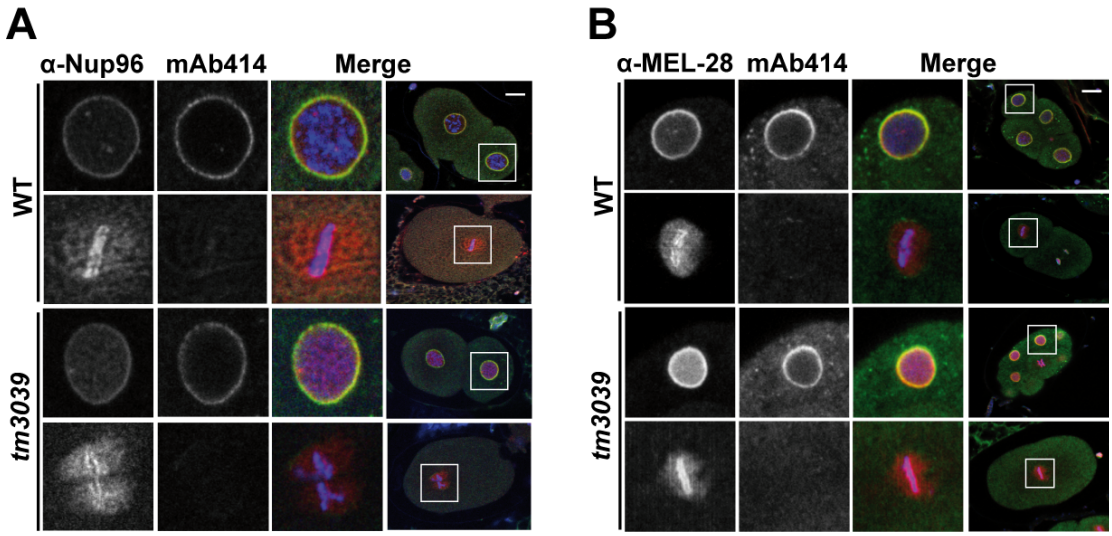

Figure 22. WT and *tm3039* embryos fixed and stained with α-Nup96 antiserum (A) and α-MEL-28 antiserum (B). Wild type and *tm3039* embryos were fixed and stained with (A) α-Nup96 and (B) α-Mel-28 antiserum (red) and monoclonal antibody mAb414 (green). Chromatin was detected using Hoechst 33258 (blue). Boxed regions in the merge panels are shown at higher magnification to the left, illustrating (A) Nup96, (B) MEL-28 and mAb414 staining individually. Scale bars, 10 μm.

Nuclear rim accumulation of Nup133 was similarly unaffected by Nup107 depletion (**Fig. 23**). However, recruitment to kinetochores in mitosis was detected only in wild type embryos but not in *tm3039* embryos.

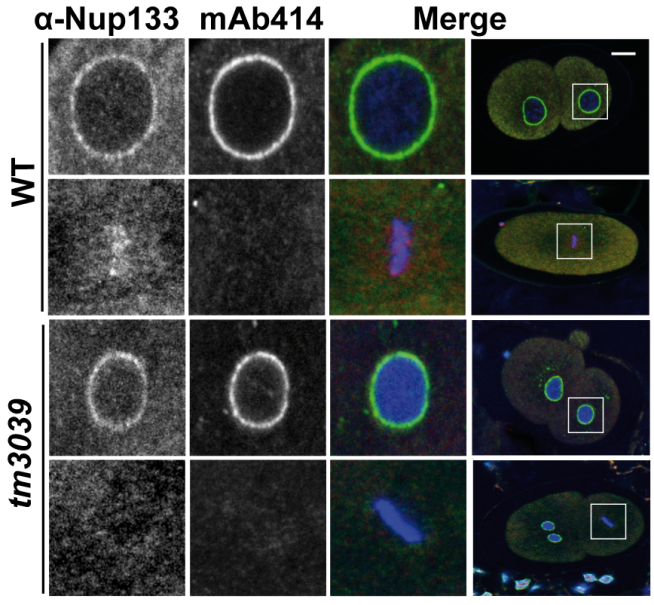

Figure 23. WT and *tm3039* embryos fixed and stained with α-Nup133 antiserum. Wild type and *tm3039* embryos were fixed and stained with α-Nup133 antiserum (red) and monoclonal antibody mAb414 (green). Chromatin was detected using Hoechst 33258 (blue). Boxed regions in the merge panels are shown at higher magnification to the left, illustrating Nup133 and mAb414 staining individually. Scale bar, 10 μm.

The observation that NPC localization of Nup133 was Nup107-independent was unexpected since a GFP-tagged version of human Nup133 mutated in residues that mediate direct contacts with Nup107 did not accumulate at the nuclear periphery (Boehmer et al., 2008). We therefore expressed GFP-Nup133 in Nup107 mutants and control animals, which revealed that NPC localization of the fusion protein is Nup107-dependent in *C. elegans* as in mammalian cells (**Fig. 24**).

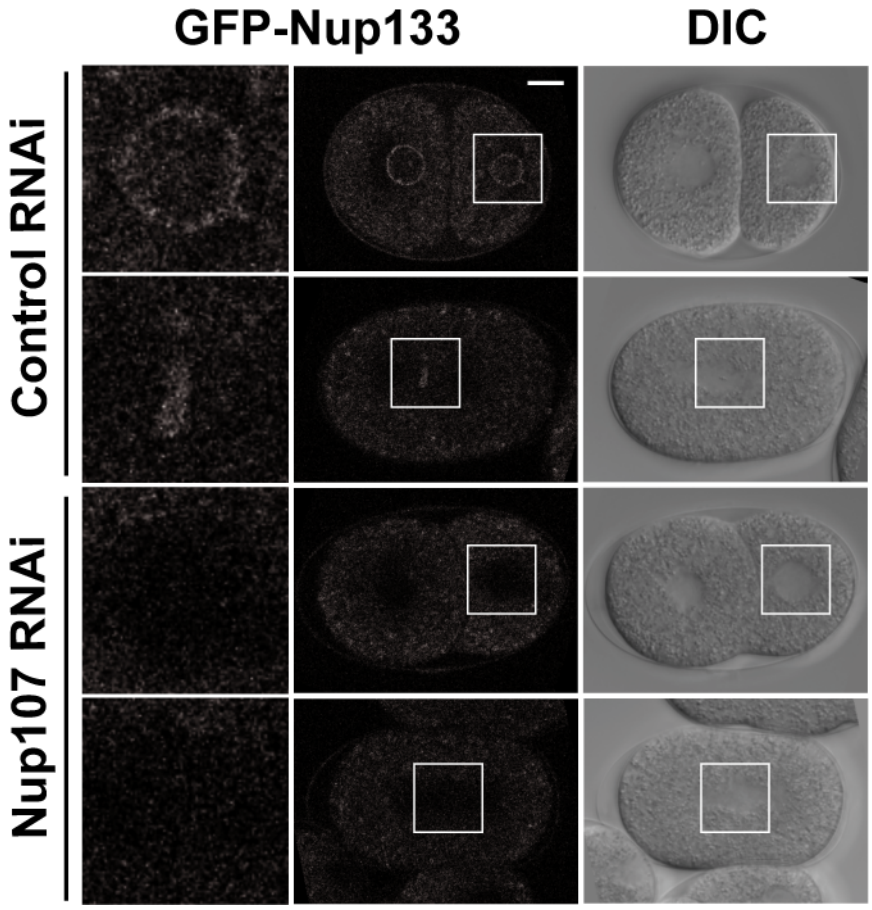

Figure 24. GFP-Nup133 localization in Nup107 RNAi embryos. GFP-Nup133 localization is impaired in Nup107 RNAi embryos. Mock-depleted and embryos depleted of Nup107 by RNAi and expressing GFP-Nup133 were imaged using time-lapse confocal microscopy. Scale bar, 10 µm.

To investigate additional members of the Nup107 complex we made transgenic strains expressing GFP fused to either Nup43 (D'Angelo et al., 2009) or Nup85, neither of which has been visualized previously in *C. elegans*. As expected, both nucleoporins localized to NPCs and kinetochores in the wild type (**Fig. 25A; B**).

While nuclear rim and kinetochore recruitment of GFP-Nup43 was diminished in *tm3039* embryos (**Fig. 25A**) GFP-Nup85 was present at normal levels at the nuclear periphery in *tm3039* animals (**Fig. 25B**).

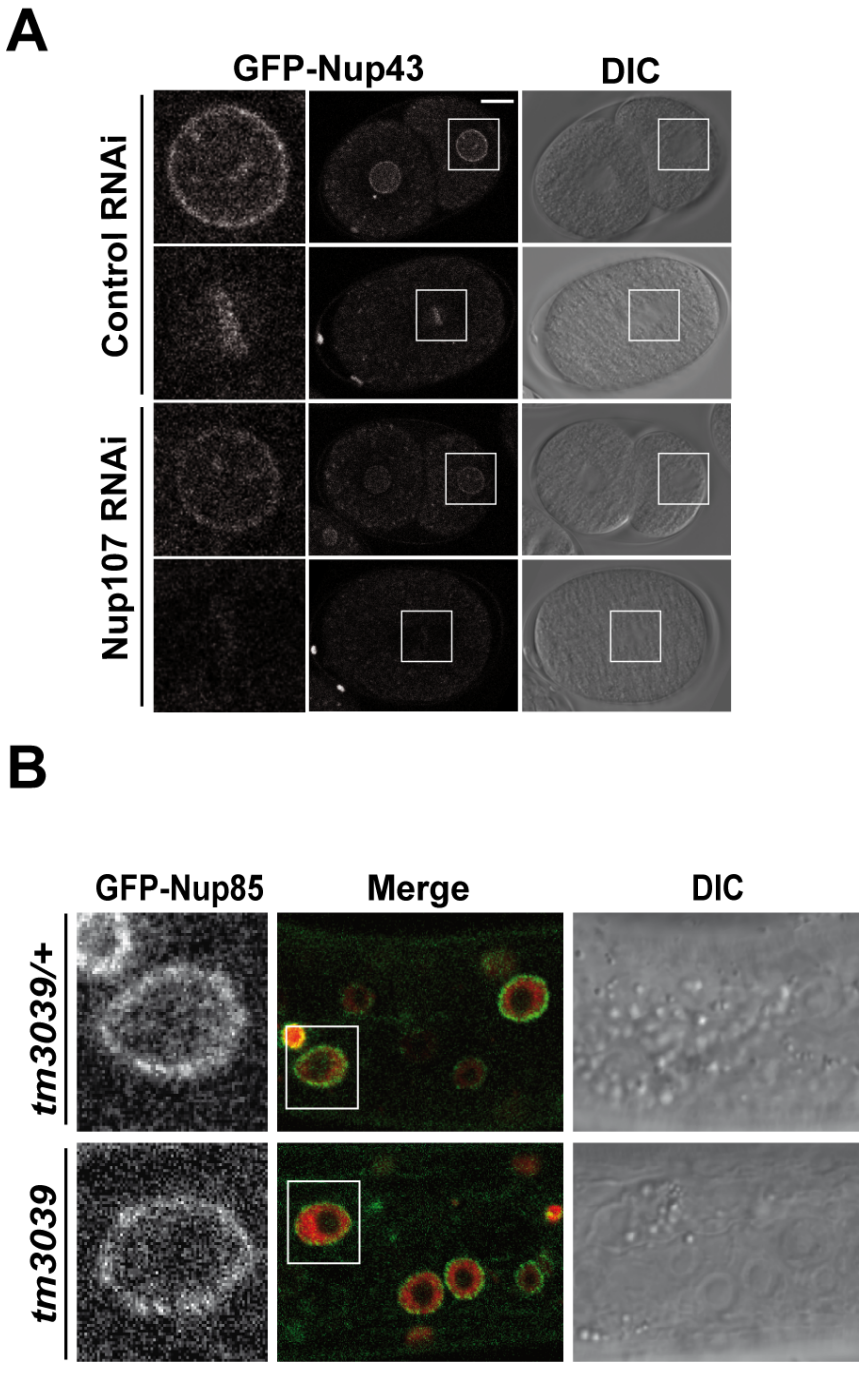

Figure 25. Expression of GFP-Nup43 and GFP-Nup85. Expression of GFP-Nup43 and GFP-Nup85/mCherry-HisH2B was analyzed by live microscopy. Whereas depletion of Nup107 inhibited recruitment of GFP-Nup43 ($n \geq 24$ for each treatment) (A), GFP-Nup85 was unaffected (B) ($n \geq 8$ for each treatment). Boxed regions in the merged panels are shown at higher magnification to the left. Scale bars, 10 µm.

Our GFP-Nup85 reporter was only expressed in postembryonic cells, which precluded a detailed analysis of mitosis in second-generation mutants since divisions have largely ceased in these animals. In first generation mutants at the larval L2-L3 stage GFP-Nup85 localized to kinetochores during division of seam cells (data not shown), but we cannot exclude the presence of low amounts of maternally contributed Nup107 protein in these animals. In conclusion, in the absence of Nup107 only Nup133 showed a dramatic reduction and only at the kinetochore, suggesting that NPC assembly and stability of the Nup107 complex is largely Nup107-independent.

1.4 <u>Localization of Nup107 depends on most other subcomplex members</u>: Having observed that most nucleoporins behave normally in Nup107-depleted animals we asked the reciprocal question: which members of the Nup107 complex are required to properly localize Nup107? Using the rescuing GFP-Nup107 strain (**Table 3**) we analyzed Nup107 dynamics in control and RNAi-treated embryos. Upon depletion of Nup85 the signal of GFP-Nup107 was reduced at both the nuclear periphery and at kinetochores whereas RNAi against Nup96 and Nup160 completely abolished Nup107 recruitment (**Fig. 26**).

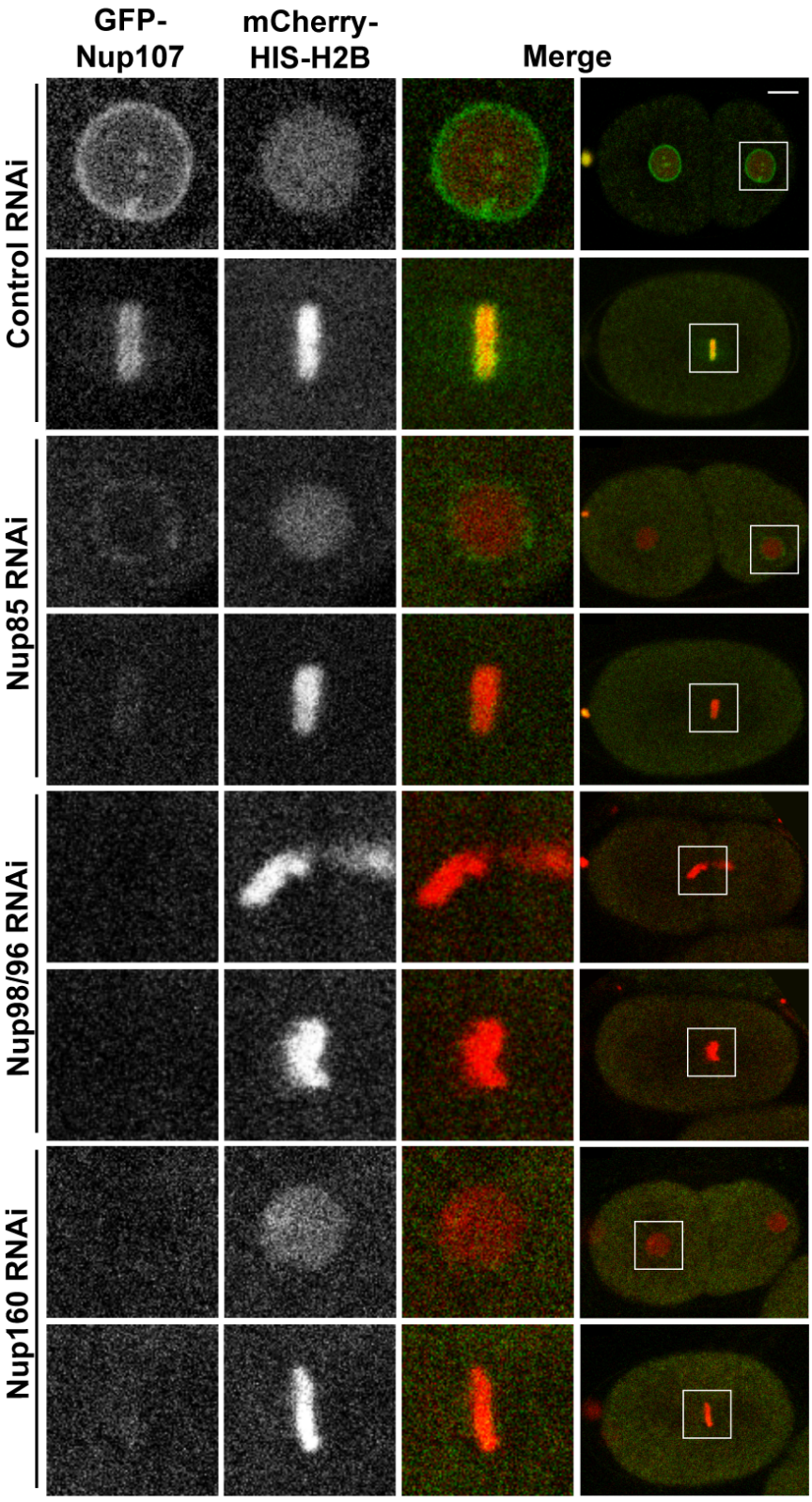

Figure 26. Nup107 localization is sensitive to perturbations of other Nup107 complex members. Still images from time-lapse confocal microscopy of embryos expressing GFP-Nup107 (green) and mCherry-HIS-58 (red). RNAi against Nup85, Nup96/98 or Nup160 inhibited proper localization of GFP-Nup107 during interphase (top rows) and metaphase (bottom rows) ($n \geq 8$ for each treatment). Boxed regions in the right panels are shown at higher magnification to the left. Scale bar, 10 μm.

Targeting Nup96 caused moreover severe chromosome segregation defects in mitosis. Because Nup96 and Nup98 are translated as a precursor polypeptide from a common mRNA, RNAi efficiently knocks down expression of both nucleoporins (Galy et al., 2003). Thus, these phenotypes may be contributed to the lack of either Nup96 or Nup98 or both. Analyzing endogenous Nup107 by immunofluorescence confirmed the dependency on Nup96/98, Nup160 and MEL-28/ELYS for correct localization of Nup107 (**Fig. 27**). In contrast, we found that RNAi against Seh1 did not impede recruitment of Nup107. Together, this suggests that while the Nup107 complex is stable in the absence of Nup107, Nup107 itself is very sensitive to perturbations of the NPC subcomplex.

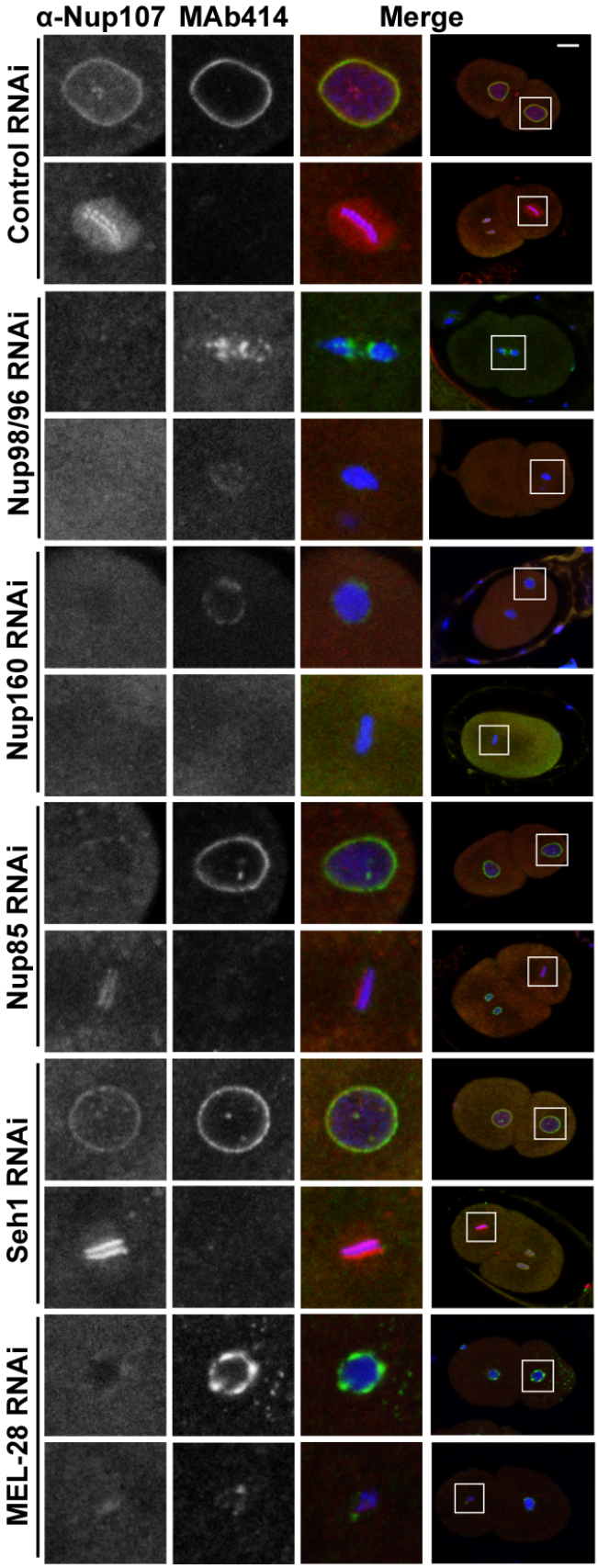

Figure 27. Perturbations of the Nup107 complex prevent proper localization of Nup107. RNAi treated embryos were fixed and stained with α-Nup107 antiserum (red) and monoclonal antibody mAb414 (green). Chromatin was detected using Hoechst 33258 (blue). Boxed regions are shown at higher magnification to the left. Scale bars, 10 μm.

1.5 <u>Nup107 is required for efficient assembly of kinetochores and Aurora B recruitment</u>: The mitotic localization of the Nup107 complex to kinetochores led to the hypothesis that nucleoporins could be directly involved in chromosome segregation (Belgareh et al., 2001). In support of this, HeLa cells with reduced Nup107 and Seh1 loading onto kinetochores showed increase frequency of misaligned chromosomes during metaphase (Zuccolo et al., 2007). To test if depletion of Nup107 affects proper kinetochore assembly in *C. elegans* we monitored the behavior of outer kinetochore proteins Nuf2/HIM-10 and Mis12/MIS-12, members of the Ndc80 and Mis12 complexes, respectively. Quantification of GFP-Nuf2 at kinetochores of metaphase chromosomes revealed a 39% reduction in *tm3039* embryos (**Fig. 28A**; $p<0.01$), whereas GFP-Mis12 localization was Nup107-independent (**Fig. 28B**; $p\approx0.62$). These results suggest that Nup107 is required for specific aspects of outer kinetochore assembly.

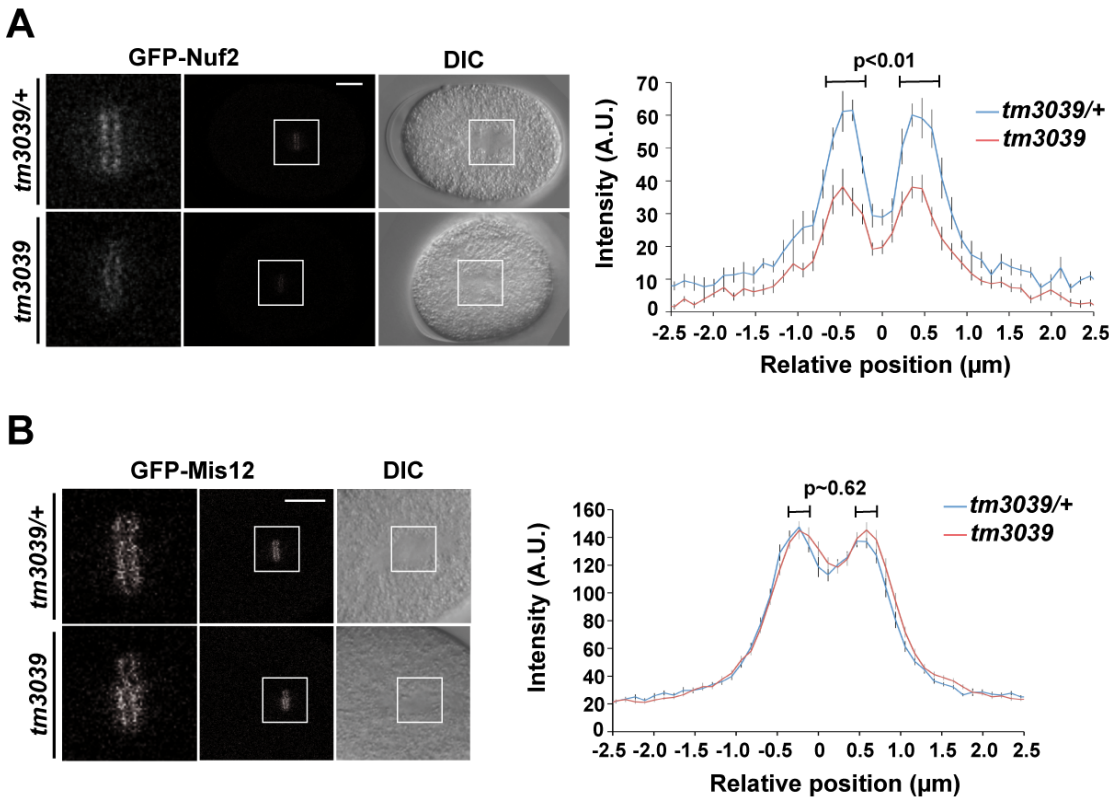

Figure 28. Nup107 is required for efficient localization of Nuf2. Still images from time-lapse confocal microscopy of control (*tm3039/+*) and *tm3039* embryos expressing GFP-Nuf2 (A) and GFP-Mis12 (B). Boxed regions in the central panels are shown at higher magnification to the left. Scale bars, 10 µm. Graphs on the right represent mean fluorescence intensities measured in 5*2.3 μm^2 rectangles perpendicular to the metaphase plates. Position is relative to the centre of metaphase chromosomes. Error bars indicate the standard error of the mean. $n\geq15$ in both experiments.

The fidelity of bipolar microtubule attachment to kinetochores is monitored by the CPC, which includes INCENP, Survivin, Borealin and the protein kinase Aurora B. We tested if CPC recruitment is Nup107-dependent by measuring GFP-Aurora B/AIR-2 levels on mitotic chromatin. This revealed a 34% reduction of chromatin-associated GFP-Aurora B during metaphase in *tm3039* embryos as compared to control embryos (**Fig. 29**; p<0.01). Thus, we concluded that Nup107 is required for proper localization of specific kinetochore and CPC components.

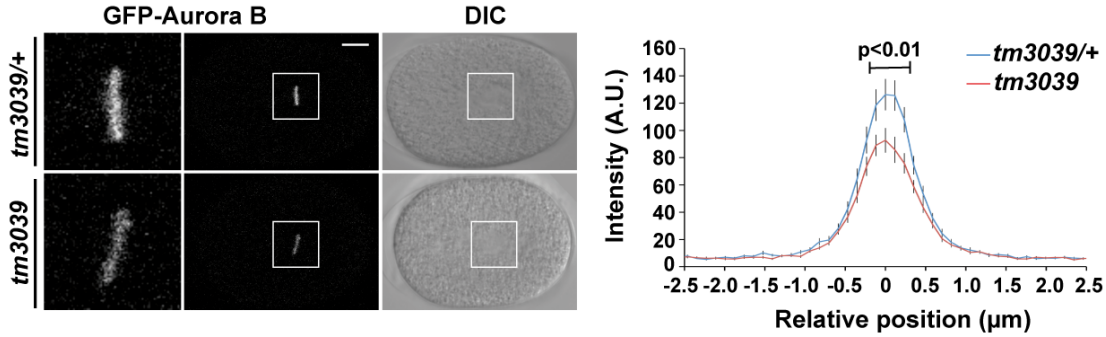

Figure 29. Nup107 is required for efficient localization of Aurora B. Still images from time-lapse confocal microscopy of control (*tm3039/+*) and *tm3039* embryos expressing GFP-Aurora B. Boxed regions in the central panels are shown at higher magnification to the left. Scale bar, 10 µm. Graphs on the right represent mean fluorescence intensities measured in 5*2.3 μm^2 rectangles perpendicular to the metaphase plates. Position is relative to the centre of metaphase chromosomes. Error bars indicate the standard error of the mean. $n \geq 15$

1.6. Microtubule density at kinetochores is unaffected in Nup107 mutants:

The defects observed at kinetochore assembly and the reduced recruitment of Aurora B to mitotic chromatin in the absence of Nup107 prompted us to investigate the dynamics of microtubules in Nup107 mutant embryos. We crossed the *npp-5(tm3039)* mutants with a strain expressing GFP-tubulin and mCherry-H2B and quantified the amount of microtubules in proximity of the metaphase plate in one cell embryos.

We observed that the density of microtubules at the metaphase plate is slightly reduced in homozygous Nup107 mutants compared to heterozygous mutants, but this difference was not statistically significant (**Fig. 30**; p>0.2). Thus, depletion of Nup107 does not significantly alter the amount of microtubules at

the metaphase plate although we cannot exclude the possibility that the attachment of microtubules to kinetochores is affected in Nup107 mutants.

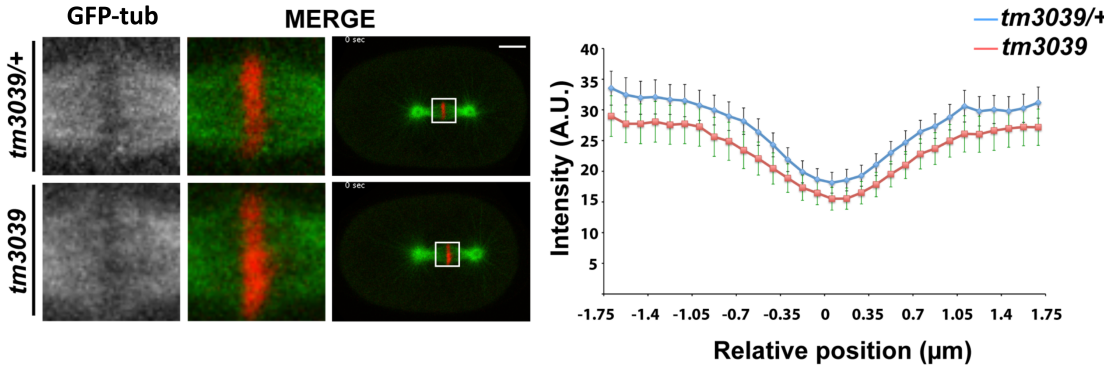

Figure 30. Microtubule density in proximity of the metaphase plate in Nup107 mutants. Still images from time-lapse confocal microscopy of control (*tm3039/+*) and *tm3039* embryos expressing GFP-tubulin. Boxed regions in the central panels are shown at higher magnification to the left. Scale bars, 10 µm. Graphs on the bottom represent mean fluorescence intensities measured in 3*6 µm^2 rectangles at the metaphase plates. Position is relative to the centre of metaphase chromosomes. Error bars indicate the standard error of the mean. $n \geq 15$

1.7 <u>The spindle assembly checkpoint can be activated in the absence of Nup107</u>: Unattached kinetochores due either to defective kinetochore assembly or Aurora B-mediated correction of syn- and merotelic MT-kinetochore attachments activate the spindle assembly checkpoint (SAC) (Lampson and Cheeseman, 2010; Tanaka, 2010). Based on our observation that Nuf2 and Aurora B localization is partially compromised in *tm3039* embryos we addressed two questions: Does the absence of Nup107 at kinetochores in itself trigger activation of the SAC? Can the SAC be activated in cells lacking Nup107? To answer the first question we investigated whether SAC proteins Mad1/MDF-1 and Mad2/MDF-2 localized to mitotic chromatin in *tm3039* embryos. In contrast to the situation in most vertebrate cells, *C. elegans* Mad1 and Mad2 accumulate on chromatin only if cells are stressed during mitosis (Essex et al., 2009; Yamamoto et al., 2008). Live recordings of Nup107-depleted embryos revealed faint but reproducible accumulation of GFP-Mad1 on chromatin during metaphase, suggesting that absence of Nup107 lead to activation of the SAC (**Fig. 31A**). GFP-Mad2 recruitment was however not observed, possibly due to a strong fluorescent signal from soluble protein (**Fig. 31B**).

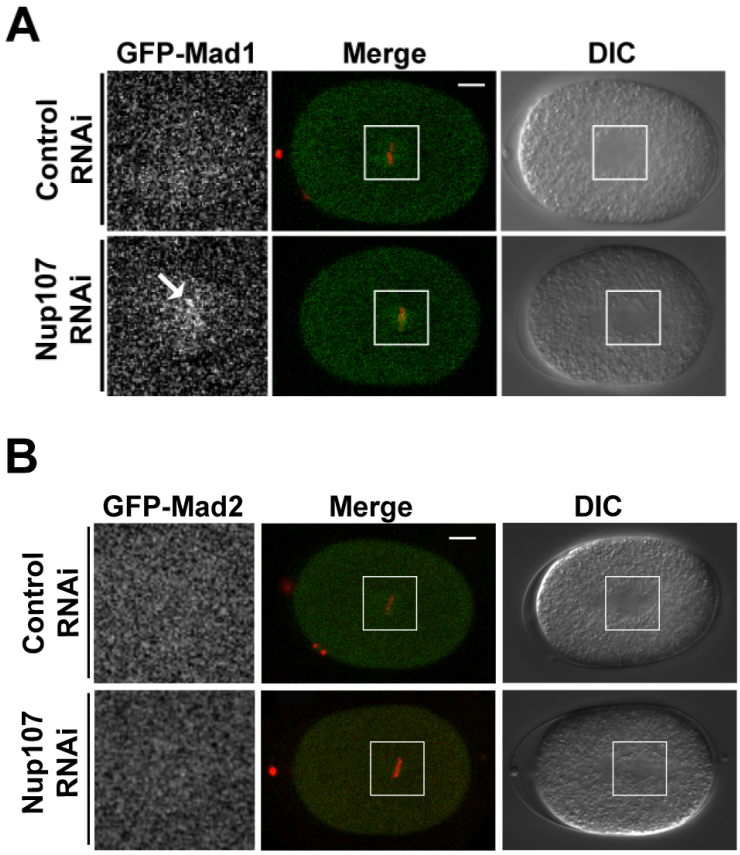

Figure 31. Mad1 and Mad2 localization in Nup107 depleted embryos. Still images from time-lapse confocal microscopy of embryos expressing GFP-Mad1 (A) or GFP-Mad2 (B) and mCherry-HisH2B. (A) Depletion of Nup107 induces recruitment of GFP-Mad1 to metaphase chromosomes (arrow) (*n*=10). (B) Depletion of Nup107 does not trigger detectable accumulation of GFP-Mad2 on mitotic chromatin (n=12). Boxed regions in the merge panels are shown at higher magnification to the left. Scale bars, 10 µm.

We next induced a situation of massive mono- and syntelic MT-kinetochore attachment by preventing centrosome duplication through RNAi-mediate loss of ZYG-1 protein (Essex et al., 2009; Yamamoto et al., 2008). As previously shown, SAC proteins strongly accumulated on mitotic chromatin of two-cell stage *zyg-1(RNAi)* embryos (**Fig. 32**). Since depletion of Nup107 did not interfere with localization of GFP-Mad1 or GFP-Mad2 in *zyg-1(RNAi)* embryos (**Fig. 32A; B**), we concluded that Nup107 is dispensable for SAC activation, at least upon strong stimuli, such as monopolar spindle formation. Similarly, the Nup107 complex is not required for triggering the SAC in cell-free *Xenopus* extracts (Orjalo et al., 2006).

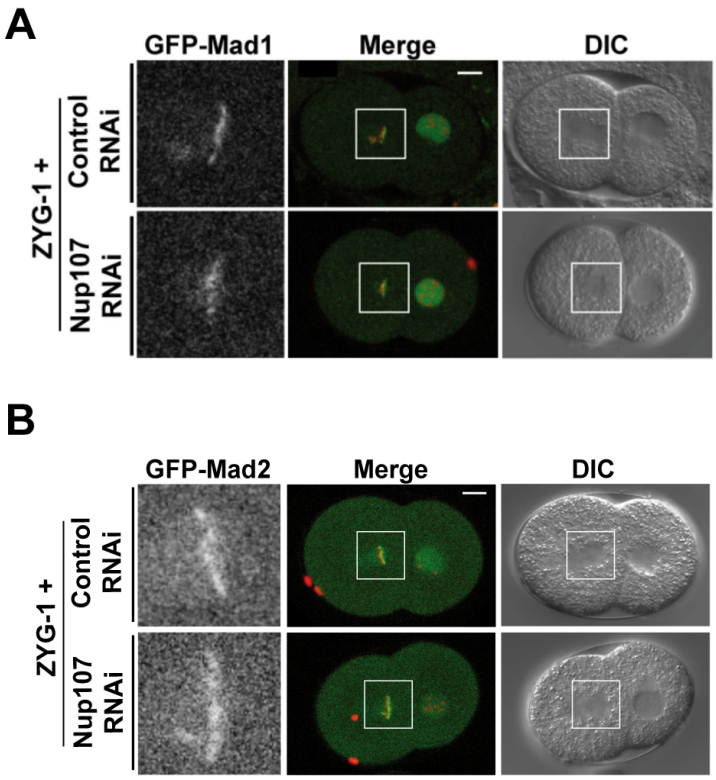

Figure 32. Recruitment of Mad1 and Mad2 when the SAC is activated. GFP-Mad1 (A) and GFP-Mad2 (B) accumulation on chromosomes attached to monopolar spindles in *zyg-1(RNAi)* embryos is unaffected by depletion of Nup107 (*n*=3). Boxed regions in the merged panels are shown at higher magnification to the left. Scale bars, 10 µm.

1.8 Mad1 localizes to NPCs through a direct interaction with Nup107:

Initially described in budding yeast, Mad1 and to some degree also Mad2 accumulate at NPCs in several cell types during interphase (Campbell et al., 2001; Iouk et al., 2002). In interphase cells of *C. elegans* embryos, GFP-Mad1 also shows enhanced signal at the NE in addition to diffuse nucleoplasmic staining (**Fig. 33A top**). Strikingly, the NE accumulation of GFP-Mad1 was absent in Nup107-depleted embryos, whereas the intranuclear signal was normal (**Fig. 33A bottom**). Immunofluorescence analysis of endogenous Mad1 in control and *tm3039* embryos confirmed these observations (**Fig. 33B**), demonstrating that Nup107 is strictly required to localize Mad1 to the NE.

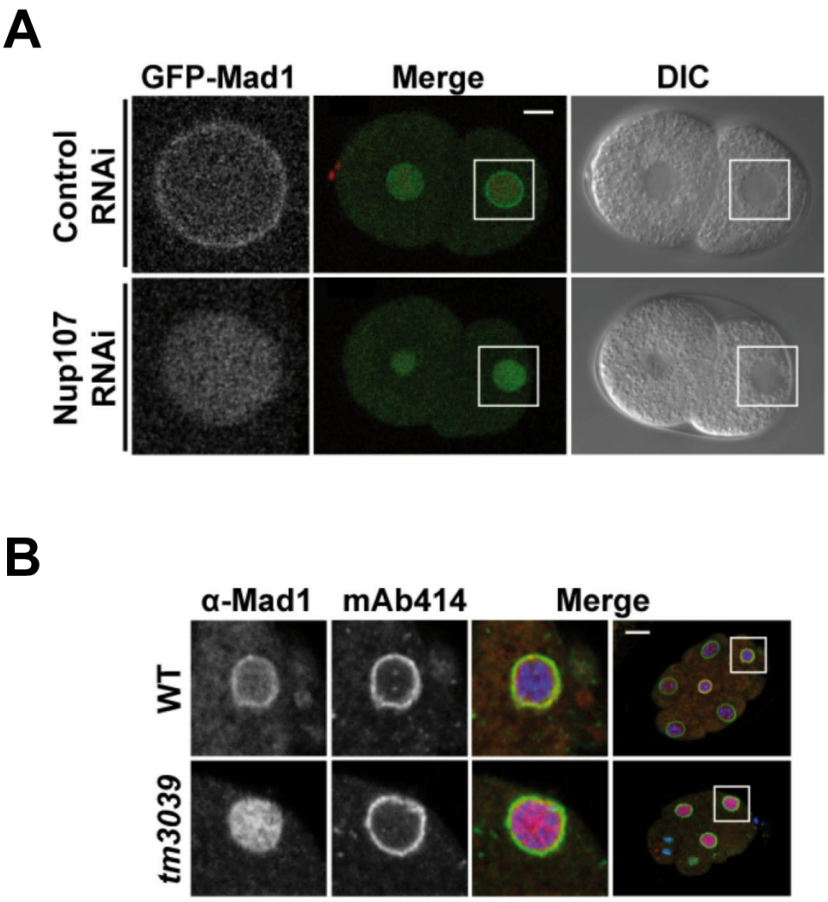

Figure 33. NPC localization of spindle assembly checkpoint protein Mad1 depends on Nup107. (A) Still images from time-lapse confocal microscopy of embryos expressing GFP-Mad1 (green) and mCherry-HisH2B (red). Localization of GFP-Mad1 to NPCs in interphase is abolished in the absence of Nup107 (*n*=14). (B) Wild type and *tm3039* embryos were fixed and stained with α-Mad1 antiserum (red) and mAb414 (green). Chromatin was detected using Hoechst 33258 (blue). Boxed regions in the merged panels are shown at higher magnification to the left. Scale bars, 10 μm.

To investigate if Mad1 accumulates at NPCs via a physical interaction with Nup107 we expressed the two proteins in budding yeast, fused to either the Gal4 activation domain or the Gal4 DNA binding domain. Only when Mad1 and Nup107 fusion proteins were expressed simultaneously did the yeast grow on media lacking the selectable markers histidine and adenine (**Fig. 34 top**), suggesting that the two proteins interact directly. Because budding yeast Mad1p and Nup53p have been demonstrated to interact physically (Scott et al., 2005) we also tested whether this was the case for the *C. elegans* homologs Mad1/MDF-1 and Nup35/NPP-19. However, we did not observe any interaction in the yeast-two-hybrid assay (**Fig. 34 bottom**), which indicates that Mad1 interacts with the NPC in a species-specific manner.

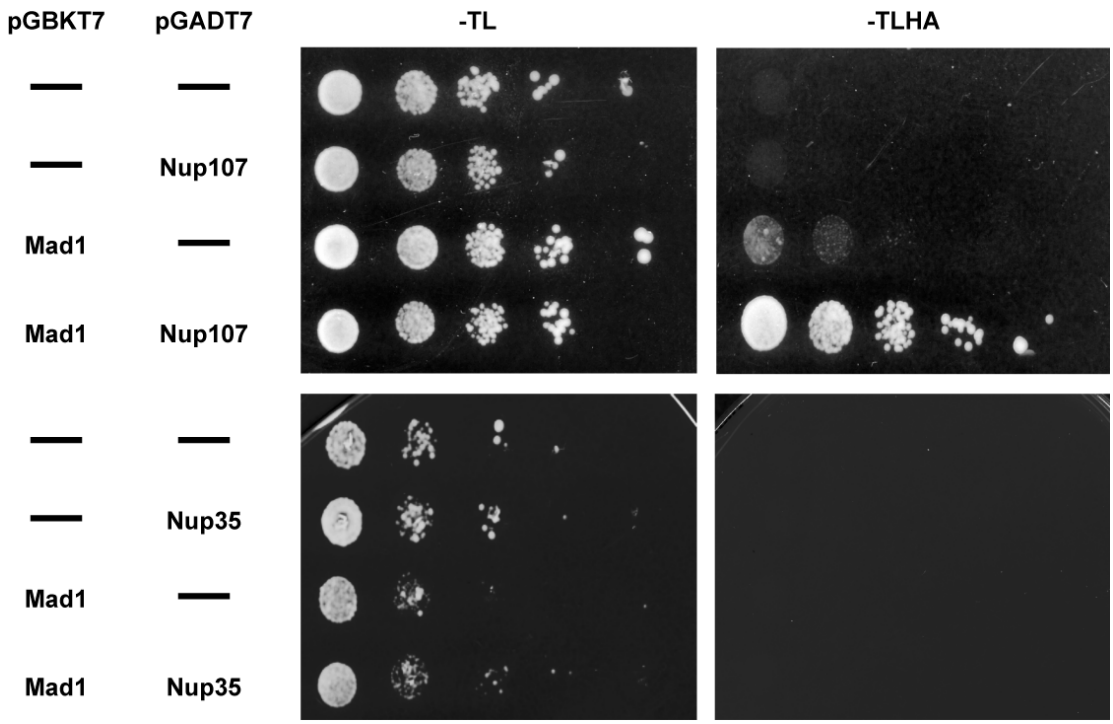

Figure 34. Nup107 physically interacts with Mad1 in yeast 2-hybrid assays. Full-length cDNAs of Nup107 and Mad1 were cloned into prey and bait vectors, respectively, and used to transform yeast cells. Growth on selective (–TLHA) medium was only supported when the two genes were present together. No interaction was observed between Nup35 and Mad1.

1.9 Nup107-deficient embryos are hypersensitive to Mad1 perturbation:

Our observation that Nup107 is partially responsible for Mad1 localization prompted us to investigate if they interact genetically. Indeed, we found that while depletion of the proteins singly caused only 3-5% embryonic lethality, RNAi against Mad1 in *tm3039* animals led to 85±7% embryonic lethality (**Fig. 35**; $p<0.001$). Mad2/MDF-2, which forms a complex with Mad1 showed an intermediate degree of synthetic embryonic lethality with Nup107 (32±6%; $p<0.001$), whereas depletion of SAC proteins BubR1/SAN-1 or Bub3/BUB-3 did not enhance lethality in *tm3039* embryos ($p>0.73$). Thus, Nup107 displayed a synthetic lethality phenotype specifically with the Mad1/Mad2 complex of the SAC.

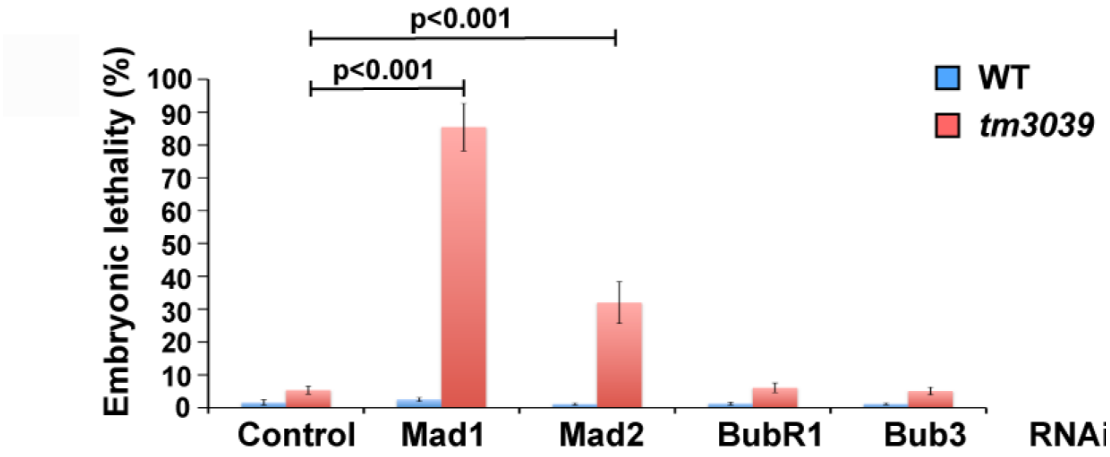

Figure 35. Nup107 and Mad1 interact genetically. Embryonic lethality was measured following RNAi against different members of the SAC in wild type and *tm3039* animals (*n*>600 embryos in all experiments).

The implication of Nup107 in kinetochore assembly and Aurora B localization suggested that chromatin segregation might be impaired in the absence of Nup107. Moreover, the synthetic interaction of Nup107 with Mad1 and Mad2 could reflect that these SAC proteins are required to prevent chromatin segregation defects in *tm3039* embryos by inducing an anaphase delay. Indeed, immunofluorescence analysis of *tm3039* mutants revealed chromatin bridges in 10% of the embryos ($p<0.05$), a phenotype never observed in control embryos (**Fig. 36**). RNAi against Mad1 caused 5% chromatin bridges in control embryos, whereas a dramatic increase to 49% ($p<0.001$) was observed upon depletion of Mad1 from *tm3039* embryos. Thus, Mad1 is required to prevent chromosome missegregation in the absence of Nup107.

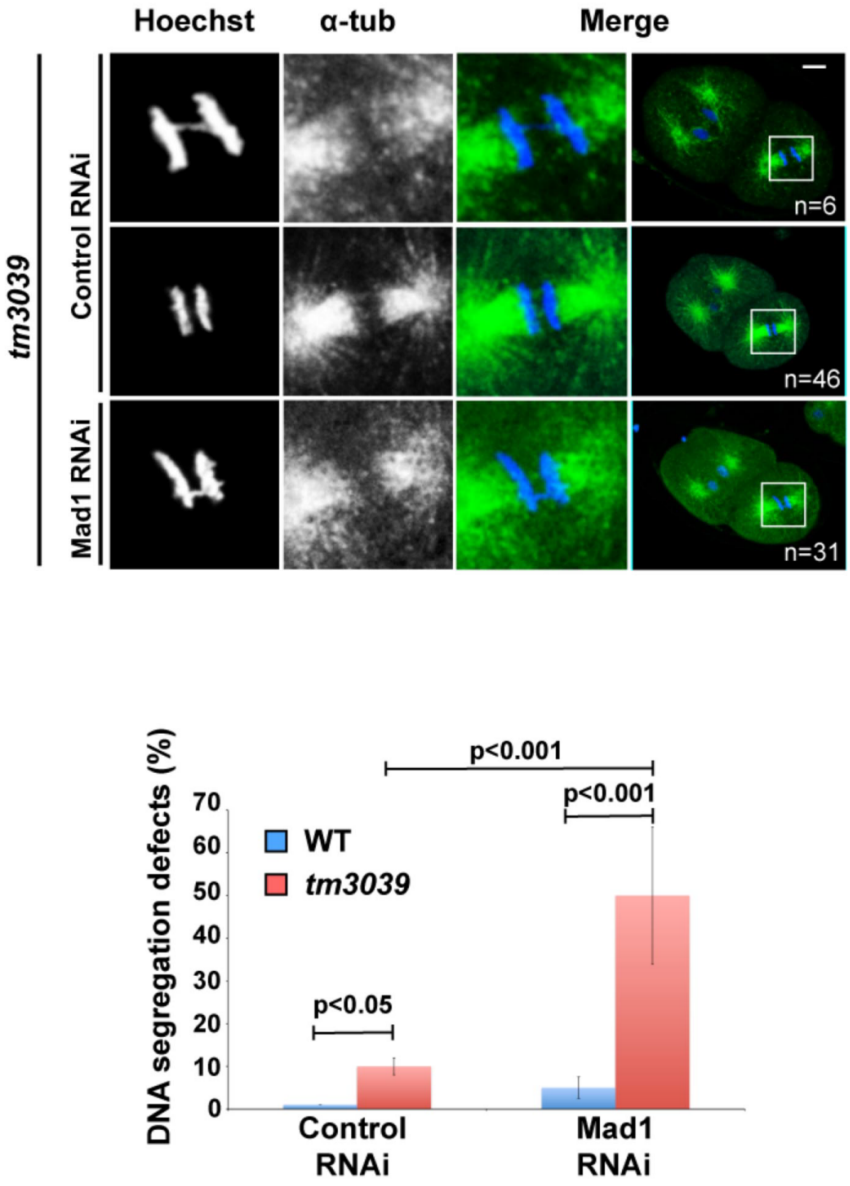

Figure 36. *tm3039* embryos show problems of DNA segregation when Mad1 is depleted. Wild type and *tm3039* animals treated with control or Mad1 RNAi were fixed and stained with α-alpha-tubulin (green). Chromatin was detected using Hoechst 33258 (blue). Boxed regions in the merged panels are shown at higher magnification to the left. Percentages of embryos presenting DNA segregation defects are indicated in the graph, demonstrating a synthetic phenotype in embryos simultaneously depleted for Nup107 and Mad1.

It was recently found that loss of cyclin B3 induces a strong SAC-dependent mitotic arrest (Deyter et al., 2010), which we hypothesized might also require Nup107. Since chromatin segregation is virtually abolished upon depletion of cyclin B3 (Deyter et al., 2010) we used other events to monitor mitotic progression: we defined 'anaphase' based on centrosome behavior and cleavage

furrow ingression (~80 sec after anaphase onset in control embryos). Compared to control embryos, time from pronuclear meeting (prophase) to anaphase was increased by 115% in embryos depleted for cyclin B3 (**Fig. 37**; p<0.001). Timing was unaffected in Nup107 mutants incubated on control RNAi plates (p=0.10), but the cyclin B3-induced mitotic delay was partially alleviated by removal of Nup107 (17%; p=0.01).

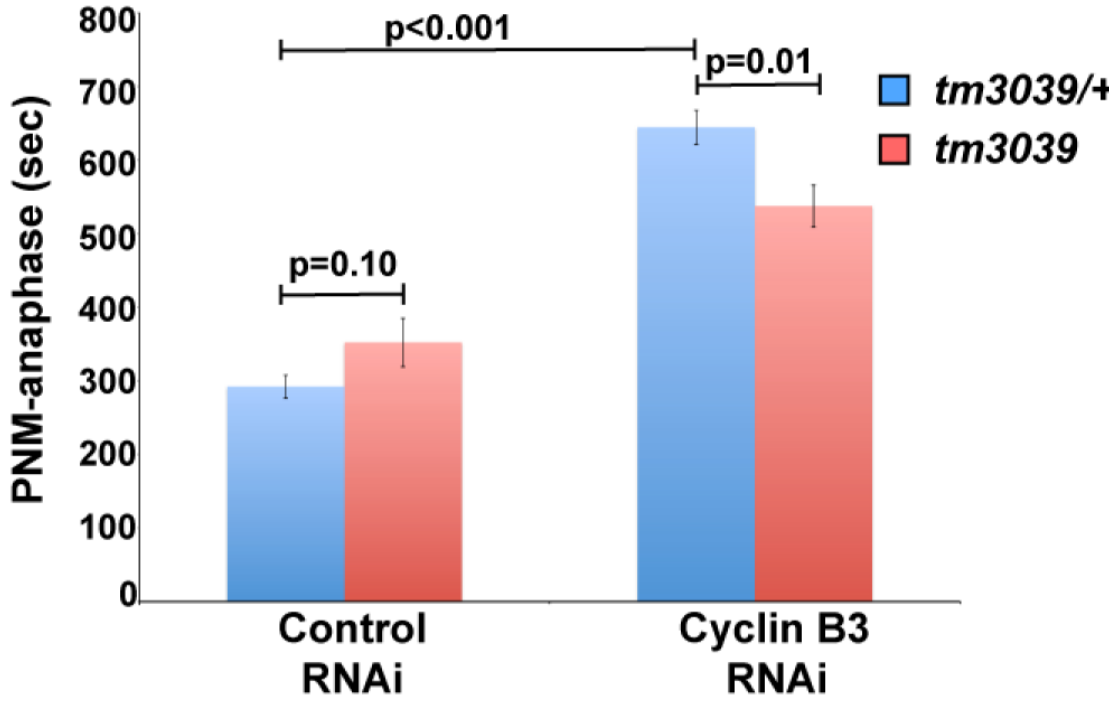

Figure 37. Mitotic delay induced by depletion of cyclin B3 is partially alleviated by depletion of Nup107. Time from pronuclear meeting (PNM) to anaphase was measured following incubation on control or cyclin B3 RNAi plates for 30 h (n≥5 for all treatments). Error bars indicate the standard error of the mean.

As an alternative way to test if Nup107 is required for proper SAC function we examined response to oxygen deprivation. *C. elegans* embryos have a remarkable capacity to withstand anoxic stress. Under conditions of low oxygen embryos arrest development and enter a stage known as suspended animation. This behavior is SAC-dependent, implying a metaphase arrest although cells may also be blocked in prophase (Hajeri et al., 2010; Nystul et al., 2003). To investigate if embryos lacking Nup107 are fully competent to enter suspended animation we placed control and *tm3039* embryos under hypoxic conditions for 21h before

returning them to normal atmosphere. Strikingly, while the hypoxia stress only modestly decreased the frequency of control embryos developing into fertile adults (7.5% decrease, p<0.001), only 1.1% of *tm3039* embryos developed into fertile adults following the hypoxia treatment (87% decrease, p<0.001; **Fig. 38**). This suggests that loss of Nup107 sensitizes cells so they cannot withstand stress which otherwise would have been tolerated via a SAC-induced mitotic arrest. From these results we concluded that Nup107 is required for efficient cell cycle arrest under stress induced by either perturbation of cell cycle regulators or hypoxia.

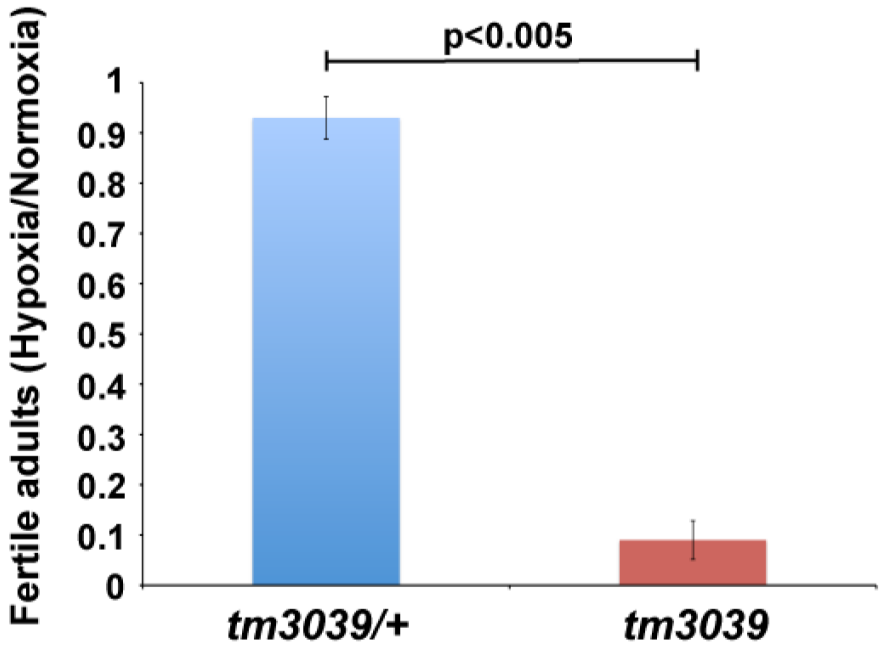

Figure 38. *tm3039* and *tm3039/+* under hypoxia conditions. Embryos from *tm3039/+* and *tm3039* animals were exposed to hypoxia for 21h. After recovery under normoxic conditions development into fertile adults was determined, revealing a severe effect in *tm3039* mutants (*n*>600 embryos in all experiments). Error bars indicate the standard error of the mean.

1.10 <u>Nup107 and the aging phenomena</u>: Nucleoporins that build the scaffold NPC, such as the Nup107 complex, are very stably associated with the NPC (Rabut et al., 2004) and are proposed to exchange only once per cell cycle, when the NE breaks down (D'Angelo et al., 2009). According to this theory, cells that have stopped dividing would thus have the same NPCs throughout their

entire life span, which means that NPCs would be subject to age-dependent damage affecting their function and nuclear integrity.

In support of this idea, there have been different studies that relate alterations of the nuclear structure with the aging phenomenon (Haithcock et al., 2005; Herndon et al., 2002). Haithcock et al. showed that the nuclear structure suffers age-dependent alterations, such as loss of perinuclear heterochromatin and nuclear shape. In particular, they proposed that the nuclear lamina is an excellent marker for the aging process, since it changes morphologically as the cell ages. They showed that mutants for lamin in *C. elegans* (*lmn-1(tm1502)*) live significantly shorter than the wild type. Conversely, long-lived mutants affected in the insulin signaling pathway maintained smooth and uniform nuclear appearance longer than wild type animals. Similarly to the reported phenotype for *lmn-1(tm1502)* mutants, we also observed that *npp-5 (tm3039)* mutants live considerably shorter than wild type nematodes (**Fig. 39**).

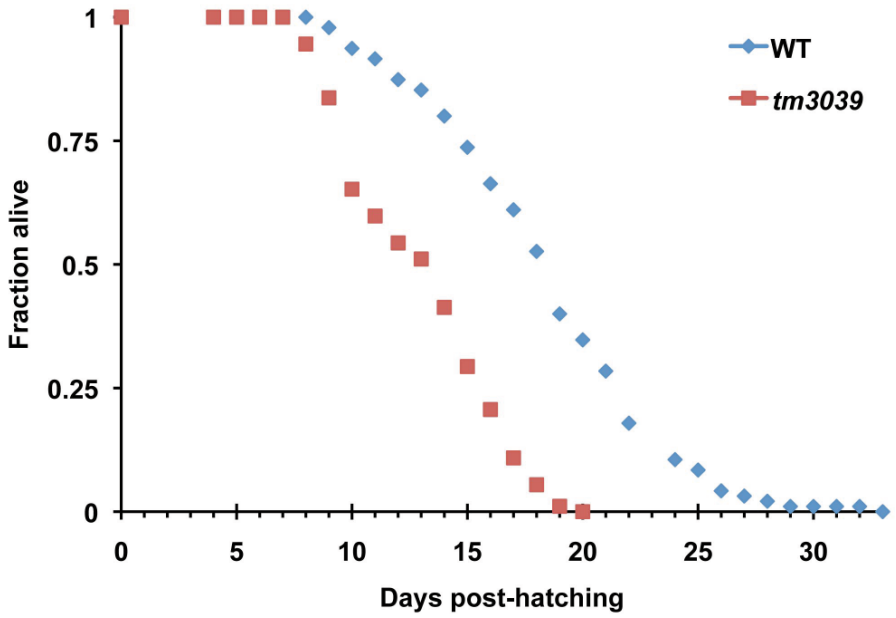

Figure 39. Life span of *tm3039* is shorter than WT's. *tm3039* and WT nematodes were separated from their progeny and their life span was monitored. The life span of *tm3039* mutants is 28% shorter than WT's.

Following this observation, we were interested in exploring if Nup107 had any implication in the aging process. Therefore we monitored the behavior of LMN-1-GFP at nuclei of hypodermal cells in *tm3039* mutants compared to the wild

type over time. Based on the nuclear morphology and the GFP signal distribution, we characterize the behavior of LMN-1-GFP over time into four different classes (**Fig. 40**).

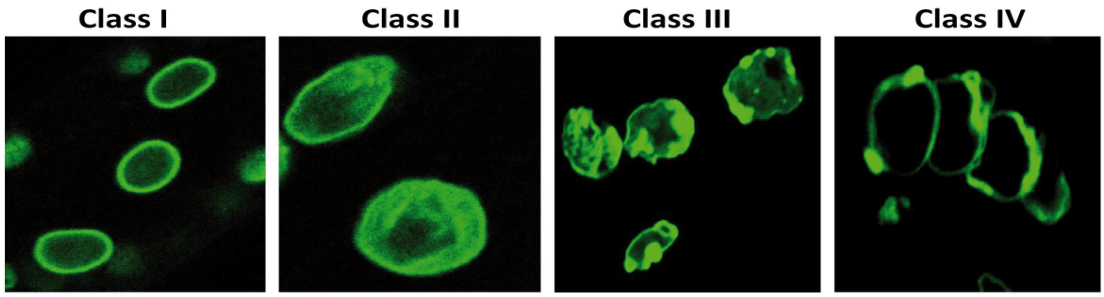

Figure 40. Morphology of the nucleus over time can be categorized into 4 distinct classes. Class I: Nucleus present a regular shape; Class II: LMN-1-GFP shows enhanced intranuclear signal; Class III: LMN-1-GFP aggregates in strong foci and the nucleus looses its regular shape; Class IV: Nuclei start to aggregate.

We captured images of the head, tail and central part of *tm3039* and wild type nematodes at the confocal microscope every two days and classified the nuclei of hypodermal cells. After 5.5 days 54% of nuclei in wild type animals belonged to classes I and II (t=0 was considered ~L1 stage), whereas 91% of nuclei in tm3039 mutants had accumulated changes typical of classes III and IV (**Fig. 41**). Thus, nuclei of *tm3039* mutants seem to age faster than the wild type and class IV nuclei are exclusively found in the older *tm3039* nematodes. The hypodermis of *C. elegans* consists of several syncytial cells of which the hyp7 containing 139 nuclei covers the majority of the body (WormAtlas, Altun, Z.F., Herndon, L.A., Crocker, C., Lints, R. and Hall, D.H. (ed.s) 2002-2010 http://www.wormatlas.org). Our observations suggest that Nup107 could be an essential protein for the proper positioning of the nuclei of hypodermal cells within the syncytium in older animals.

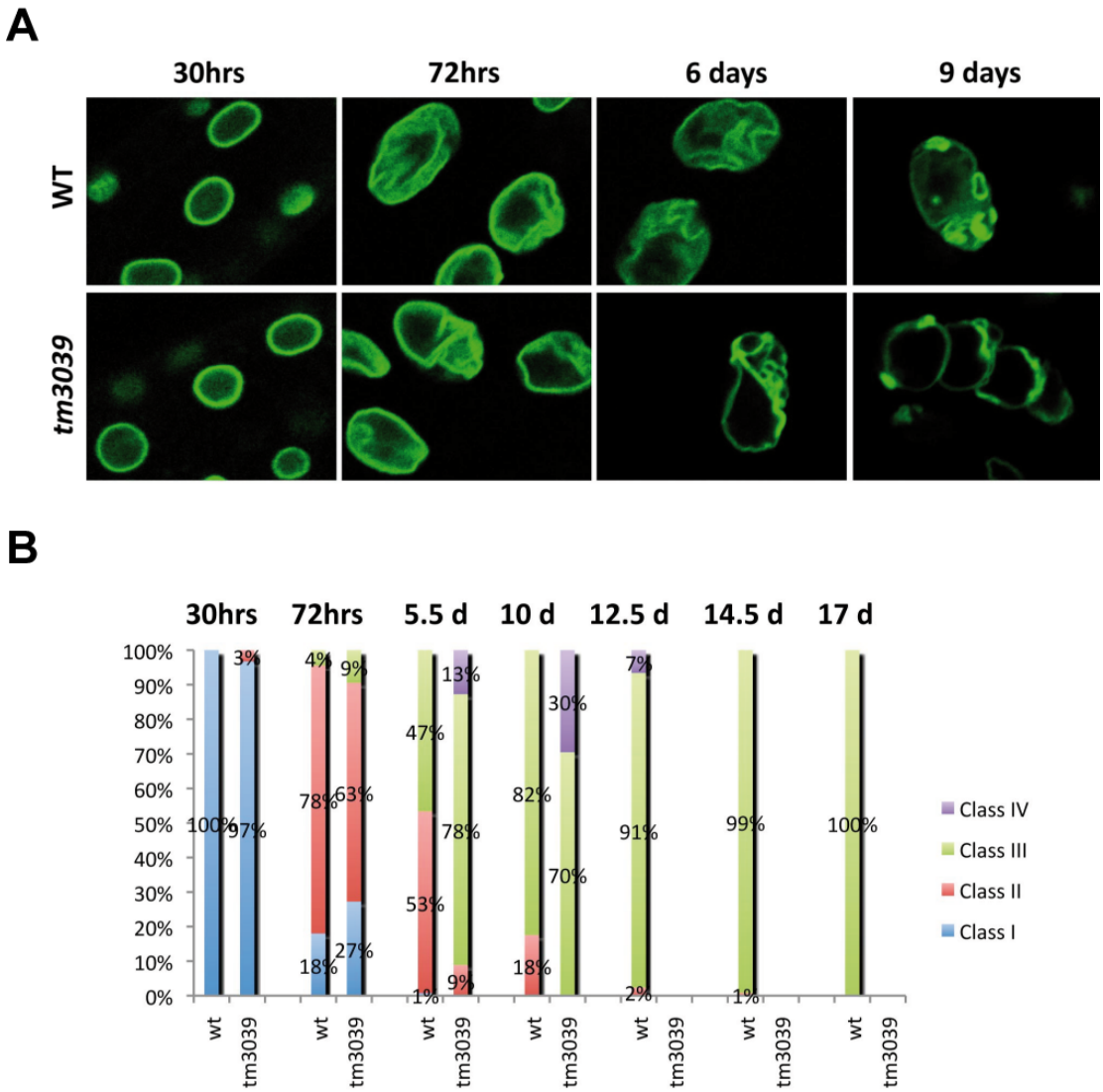

Figure 41. Nuclear morphology over time in *tm3039* and wild type nematodes. (A) Confocal images of the nuclei of hypodermal cells over time using as a marker LMN-1-GFP. Note that the nuclei morphology after 6 days in *tm3039* mutants resembles the nuclei morphology of WT after 9 days. (B) Graphic representation of the morphology of the nuclei over time of the *tm3039* versus wild type nematodes. Note that after 12.5 days all the *tm3039* mutants were dead, considering t=0 as the L1 stage.

2. Early embryonic requirement for nucleoporin Nup35/NPP-19 in nuclear assembly

During this thesis we were also interested in understanding the role of another nucleoporin that belongs to the NPC called Nup35. As mentioned in the introduction, postmitotic NPC biogenesis involves four essential steps. Others and we were able to place the Nup107 complex at the second step of NPC biogenesis, just after MEL-28 is recruited to chromatin, to form what is known as the "prepore" (Franz et al., 2007; Galy et al., 2006; Gillespie et al., 2007; Rasala et al., 2006).

On the other hand, Nup35 and other soluble nucleoporins have been shown to be involved at the last step of postmitotic NPC assembly (Franz et al., 2005; Hawryluk-Gara et al., 2008; Rodenas et al., 2009). Below we show the results that confirmed that indeed Nup35 plays a critical role at the fourth and last step of postmitotic NPC assembly (Rodenas et al., 2009).

2.1 Characterization of Nup35/NPP-19 mutant allele *tm2886*:

To investigate the function of Nup35/NPP-19 in *C. elegans* we combined RNAi experiments with other genetic approaches. Initially, we characterized a novel mutant allele, *tm2886* (kindly provided by Dr. Shohei Mitani). Reverse transcriptase PCR and Western blot analyses showed that embryos from homozygous *npp-19(tm2886)* hermaphrodites (hereafter termed *tm2886* embryos) express Nup35 lacking amino acid residues (aa) 217–286 (**Figs. 42A**; **B**). Interestingly, the amount of mutant Nup35 protein present in *tm2886* embryos is reduced to approximately 20–25% of wild type levels suggesting that the mutant mRNA and/or the truncated protein is unstable (**Fig. 42B**). *tm2886* animals can be propagated under standard conditions but show 43–56% embryonic lethality at 15–20 °C (**Table 4**). At 25 °C the embryonic lethality increases significantly to 86%, which is similar to the lethality observed when expression of Nup35 is knocked down by RNAi (96%; **Table 4**, **Fig. 42D**;(Galy et al., 2003)). Western blot analysis of *tm2886* embryos after incubation for 10 h at either 20 °C or 25 °C revealed that the amount of mutant Nup35 protein is temperature- independent (**Fig. 42C**), ruling out that increased lethality observed at 25 °C is caused by a further reduction in Nup35 levels. Instead, we

propose that embryos require additional Nup35 activity at 25 °C as compared to 20 °C. Alternatively, mutant Nup35 protein may not properly fold at elevated temperatures. Expression of Nup35 fused to GFP restored embryonic viability of *tm2886* embryos at 20 °C and partially at 25 °C (**Table 4**). These data demonstrate that the phenotypes observed in *tm2886* are due to the deletion in the *npp-19* gene and indicate that GFP-Nup35 can functionally replace endogenous Nup35. Finally, we note that the *tm2886* embryos that hatch develop in most cases into fertile adults (87%, **Table 4**), suggesting that Nup35 function is most critically required during embryogenesis. The remaining animals die during larval stages (13%, data not shown).

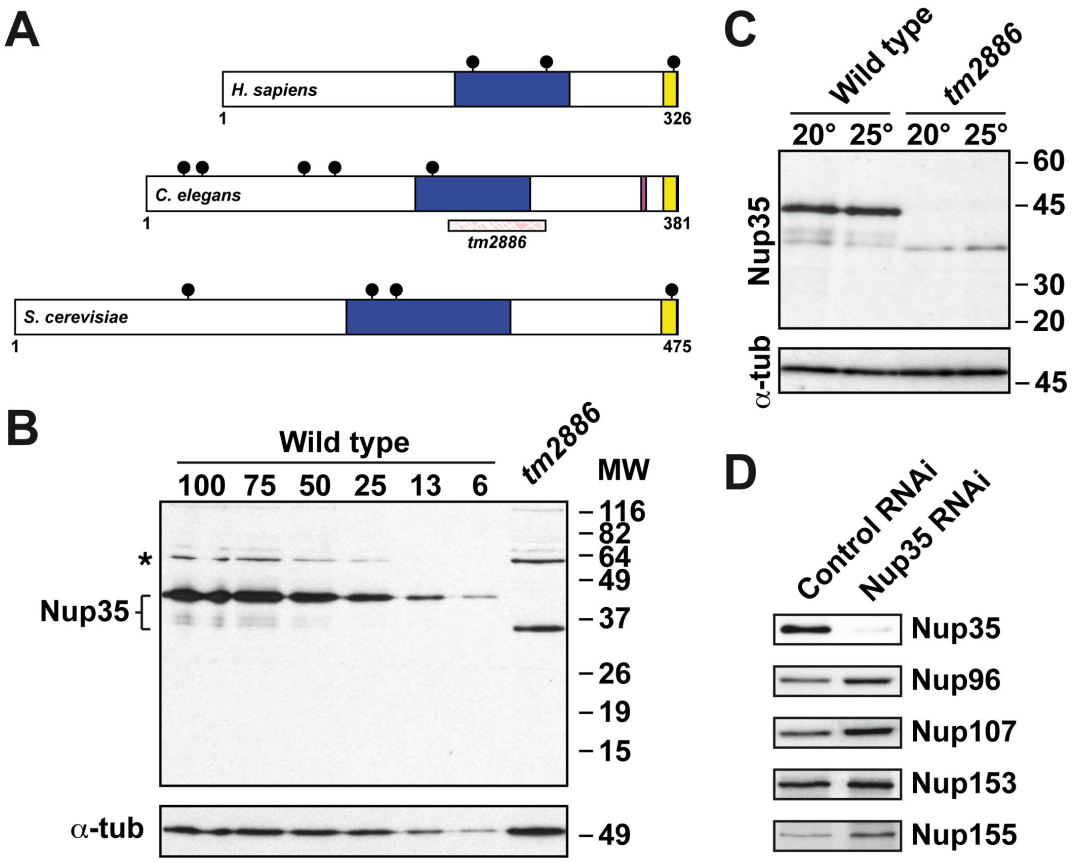

Figure 42. NPP-19 levels are reduced in *tm2886* and *npp-19(RNAi)* embryos. (A) Schematic representation of human Nup35 (AAM76704), *C. elegans* NPP-19 (Q09601) and budding yeast Nup53p (Q03790). Blue boxes indicate a highly conserved MPPN (RRM-like) domain (Handa et al., 2006); yellow boxes indicate a putative membrane-associated amphipathic alpha helix (Marelli et al., 2001); pins mark the position of phenylalanine-glycine (FG) dipeptides. A magenta box in *C. elegans* NPP-19 represents three aa (ILQ) present in the NPP-19b splice isoforms, which are absent in the NPP-19a isoform. A red scratchboard bar indicates the region deleted in *tm2886*. (B) Western blot analysis of approximately 1200 *tm2886* embryos compared with a titration of wild type embryos (6-100%; ~70-1200 embryos). Upper and lower panels show probing with α-Nup35 antiserum and α-alpha-tubulin antibodies, respectively. In wild type embryos, Nup35 appeared with a molecular weight of ~46 kDa, while in mutant embryos a specific Nup35 band was observed at ~36 kDa, consistent with the molecular lesion in the *tm2886* allele. A non-specific cross-reacting band of ~61 kDa is indicated (asterisk). (C) Wild type and *tm2886* embryos developing at 20°C or 25°C were analyzed with affinity purified α-Nup35 (top) or α-alpha-tubulin (bottom) antibodies. (D) Control and Nup35 RNAi embryos analyzed by Western blotting using antibodies directed against Nup35/NPP-19, Nup96/NPP-10-C, Nup107/NPP-5, Nup153/NPP-7 or Nup155/NPP-8.

Strain	*n*[a]	Embryonic lethality[b] (average ±S.D.[d])	Hatched embryos → fertile adult[c] (average ±S.D.)
N2 wild type, 15°C	555	0.6±0.5%	N.D.[e]
N2 wild type, 20°C	1206	0.6±1.0%	99.3±1.4%
N2 wild type, 25°C	748	2.2±2.4%	N.D.
npp-19(tm2886), 15°C	419	55.6±18.0%*,†	N.D.
npp-19(tm2886), 20°C	1133	42.5±15.7%*	86.8±7.2%*
npp-19(tm2886), 25°C	632	86.2±12.1%*,†	N.D.
npp-19(tm2886); gfp::Nup35, 20°C	243	4.7±6.2%*,†	N.D.
npp-19(tm2886); gfp::Nup35, 25°C	138	21.6±7.1%*,‡	N.D.
N2 control RNAi, 20°C	431	0.4±0.4%	N.D.
N2 Nup35 RNAi, 20°C	662	96.0±5.6%*	N.D.

Table 4. Development of *tm2886* and Nup35 RNAi embryos. Young gravid hermaphrodites were incubated for 1 h on NGM plates at indicated temperatures. The number of embryos analyzed[a], percentage of embryonic lethality[b] and percentage of hatched embryos that developed into fertile adults[c] was determined after 0h, 24h and 96h, respectively. [d] Standard deviation. [e] Not determined. Significant differences by Chi-square test: * different from the wild type or control RNAi at same temperature ($p<0.001$); † different from *npp-19(tm2886)* at 20°C ($p<0.001$); ‡ different from *npp-19(tm2886)* at 25°C ($p<0.001$).

2.2 Reduced Nup35 activity causes chromosome missegregation and nuclear morphology defects: To examine if *tm2886* and Nup35 RNAi embryonic lethality can be attributed to abnormal NE structure, embryos were analyzed by immunofluorescence microscopy. Monoclonal antibody mAb414 that recognizes *C. elegans* nups Nup96/NPP-10-C, Nup98/NPP-10-N, and Nup358/NPP-9 was used together with specific antibodies against MEL-28, a nucleoporin discovered recently based on its role in NE assembly (Fernandez

and Piano, 2006; Galy et al., 2006). More than 95% of nuclei in *tm2886*embryos (n>100) obtained from nematodes grown at 20 °C showed normal mAb414 and α-MEL-28 staining (**Fig. 43A, top; Fig. 44**). In contrast, *tm2886* and Nup35 RNAi embryos developing at 25 °C and 20 °C, respectively, displayed severe defects in nuclear morphology and mAb414 staining (**Figs. 43A, bottom right; B, right**). As expected from the Western blot analysis above, Nup35 localization to the nuclear periphery was strongly reduced in *tm2886* embryos as well as in Nup35 embryos (**Fig. 43**). However, the remaining Nup35 detected at the nuclear rim in *tm2886* embryos indicates that Nup35 aa 217–286 are dispensable for NE targeting. Strikingly, during cytokinesis we observed chromatin associated with the cleavage furrow in more than half of Nup35 RNAi and *tm2886* embryos at restrictive temperature (n>100), suggesting that wild type Nup35 activity is required for correct chromosome segregation during mitosis (**Figs. 43A, bottom right; B, right**).

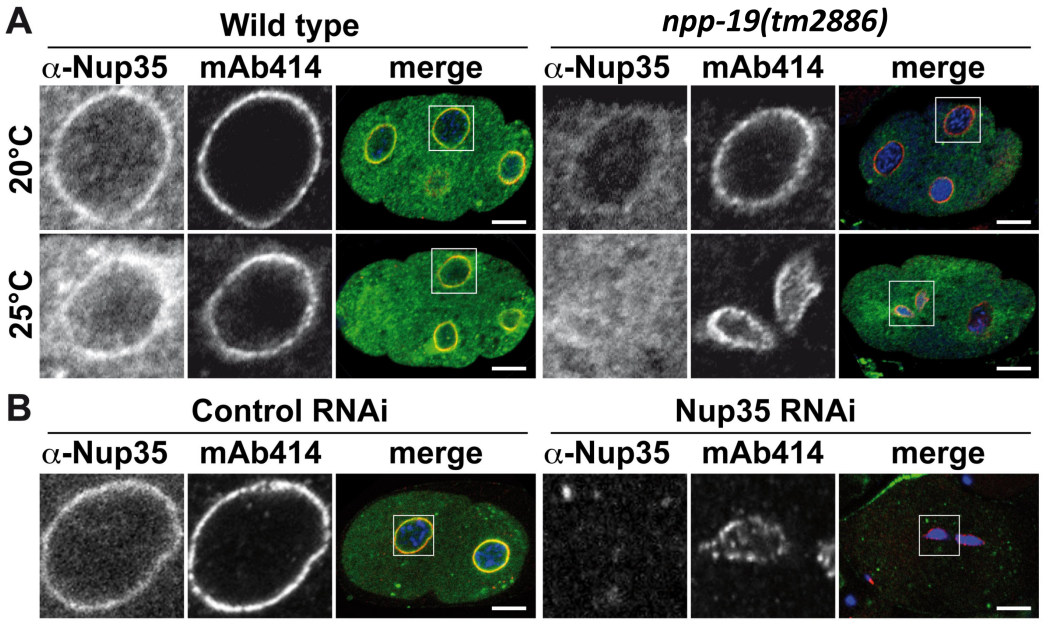

Figure 43. Perturbation of NPP-19 activity results in nuclear morphology and chromatin segregation defects. Control, *tm2886* (A) and Nup35 RNAi (B) embryos were fixed and stained using α-Nup35 antiserum (green) and monoclonal antibody mAb414 (red). Chromatin was detected using Hoechst 33258 (blue). Boxed regions in the merged panels are shown at higher magnification to the left, illustrating Nup35 and mAb414 staining individually. Scale bars, 10 µm.

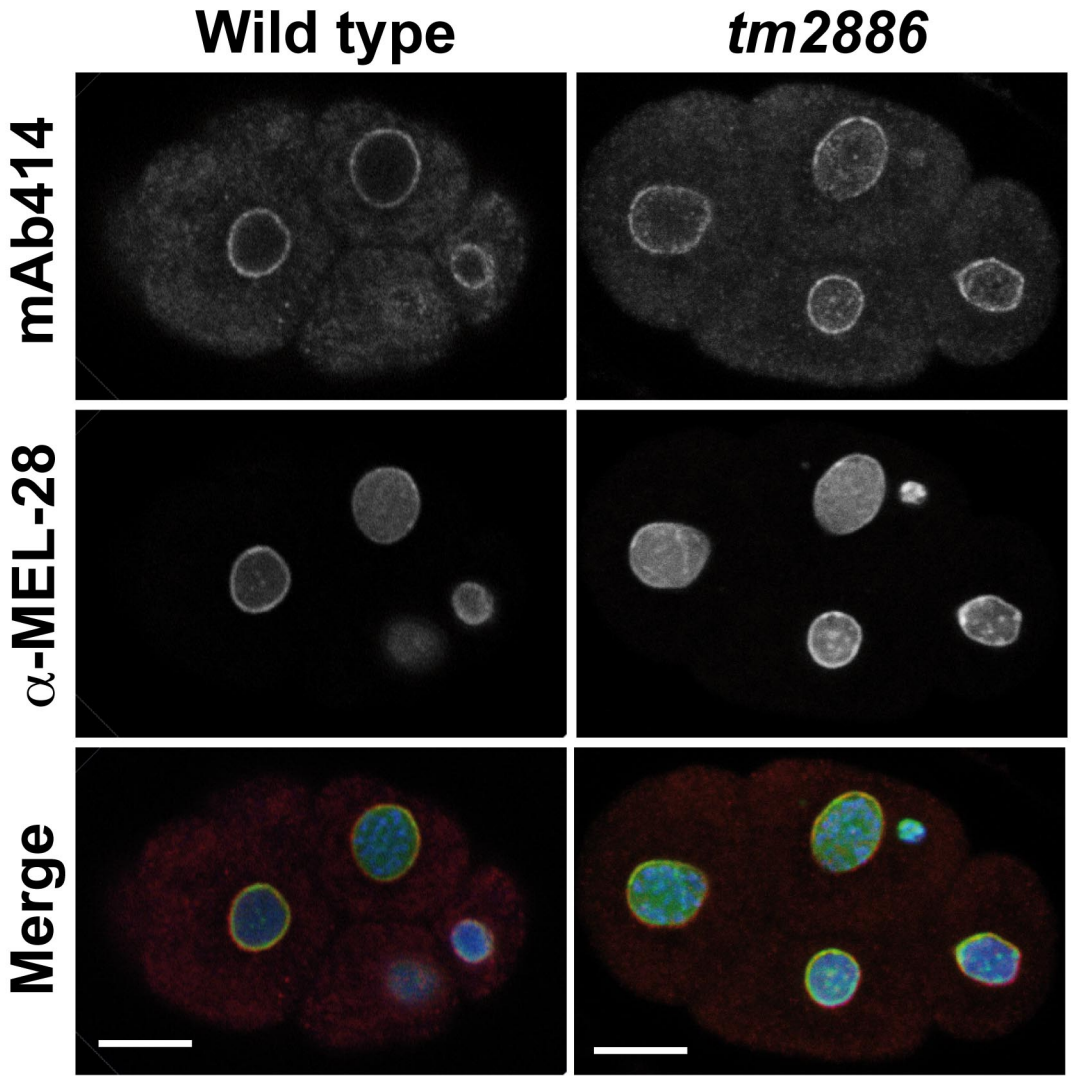

Figure 44. NPCs are assembled normally in *tm2886* mutants at 20°C. Embryos from wild type and *tm2886* homozygous mutant animals grown at 20°C were fixed and stained using α-MEL-28 antiserum (green) and monoclonal antibody mAb414 (red). Chromatin was stained using Hoechst 33258 (blue). Scale bars, 10 µm.

2.3 <u>Live imaging of *tm2886* and Nup35 RNAi embryos</u>: We next crossed *tm2886* with strains expressing fluorescent NE and chromatin markers to characterize in greater detail the defects in embryos with reduced Nup35 activity. For all strains (including RNAi experiments described below), at least five embryos were observed by confocal time-lapse microscopy and the most frequent phenotype (≥80%) is reported here. Initially, we focused on Nup107/NPP-5 as a marker for the Nup107–160 NPC subcomplex, which is essential for NPC formation (Franz et al., 2005; Harel et al., 2003b; Walther et al.,

2003a). In wild type embryos, GFP-Nup107 accumulated at the NE prior to mitosis and relocalized to kinetochores subsequent to NEBD (**Fig. 45A, left**; (Franz et al., 2005)). Completion of oocyte meiosis and polar body extrusion appeared normal in *tm2886* zygotes developing at 25 °C (data not shown). GFP-Nup107 still localized to the nuclear periphery but nuclear morphology and behavior was abnormal: Indicative of NE defects, pronuclei were considerably smaller than in wild type embryos and failed to juxtapose properly (**Fig. 45A, middle, −3:40**) (Askjaer et al., 2002). Frequently, the sperm-derived pronucleus was more severely affected than its oocyte-derived counterpart (arrow in **Fig. 45A, middle, – 3:40**; 66%, n = 32). Moreover, alignment of chromosomes (visualized by mCherry-histone H2B/HIS-58) on the metaphase plate was defective and chromosomes failed to be properly incorporated into the mitotic spindle of 1-cell stage *tm2886* embryos (arrow in **Fig. 45A, middle, 0:00**). Unsuccessful segregation of chromosomes caused chromatin to become trapped in the cytokinetic furrow and resulted in an abnormal nuclear appearance (**Fig. 45A, middle, 6:00**). Similarly, in Nup35 RNAi embryos, GFP-Nup107 continued to localize to chromatin, but recruitment to the nuclear periphery in interphase cells was irregular (**Fig. 45B, right**). Moreover, upon extended periods of RNAi treatment (~40 h) we frequently observed that the pronuclei failed to properly interact and centrosomes often detached from the sperm-derived pronucleus. Together, these defects likely prevented normal chromosome congression during mitosis (**Fig. 45B, right, – 4:40–0:00**).

To investigate if the failure to properly congress chromosomes on the metaphase plate may be a consequence of nuclear morphology defects, we took advantage of the temperature-sensitive properties of *tm2886*. Mutant embryos were incubated at 20 °C until approximately 2 min before NEBD, at which point embryos were shifted to 25 °C. Pronuclei in these embryos were only slightly smaller than in wild type embryos and were juxtaposed correctly (**Fig. 45A, right, −3:40**). Importantly, chromosome alignment on the metaphase plate as well as kinetochore and NE recruitment of GFP-Nup107 were normal (**Fig. 45A, right**). Nuclear growth after mitosis was however reduced. Thus, defects in chromosome alignment and segregation appear to correlate with defects in pronuclear morphology. Shifting *tm2886* embryos from 25 °C to 20 °C at the 2-

cell or 4-cell stage did not improve viability as compared to embryos kept constantly at 25 °C (**Table 5**). Conversely, up-shift of 2–4-cell stage *tm2886* embryos from 20 °C to 25 °C did not increase lethality as compared to embryos kept constantly at 20 °C (**Table 5**). This demonstrates that wild type Nup35 activity is most critically required in the 1-cell zygote and possibly also during oocyte maturation. Despite the dramatic defects at the 1- and 2-cell stages, cells of *tm2886* embryos continued to divide for approximately 100 min (4–5 division rounds) after which development slowed down and eventually arrested in mid-gastrulation after ~200 min (**Fig. 46**).

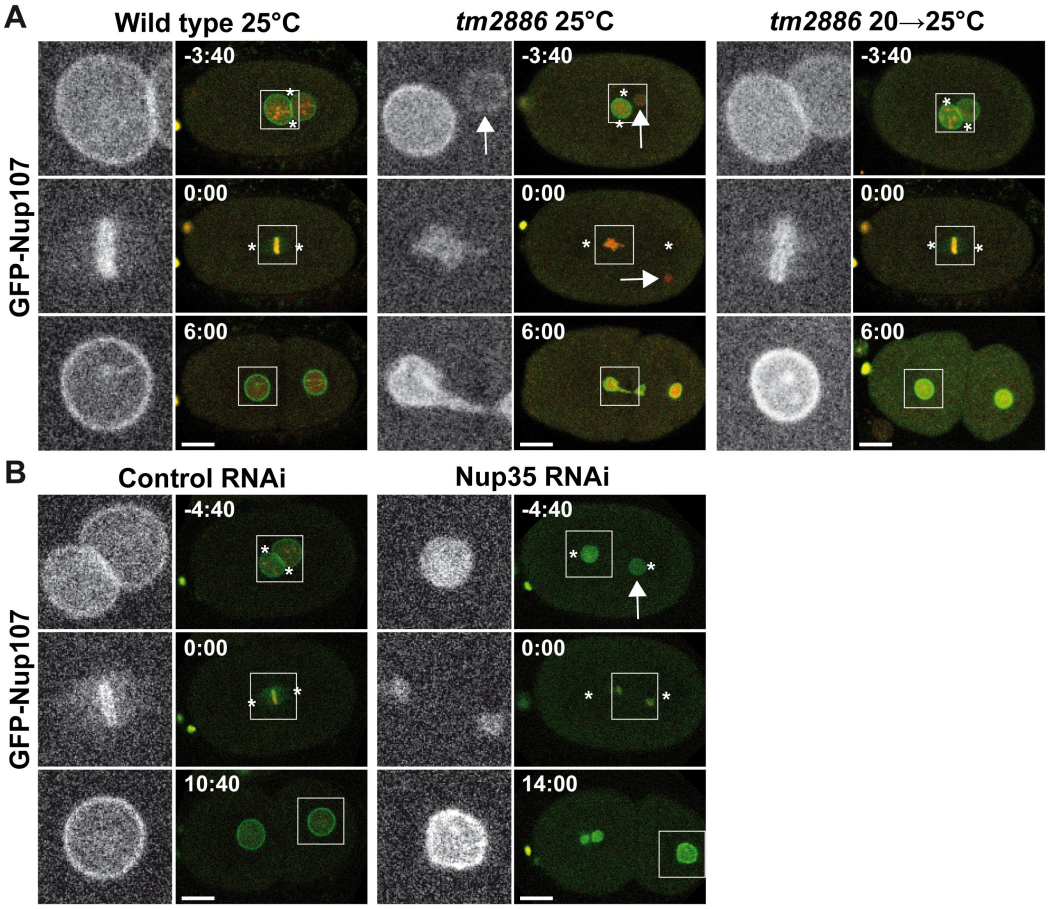

Figure 45. Live observation of *tm2886* and Nup35 RNAi embryos reveals early embryonic defects. Selected frames from time-lapse confocal microscopy of control, *tm2886* (A) and Nup35 RNAi (B) embryos expressing GFP-Nup107 (green) and mCherry-HIS-58 (red). Time (min:sec) relative to onset of the first zygotic anaphase is indicated. Boxed regions in merged panels are shown on the left, illustrating GFP-Nup107 localization at higher magnification. Arrows highlight sperm-derived pronuclei, and asterisks indicate centrosome localization (inferred from DIC images) in selected frames. Scale bars, 10 µm.

Temp pre-dissection[a]	Temp post-dissection[b]	Embryonic stage[c]	*n*	Embryonic lethality[d] (average ±S.D. [e])
20°C	20°C	>4-cell	382	44.1±18.8%
	25°C	2-4-cell	137	33.8±10.5%
25°C	20°C	2-4-cell	138	87.6±7.9%[*,†]
	25°C	>4-cell	445	90.0±11.0%[*,†]

Table 5. Temperature shift of *tm2886* reveals an early embryonic Nup35 requirement.
[a] Gravid *tm2886* hermaphrodites were incubated for 6 h at indicated temperature prior to dissection. Embryos were separated into two groups: 2-4-cell stage and >4-cell stage embryos[c] (1-cell stage embryos were discarded) that were incubated at either 20°C or 25°C[b]. [d] Embryonic lethality was determined after 24h. [e] Standard deviation. Significant differences by Chi-square test: [*] different from embryos incubated constantly at 20°C ($p<0.001$); [†] different from embryos shifted from 20°C to 25°C at 2-4-cell stage ($p<0.001$).

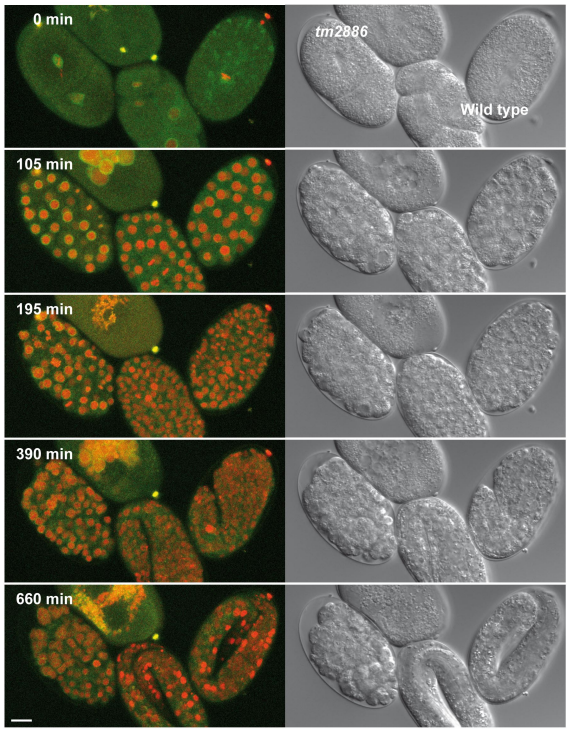

Figure 46. *tm2886* embryos arrest development during mid-gastrulation. Two wild type embryos (right) co-expressing GFP-LEM-2 (green) and mCherry-HIS-58 (red) and two *tm2886* embryos (left) co-expressing GFP-Nup107 (green) and mCherry-HIS-58 (red) were mounted together and imaged using confocal time-lapse microscopy at ~25°C. Selected maximum projections of 5 serial sections (in the z-axis) taken at 15 min intervals are shown with corresponding DIC images. Time relative to the start of recording is shown, which corresponds to the first embryonic cell division of the left-most *tm2886* embryo and the right-most control embryo. The upper *tm2886* embryo suffered osmotic damage during dissection and should be ignored. An arrow highlights abnormal chromatin distribution in the AB cell of the *tm2886* embryo, which terminates development after ~200 min. Scale bar, 10 µm.

2.4 <u>Lack of Nup35 affects asynchronous cell division</u>: Monitoring the second round of division in *tm2886* and Nup35 RNAi embryos revealed that Nup35 is required for proper cell cycle timing in both daughter cells of the P0 zygote. Measured from first cytokinesis, anaphase onset in the anterior AB cell was delayed 8% in *tm2886* embryos and 29% in Nup35 RNAi embryos (**Table 6**). For the posterior P1 cell, the effect was more pronounced with a delay of 42% in *tm2886* embryos and 63% in Nup35 RNAi embryos. AB and P1 have different sizes and fates and AB divides normally ~2.5 min before P1 (Bao et al., 2008; Deppe et al., 1978). However, this asynchrony was dramatically increased in both *tm2886* embryos (~7 min) and Nup35 RNAi embryos (~7.5 min) (**Figs. 47A, B; Table 6**). In 79% of *tm2886* and Nup35 RNAi embryos (n = 33), lagging chromosomes were detected during division of the AB cell whereas this phenotype was observed in only 10% of diving P1 cells (**Fig. 47A**). Thus, the longer cell cycle delay observed in P1 as compared with AB correlated inversely with defects in chromosome segregation.

The delay in cell cycle timing upon depletion of Nup35 suggested that a checkpoint(s) may be activated in the absence of this nucleoporin. To investigate the role of the spindle assembly checkpoint we depleted *tm2886* embryos for MDF-2, the *C. elegans* homolog of yeast Mad2p (Encalada et al., 2005). Compared to control embryos, *tm2886*; Mad2 RNAi embryos did not exhibit significant delays in either AB or P1 cell divisions, although the asynchrony between the divisions remained slightly elevated (**Fig. 47B; Table 6**). We conclude that the spindle assembly checkpoint is activated in the AB and P1 cells in the absence of Nup35 and contributes to delaying cell division. We next examined the role of the DNA replication checkpoint by depleting ATL-1, which is required to both protect cells against damage arising from defective DNA replication and repair and establish asynchrony between the AB and P1 divisions (Brauchle et al., 2003). In accordance with this latter function, depletion of ATL-1 in *tm2886* embryos specifically affected timing of P1 cell division (**Table 6**), thereby restoring normal degree of asynchrony between AB and P1 division (**Fig. 47B; Table 6**). This suggests that the P1 cell is particularly sensitive to decreased Nup35 activity and that depletion of Nup35 leads to activation of an ATL-1-

dependent checkpoint in this blastomere.

Strain	*n*[a]	AB division[b] (average ±S.D.[c])	P1 division[d] (average ±S.D.)	P1 delay[e] (average ±S.D.)	P1/AB ratio[f] (average ±S.D.)
Control	17	661±54 sec	809±50 sec	147±19 sec	1.22±0.04
Nup35 RNAi	33	853±75 sec*	1316±113 sec*	467±122 sec*	1.56±0.18*
tm2886	18	714±110 sec	1149±227 sec*	460±192 sec*	1.67±0.26*
tm2886; ATL-1 RNAi	9	726±69 sec	931±76 sec‡	206±100 sec†	1.29±0.16†
tm2886; Mad2 RNAi	5	540±97 sec‡	768±176 sec‡	228±90 sec‡	1.42±0.11‡

Table 6. Depletion of Nup35 induces checkpoint-dependent cell cycle delays. [a] Number of embryos monitored by time-lapse confocal microscopy. [b] Time from P0 cytokinesis to AB anaphase onset. [c] Standard deviation. [d] Time from P0 cytokinesis to P1 anaphase onset. [e] Time from AB anaphase onset to P1 anaphase onset. [f] Ratio between AB division and P1 division. Significant differences by two-tailed t-test: * different from control embryos ($p<0.002$); † different from *npp-19(tm2886)* embryos ($p<0.005$); ‡ different from *npp-19(tm2886)* embryos ($p<0.05$).

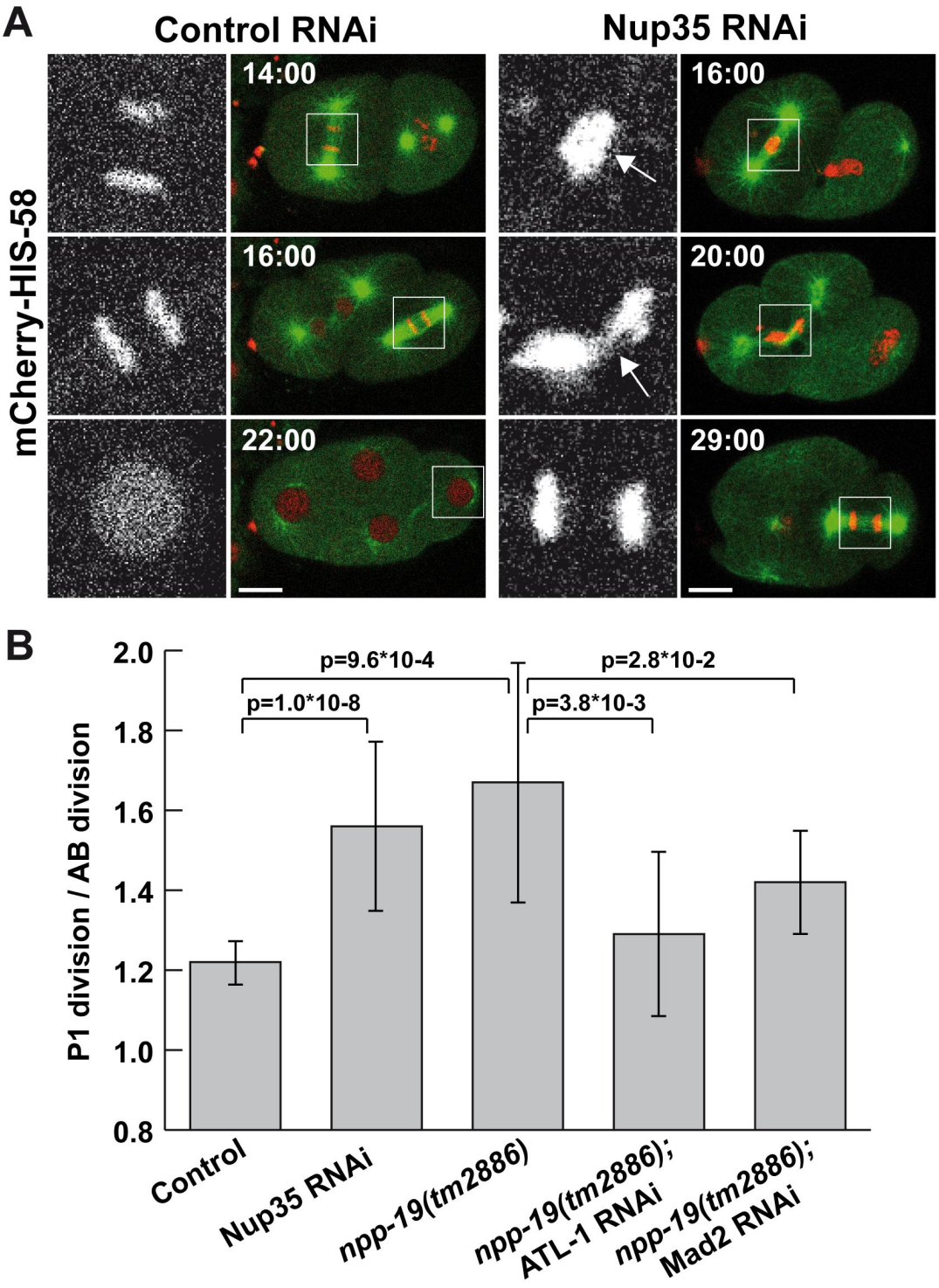

Figure 47. Depletion of Nup35 slows cell cycle progression and increases asynchrony between the AB and P1 cell divisions. (A) Control and Nup35 RNAi embryos co-expressing GFP-α-tubulin/TBA-2 (green) and mCherry-HIS-58 (red) were imaged using time-lapse confocal microscopy as described in Fig. 17. Boxed regions in merged panels are shown at higher magnification on the left, illustrating chromatin morphology. Arrows highlight defects in chromosome segregation. Scale bars, 10 µm. (B) Asynchrony between the AB and P1 cell divisions in control, Nup35 RNAi, *tm2886*, *tm2886*; ATL-1 RNAi and *tm2886*; Mad2 RNAi embryos expressed as the ratio of time between P0 cytokinesis to P1 anaphase over the time between P0 cytokinesis to AB anaphase. Probability values (p) from two-tailed t-tests are shown.

2.5 <u>Depletion of Nup35 induces structural NE defects</u>: To characterize the structural and molecular defects induced by Nup35 depletion, we analyzed NE dynamics in further detail. Nup155/ NPP-8 is essential for NPC formation (Franz et al., 2005) and has been shown to interact physically with Nup35 in vertebrates (Hawryluk-Gara et al., 2008; Hawryluk-Gara et al., 2005). We therefore decided to investigate the behavior of Nup155 in the absence of Nup35. GFP-Nup155 localization to the NE in late anaphase was disrupted following Nup35 depletion (**Fig. 48A, 3:00**). Later in interphase, GFP-Nup155 eventually appeared at the nuclear periphery in Nup35 RNAi embryos at significantly reduced levels (**Fig. 48A, 9:20**). Analysis of endogenous Nup155 by immunofluorescence likewise demonstrated a decreased NE localization in Nup35 RNAi embryos (**Fig. 49A**). We have previously observed that depletion of Nup155 prevents nuclear rim accumulation of Nup35 (Franz et al., 2005). Thus, Nup35 and Nup155 show a mutual dependency for NE localization. Depleting Nup35 from embryos expressing GFP-Nup45/58/NPP-4 induced an identical phenotype as obtained for GFP-Nup155 (data not shown). From these experiments, we conclude that Nup35 regulates Nup155 and Nup45/58 recruitment. Additionally, Nup35 is required for the correct distribution of Nup107, suggesting an important role for Nup35 in NPC assembly.

In addition to NPCs, the NE consists of inner and outer nuclear membranes and an underlying nuclear lamina (Hetzer et al., 2005). To analyze if Nup35 is required for assembly of these essential structures, we monitored the behavior of the inner nuclear membrane protein LEM-2 and lamin/LMN-1 fused to fluorescent proteins. Similar to the defects in Nup155 and Nup45/58 recruitment, YFP-LMN-1 levels at the nuclear periphery were strongly reduced in Nup35 RNAi embryos, implying that nuclear lamina assembly is Nup35-dependent (**Fig. 48B**). In contrast, GFP-LEM-2 recruitment was unaffected in Nup35 RNAi (**Fig. 48C**) and *tm2886* embryos (**Fig. 50**). Thus, Nup35 appears to be dispensable for targeting of nuclear membrane to the chromatin surface after mitosis.

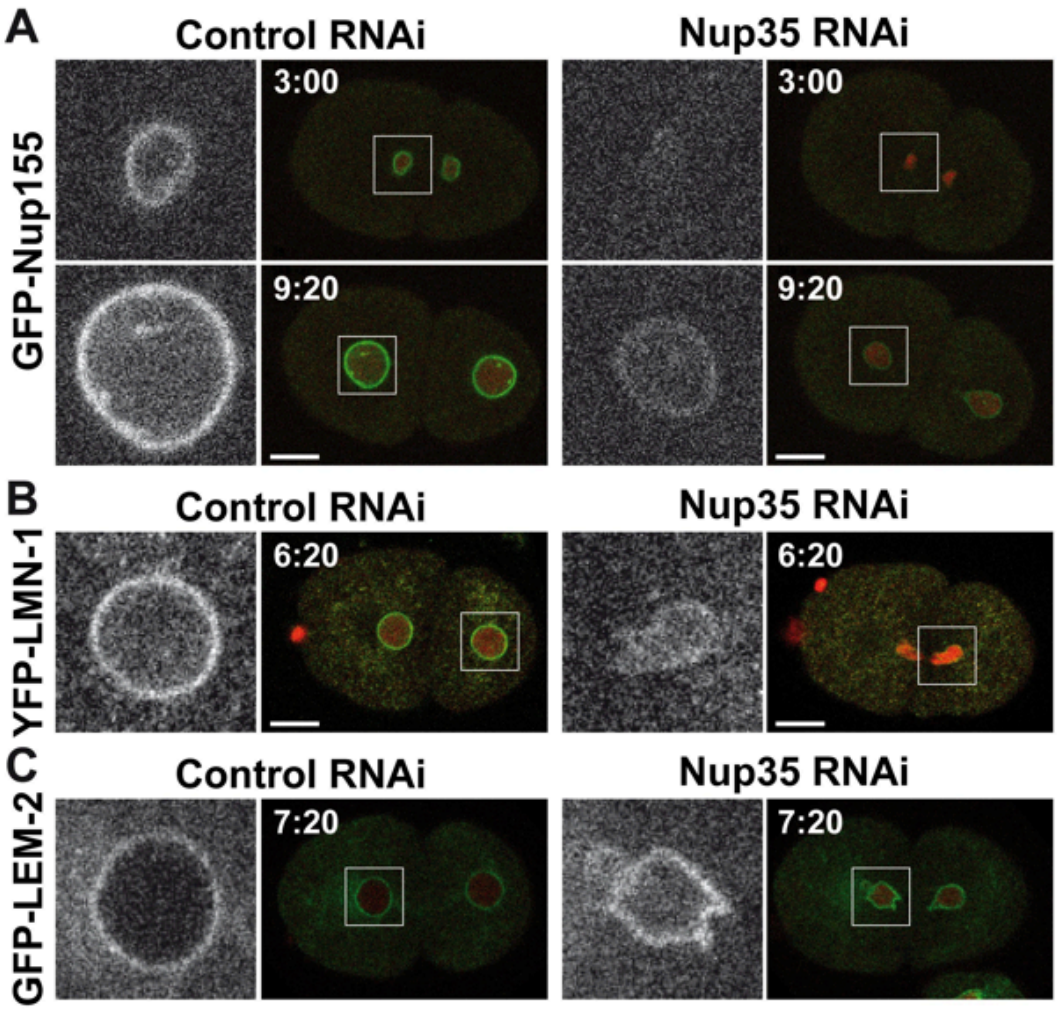

Figure 48. Depletion of Nup35 inhibits NPC and nuclear lamina formation. Control and Nup35 RNAi embryos co-expressing mCherry-HIS-58 with various GFP/YFP fusion proteins were imaged using time-lapse confocal microscopy as described in Fig. 17. Higher magnification views of boxed regions shown in merged panels highlight localization of (A) GFP-Nup155, (B) YFP-LMN-1, and (C) GFP-LEM-2. Scale bars, 10 μm.

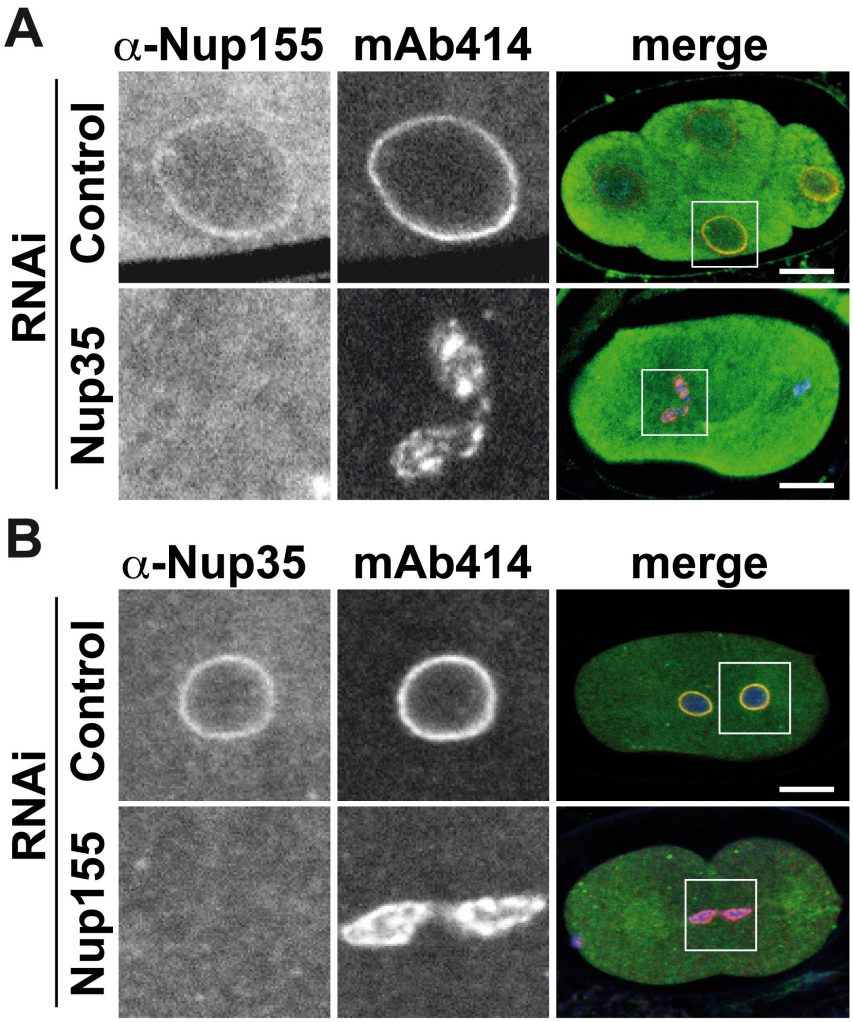

Figure 49. The localizations of Nup155 and Nup35 to the NE are inter-dependent. Control, Nup35 RNAi (A) and Nup155 RNAi (B) embryos were fixed and stained with monoclonal antibody mAb414 (red) and either α-Nup155 antiserum (A, green) or α-Nup35 antiserum (B, green). Chromatin was stained with Hoechst 33258 (blue). Higher magnification views of boxed regions are shown on the left. Scale bars, 10 μm.

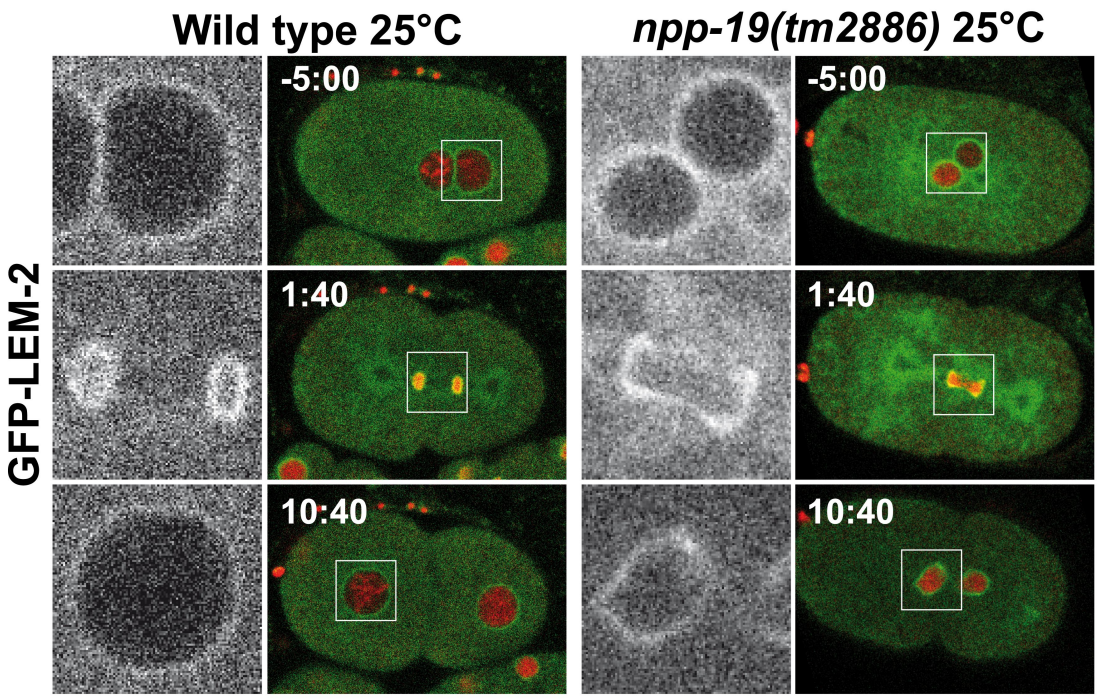

Figure 50. GFP-LEM-2 is recruited to the chromatin surface in *tm2886* embryos. Wild type and *tm2886* embryos expressing GFP-LEM-2 (green) and mCherry-HIS-58 (red) were imaged using time-lapse confocal microscopy. Time (min:sec) relative to the onset of the first zygotic anaphase is indicated. Boxed regions in merged panels are shown at the left at higher magnification. Scale bars, 10 μm.

2.6 <u>NE function depends on Nup35</u>: The alterations in nucleoporins recruitment and distribution in the absence of Nup35 prompted us to investigate if a functional NE is formed in Nup35 RNAi embryos. We initially analyzed whether a cytoplasmic protein, α-tubulin/TBA-2, fused to GFP, is excluded from the nuclear space upon Nup35 knockdown. In control embryos, the NE assembled while the chromatin was still highly compacted (see **Fig. 48A, left, 3:00**), and as nuclei grew in size, exclusion of GFP-TBA-2 was observed (**Fig. 51A, left**). In contrast, nuclear exclusion was not observed in Nup35 RNAi embryos (**Fig. 51A, right**). To analyze if nuclear protein import also depends on Nup35, we determined the localization of GFP fused to either PCNA/PCN-1, a DNA replication co-factor, or PIE-1, an RNA polymerase II repressor essential for germ-line specification. Nuclear accumulation of GFP-PCN-1 was observed significantly earlier in control embryos than in Nup35 RNAi embryos (180 ± 14 s vs. 288 ± 36 s [average ± standard deviation]) and reached higher concentrations (**Fig. 51B**), strongly suggesting that nuclear protein import is impaired in the absence of Nup35. Moreover, we speculate that nuclear GFP-PCN-1 observed in

Nup35 RNAi embryos may reflect the direct association of GFP-PCN-1 to chromatin in cells with increased NE permeability. In support of this notion, nuclear accumulation of GFP-PIE-1 was inhibited in Nup35 RNAi embryos. In control embryos, GFP-PIE-1 was present in the P2 cell, displaying strong nuclear enrichment (**Fig. 51C, left**). Asymmetric inheritance of GFP-PIE-1 was maintained in Nup35 RNAi embryos, indicating that Nup35 does not regulate early cell specification. However, in embryos lacking Nup35, GFP-PIE-1 failed to concentrate in the nucleus (**Fig. 51C, right**).

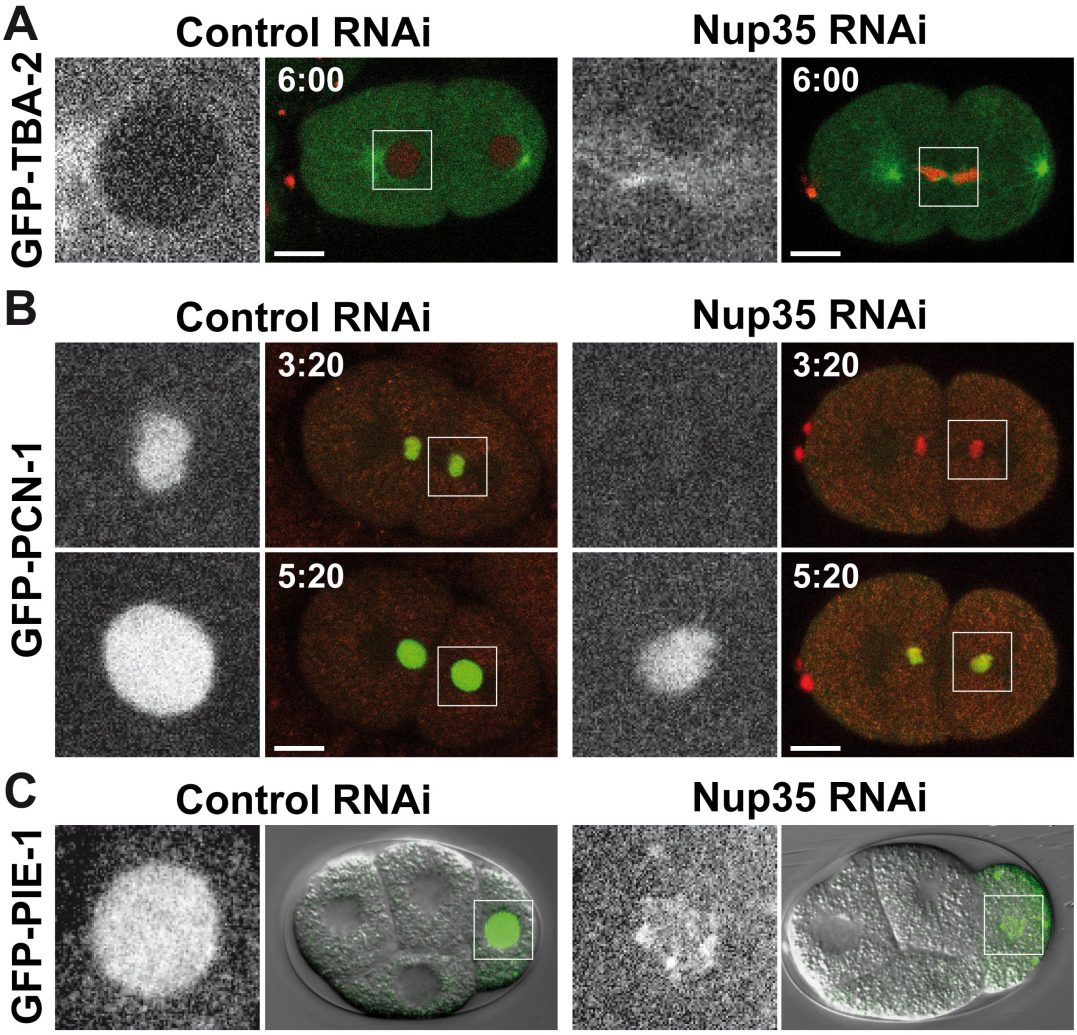

Figure 51. Nup35 is required for NE function and nuclear protein import. Control and Nup35 RNAi embryos co-expressing various fluorescent fusion proteins were imaged using time-lapse confocal microscopy as described in Fig. 17. Scale bars, 10 μm. Higher magnification views of boxed regions shown in merged panels highlight localization of (A) GFP-TBA-2, (B) GFP-PCN-1, and (C) GFP-PIE-1.

2.7 <u>Ultrastructural NE analysis in Nup35 RNAi embryos</u>: The defects in nucleoporin recruitment and nuclear protein import observed in Nup35 RNAi embryos by immunofluorescence and live-cell microscopy raised the question of whether NPCs are assembled in the absence of Nup35. To address this issue, we fixed Nup35 RNAi embryos by high pressure freezing followed by transmission electron microscopy (TEM). NPCs were detected at high density and with regular spacing in control embryos (**Fig. 52, left**). In contrast, nuclei of Nup35 RNAi embryos contained fewer NPCs, separated by long stretches of intervening nuclear membranes (**Fig. 52, middle and right**; note the different scale of control and Nup35 RNAi images). Moreover, several gaps larger than NPCs were observed in the nuclear membranes in Nup35 RNAi embryos (data not shown) as well as chromatin surfaces devoid of nuclear membranes (**Fig. 52, middle**). Live observation of *tm2886* and Nup35 RNAi embryos revealed that chromatin initially trapped in the cytokinetic furrow eventually separates and forms spherical nuclei. Thus, the two nuclei from Nup35 RNAi embryos shown in **Fig. 52** most likely represent early (**Fig. 52, middle**) and late (**Fig. 52, right**) time points after mitosis. In summary, TEM analysis showed that depletion of Nup35 causes a strong decrease in NPC formation whereas nuclear membranes are still able to cover and seal over most of the chromatin surface, consistent with our observations using live microscopy.

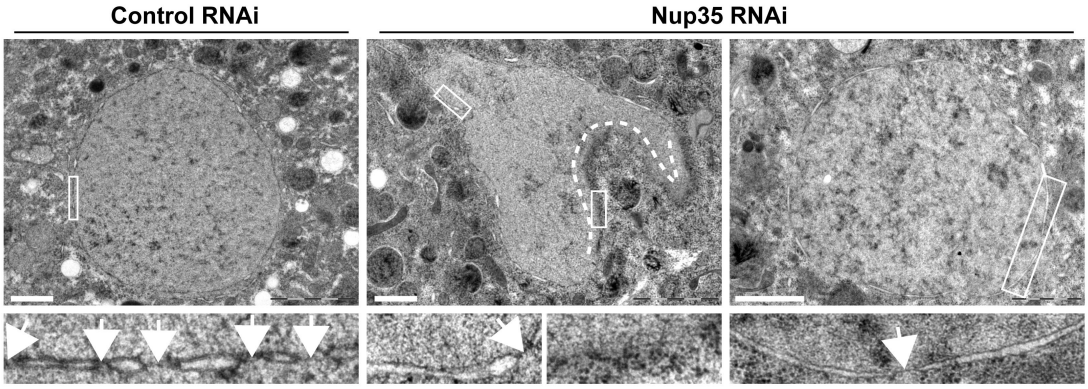

Figure 52. Depletion of Nup35 leads to lower NPC density. Control and Nup35 RNAi embryos were analyzed by transmission electron microscopy to visualize nuclear membranes and NPCs. Higher magnification views of boxed regions are shown below. Arrows highlight NPCs and dashed lines indicate regions of chromatin that lack nuclear membranes. White scale bars, 1 µm in upper panels; 100 nm in lower panels.

2.8 Nup155, but not Nup205 or Nup93, is required to localize Nup35:

Vertebrate Nup35 forms a NPC subcomplex together with at least Nup93, Nup155 and Nup205 (Hawryluk-Gara et al., 2005). Moreover, siRNA-mediated depletion of Nup93 reduces the amount of Nup35 at the NE (Hawryluk-Gara et al., 2005). To investigate the role of these nucleoporins in controlling Nup35 localization in *C. elegans* we performed RNAi experiments with *tm2886* embryos expressing GFP-Nup35. As noted earlier, GFP-Nup35 is able to rescue the embryonic lethality of *tm2886*, demonstrating its biological activity (**Table 4**). RNAi against Nup205/NPP-3 or Nup93/NPP-13 affected nuclear growth and shape and induced chromosomes to condense at the nuclear periphery as reported (**Fig. 53**; (Galy et al., 2003). In contrast to its smooth appearance in control embryos, the distribution of GFP-Nup35 at the NE was highly irregular and punctate in Nup205 and Nup93 RNAi embryos (**Fig. 53**). Presumably, this abnormal localization reflects NPC clustering rather than a decrease in NPC number (Galy et al., 2003). Co-depletion of Nup205 and Nup93 using RNAi aggravated the irregular localization of GFP-Nup35 (**Fig. 53**). In some Nup205/Nup93 RNAi embryos, the total amount of GFP-Nup35 at the NE appeared reduced, but this phenotype was variable. In contrast and as expected from previous studies (Franz et al., 2005), depletion of Nup155 caused a complete block in GFP-Nup35 recruitment (**Fig. 49B; Fig. 53**). From these experiments, we deduce that Nup155, but neither Nup205 nor Nup93, is essential for localization of Nup35 to the nuclear periphery. Moreover, Nup205 and Nup93 may have redundant roles in Nup35 recruitment.

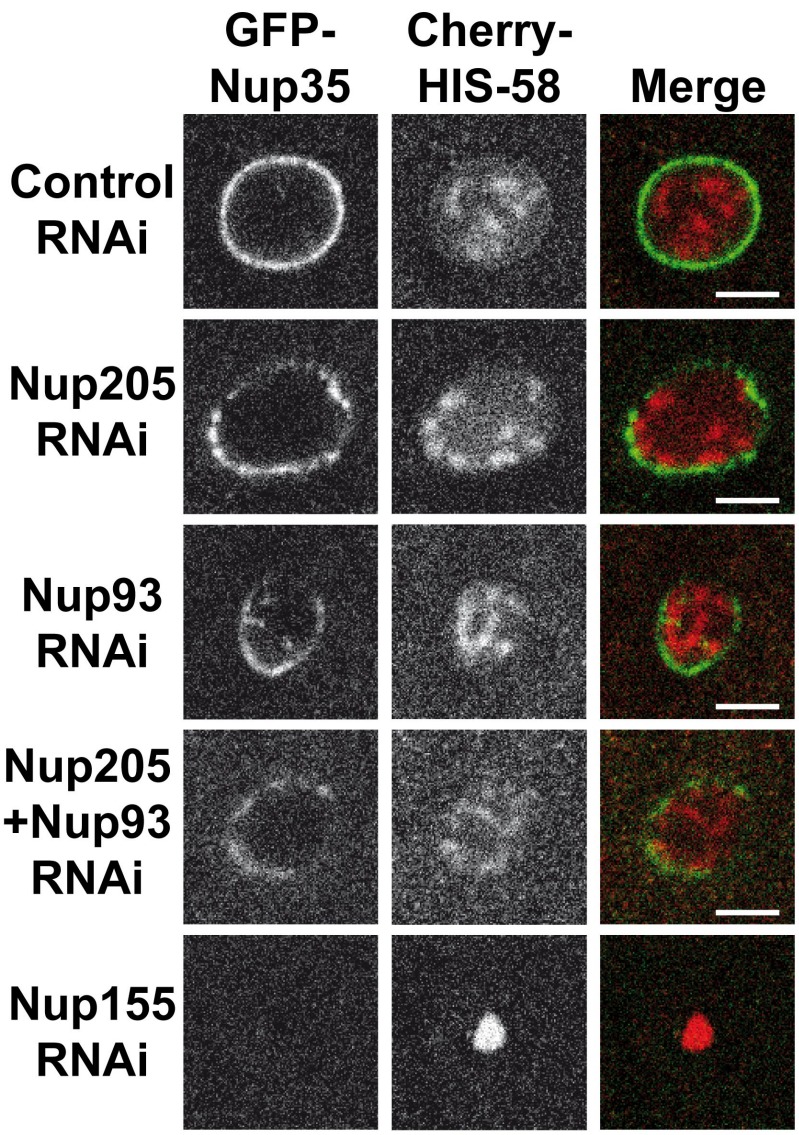

Figure 52. Nup155 is essential for NE localization of Nup35. The P1 cells of 2-cell stage Control, Nup205, Nup93, Nup205+Nup93 and Nup155 RNAi embryos expressing GFP-Nup35 (green) and mCherry-HIS-58 (merge) were imaged using time-lapse confocal microscopy. Scale bars, 5 µm.

4. Discussion

1. Nucleoporins in yeast, worms and vertebrates

Most nucleoporins are evolutionary conserved from yeast to mammals, and consequently the NPC structure is also well conserved. Around 30 different nucleoporins have been found in mammals and in yeast, although some of them are specific to only some species. Specific nucleoporins in mammals are Nup37, Pom121 and ALADIN, whereas Nup59, Nup100, Pom33 and Pom134 among others only have been identified in yeast. In *C. elegans* only ~23 nucleoporins have been so far described, and it is possible that there are still nucleoporins to be identified in this model system. Due to the lack of sequence homology of these "missing" nucleoporins in *C. elegans* it has not been possible to identify them with bioinformatics approaches, and only functional assays will allow us to recognize them.

Among nucleoporins that are well conserved in mammals, worms and yeast we can find the members of the Nup107 complex, suggesting that the scaffold NPC is very well evolutionary conserved.

2. Dissection of a conserved nuclear pore subcomplex reveals a novel role of Nup107 in mitosis

We provide here the first *in vivo* characterization of a metazoan Nup107 mutant. Moreover, we demonstrate that *C. elegans* Nup43, Nup85 and Nup133 localize at the nuclear periphery in interphase and at kinetochores during mitosis, thus behaving like *bona fide* Nup107 complex components. It was reported that depletion of Nup107 with siRNAs in HeLa cells or by immunoprecipitation from *Xenopus* extracts cause a co-depletion of several Nup107 complex members, hampering a detailed understanding of how this ~720 kD complex functions (Boehmer et al., 2003; Harel et al., 2003b; Walther et al., 2003a). However, we show that the majority of nucleoporins are expressed at normal levels in a *C. elegans* Nup107 *null* mutant, *tm3039*, paving the way to study the role of individual Nup107 complex members.

As mentioned before, postmitotic NPC assembly consists of four essential steps. First MEL-28 binds chromatin, possibly via its AT-hook domain, and in the second step of NPC biogenesis it recruits the Nup107 complex to form what is known as the "prepore". We observed that in Nup107 mutants, MEL-28 as well

as Nup85 and Nup96 – both components of the Nup107 complex - are still recruited to chromatin. The third step of NPC biogenesis, in which transmembrane proteins associate to the "prepore" via interactions with the Nup107 complex and the fourth step of NPC biogenesis, in which soluble nucleoporins such as Nup35 and Nup155 are incorporated to complete NPC assembly seem also to be unaffected in Nup107 mutants. These observations make us conclude that postmitotic assembly of the NPC is unaffected in Nup107 mutants, probably due to the fact that the Nup107 complex in Nup107 mutants is stable in *C. elegans* and is able to bind MEL-28 to form the "prepore" at the second step of NPC biogenesis.

The fact that nucleoporins are largely absent from chromatin during mitosis and recruited in a highly ordered manner makes it tempting to speculate on the coordination between chromosome segregation and NE reformation. One possible scenario to explain why the assembly of NPC only starts at late anaphase and not during early mitosis could be that the association of the Nup107 complex to kinetochores prevents its interaction with other nucleoporins and thus blocking NPC assembly. It is known that members of the Nup107 complex get phosphorylated upon entry in mitosis, so it could be possible that phosphorylation of the Nup107 complex prevents the interaction with the other nucleoporins during mitosis. In the future, it would be interesting to map the phosphorylation site of Nup107 and generate transgenic nematodes that express the mutated Nup107 lacking the phosporylation site to observe if this mutated Nup107 is still able to localize to kinetochores and if NPC assembly is still blocked during mitosis.

Strikingly, although most Nup107 mutant animals do not complete development to adulthood, NPCs are formed and neither nuclear protein import nor nuclear exclusion of soluble cytoplasmic content is significantly affected by the absence of Nup107. The high lethality, in particular at 25°C, lead us to conclude that Nup107 is an essential gene in *C. elegans*, as also reported for *Schizosaccharomyces pombe* (Bai et al., 2004) and *Drosophila melanogaster* (Katsani et al., 2008). In contrast, deletion of the homologous Nup84 genes from *S. cerevisiae* or *Aspergillus nidulans* causes milder, temperature-sensitive growth defects (Osmani et al., 2006; Siniossoglou et al., 1996).

2.1 Dissection of the Y-shaped Nup107 complex

Among nucleoporins that belong to the Nup107 complex, we found that only Nup43 and Nup133 depend on Nup107 for their correct localization. Recruitment of Nup43 is diminished both at kinetochores during mitosis and at the NPC during interphase in the absence of Nup107. The position of Nup43 within the Y-shaped Nup107 complex is unknown (Lutzmann et al., 2002), but based on our observation that other nucleoporins are still at the NPC in the absence of Nup107, we suggest that Nup43 and Nup107 may interact directly. It would be interesting in the future to see if Nup107 can pull down Nup43 in an immunoprecipitation assay (and vice versa) and if in a Y2H assay these two proteins interact. Also using Nup43 and Nup107 recombinant proteins we could test if there is direct interaction between these two nucleoporins. On the other hand, Nup133 localizes normally at NPCs during interphase in *tm3039* embryos but does not localize at kinetochores in mitosis. The observation that NPC localization of endogenous Nup133 is Nup107-independent was unexpected since GFP-tagged human Nup133 mutated for the residues that mediate its interaction with Nup107 *in vitro* do not accumulate at the nuclear periphery in HeLa cells (Boehmer et al., 2008). We propose that the addition of a GFP tag to Nup133 renders it more dependable on Nup107 for its NPC incorporation. Indeed, we observe that also *C. elegans* GFP-Nup133 is dependent on Nup107 for its localization to the NPC. The position of Nup133 at the base of the Y-shaped complex, ”below” Nup84p (Lutzmann et al., 2002) implies that removal of Nup107/Nup84p should release Nup133 from the rest of the Nup107 complex. Thus, how does Nup133 localize to the NPC in the absence of Nup107? One possibility is that Nup133 may interact physically with other nucleoporins. In fact, it was recently suggested that the Nup107 complex is arranged in a head-to-tail fashion within the NPC, through direct contacts between the Nup133 and Nup120/Nup160, forming closed rings of eight Nup107 complexes (Seo et al., 2009). Moreover, Nup133 contains an ALPS motif capable of sensing membrane curvature (Drin et al., 2007), which plays a crucial role for Nup133 recruitment during de novo interphase NPC assembly (Doucet et al., 2010). Based on these observations we propose that Nup133 may utilize several mechanisms for its

NPC incorporation and that binding to Nup107 is only required for kinetochore targeting. It is interesting to note that Western blot analysis of *tm3039* extracts reveals only a single Nup133 band, while two protein species are detected in wild type extracts. At present we do not have information as to the nature of the doublet in the wild type, but the differential behavior of Nup133 in terms of NPC and kinetochore localization in the absence of Nup107 makes us speculate that the two Nup133 bands represents different isoforms of Nup133; one localizing to kinetochores during mitosis and another to NPCs during interphase in *C. elegans*. Without Nup107 the former Nup133 isoform becomes unstable, whereas the latter is stabilized through interactions with other Nups and/or pore membrane components. *C. elegans* Nup133 is refractory to RNAi (Galy et al., 2003; Gonczy et al., 2000; Kamath et al., 2003) whereas null mutants display a complete maternal effect lethal phenotype during early larval development, which has precluded us to investigate the Nup107-Nup133 interaction in further detail. An experiment that would be interesting to perform in the future would be to analyze by mass spectrometry the different isoforms of Nup133. If such analysis would reveal differences at the level of amino acid sequences we could generate transgenic nematodes expressing individually both Nup133 isoforms tagged with GFP and observe the localization of both isoforms. Also we could generate specific antibodies against one of the isoforms and observe if indeed one of the Nup133 isoforms localize to the nuclear periphery and the other one to the kinetochores..

On the other hand, we found that depletion of other Nup107 complex proteins, such as Nup85, Nup96 and Nup160, efficiently abrogated Nup107 recruitment and NPC assembly, suggesting that these proteins are critical for Nup107 complex stability and postmitotic NE reformation. An important conclusion from our work is therefore that the previously identified requirement for the Nup107 complex during NPC assembly, which is confirmed here, is independent of Nup107 itself.

2.2 Nup107 acts at multiple steps of mitosis

Although it is well established that Nup107 localizes to kinetochores in vertebrate and nematode cells (Belgareh et al., 2001; Franz et al., 2005; Loiodice

et al., 2004), but not in *Drosophila* (Katsani et al., 2008), little is known about the functional implications. By depleting Nuf2 from HeLa cells, Zuccolo and colleagues concluded that the Ndc80 complex plays a major role in the recruitment of the Nup107 complex to kinetochores (Zuccolo et al., 2007). Our observation that kinetochore accumulation of Nuf2 is reduced in embryos lacking Nup107 suggests that proper localization of the two protein complexes is interdependent. This is in contrast to the experiments of Zuccolo and colleagues where inhibition of Nup107 complex recruitment to kinetochores through Seh1 siRNA treatment did not affect localization of Hec1, which forms heterodimers with Nuf2 (Zuccolo et al., 2007). However, since detectable levels of Seh1 were still present upon siRNA treatment, we propose that residual Nup107 complex activity at kinetochores was sufficient for the Hec1 accumulation observed by Zuccolo and coworkers, whereas complete absence of Nup107 causes a ~40% decrease in Nuf2 as reported here. Importantly, Mis12 localized normally in *tm3039* embryos, which suggest that Nup107 acts at specific steps of kinetochore assembly.

The Nuf2-Hec1 dimer is essential for microtubule attachment to kinetochores (Cheeseman et al., 2006; Wei et al., 2007). One could therefore expect that reduced accumulation of Nuf2 in Nup107 mutants would trigger reduced tension between sister chromatids when aligned on the metaphase plate. However, in agreement with recent studies of Seh1 siRNA-treated HeLa cells (Platani et al., 2009), we note that interkinetochore distance was not altered by Nup107 depletion. We speculate that the reduced levels of Aurora B on centromeric chromatin upon removal of Nup107 (this study) or Seh1 (Platani et al., 2009) may partially counterbalance the lower Nuf2 activity.

Our observation that 10% of dividing *tm3039* embryos contained lagging chromosomes during mitosis is compatible with reduced correction of syntelic microtubule-kinetochore attachments by Aurora B (Lampson and Cheeseman, 2010), as also proposed for Seh1-depleted HeLa cells (Platani et al., 2009). Moreover, alterations in kinetochore structure upon Nup107 depletion, including reduced Nuf2 accumulation, are likely to produce activation of the SAC. Indeed, we observed accumulation of GFP-Mad1 on mitotic chromosomes in embryos depleted for Nup107, as has also been reported upon interfering with

kinetochore localization of the Nup107 complex though depletion of Seh1 in HeLa cells (Zuccolo et al., 2007). Finally, *tm3039* mutant embryos were hypersensitive to depletion of Mad1, resulting in 85% embryonic lethality and lagging chromosomes in 49% of dividing cells, which further supports the possibility that the SAC is activated in the absence of Nup107. In the future it would be important to determine if the activation of the SAC is due to the defects caused by depleting Nup107 at the kinetochores or if it is caused by a direct regulation of Nup107 of the SAC. An interesting experiment would be to partially deplete Nuf2 at the same levels that we observed in Nup107 mutants, and examine how is the SAC being activated in this case looking also at Mad1-GFP. Quantifying the Mad1-GFP signal at kinetochores in both situations (Nup107 mutants and partially Nuf2 depleted embryos) we could determine if Nup107 is regulating the SAC directly or if the activation of the SAC in the Nup107 mutants is due to a defect at the kinetochore structure.

Our experiments have unexpectedly revealed that Mad1 depends strictly on Nup107 in order to accumulate at the nuclear periphery during interphase. Mad1 localization to NPCs has previously been described in different organisms. In *S. cerevisiae* the interaction with the NPC is mediated via Nup53 and Mlp1/Mlp2 (Scott et al., 2005) whereas in HeLa cells localization of Mad1 to the NPC is dependent on the Mlp1/Mlp2 homolog Tpr and on Nup153 (Lee et al., 2008; Lussi et al., 2010). Yeast two hybrid experiments presented here demonstrate that *C. elegans* Mad1 interacts directly with Nup107 but not with Nup35. Thus, our data shows that accumulation of Mad1 at NPCs is conserved and that different Mad1-Nup interactions may have arisen during evolution. Cells are more dependent on the SAC and other checkpoints in situations of stress. Our observation that suspended animation and delay in mitotic progression were compromised in the absence on Nup107 combined with the genetic and physical interaction between Nup107 and Mad1 suggest that Nup107 may play an active role in control of chromosome segregation and cell cycle progression. It is intriguing that Mad1 accumulates at NPCs in several organisms but a clear functional implication of this behavior is lacking. We propose that Nup107 may serve as binding site for Mad1 both at the NPC and at kinetochores and that the two proteins may even translocate together at the

entry into mitosis. However, future experiments will be required to analyze this interaction in further detail. An attractive approach to analyze the interphase function of Mad1 would be to narrow down the Mad1 domain that is interacting with Nup107 and then generate transgenic nematodes in a Mad1 mutant background that express Mad1 lacking this Mad1-Nup107 interaction domain fused to GFP. Once this transgenic strain is generated we could investigate whether the NPC and the NE function properly in the absence of Mad1 at the NPC. Moreover, this strain could shed light on the possibility that Mad1's function in the SAC at least partially depends on its NPC localization in interphase.

2.3 Nucleoporins and the aging process

Nucleoporins that belong to the scaffold of the NPC, such as the members of the the Nup107 complex, are extremely long lived and do not turn over in postmitotic cells (D'Angelo et al., 2009). The fact that there is not a turn over of the scaffold region of the NPCs might imply that NPC function also gets deteriorated over time. The main consequence of the failure of NPC function would be that the NPCs become leaky structures, allowing proteins from the cytoplasm to enter the nucleus randomly. Another important consequence of the aging of NPCs would be a misregulation of gene expression in older cells (Hetzer, 2010b).

Also it has been shown that mutations in lamins cause premature aging syndromes in humans, such as Hutchinson-Gilford progeria syndrome (HGPS) (Haithcock et al., 2005; Scaffidi and Misteli, 2006). Haithcock et al. used lamina fused to GFP (LMN-1-GFP) as a marker for aging and observed that the morphology of the nuclei of *C. elegans* hypodermal cells gets disrupted over time. Also looking at LMN-1-GFP, we observed that the nuclear morphology gets disrupted faster in Nup107 mutants than in wild type cells and that Nup107 mutants live shorter than wild type nematodes, suggesting that Nup107 could play a role in longevity. Another striking phenotype that we observed is that the nuclei of hypodermal cells started to aggregate in Nup107 mutants over time, suggesting that Nup107 is an essential protein for the proper positioning of the nuclei of hypodermal cells within the hypodermal syncytium over time. It would

be interesting in the future to test if Nup107 interacts with unc-83 and/or unc-84, two transmembrane proteins that have been previously shown to play an important role in nuclear positioning and migration during *C. elegans* development (Lee et al., 2002; Starr et al., 2001).

3. Early embryonic requirement for nucleoporin Nup35/NPP-19 in nuclear assembly

Using *C. elegans*, we have provided the first in vivo characterization of the Nup35/NPP-19 mutant *npp-19(tm2886)*. Doing RT-PCR we have observed that the truncated Nup35 protein expressed in *tm2886* mutants lacks aa 217–286 and that this truncated Nup35 protein is stable via Western blot at permissive (20°C) and restrictive (25 °C) temperatures (**Fig 42C**). At 20°C, *tm2886* mutant embryos do not present obvious defects in the NE assembly, but 42.5% died during gastrulation. We hypothesize that the embryonic lethality observed at 20 °C may be caused by cumulative defects arising from perturbations in nucleocytoplasmic transport. We note that mutant Nup35$^{\Delta 217-286}$ possesses weak NE targeting capacity, which may contribute to NE assembly and NPC function under permissive condition.

At 25 °C the phenotypes observed in *tm2886* mutants are much more severe. Pronuclei are smaller (specially the sperm-derived one) and they failed to juxtapose properly, they present problems of DNA segregation during mitosis and around 86% of the embryos died during gastrulation. The same phenotypes were observed when we depleted Nup35 by RNAi, suggesting that at 25 °C the truncated Nup35$^{\Delta 217-286}$ protein is not able to perform the function of the endogenous Nup35. This could be due to a higher requirement of Nup35 at restrictive temperature (25 °C), since the time of cell division and NPC assembly are accelerated at this temperature.

We also noticed by electron microscopy that the nuclei of embryos depleted of Nup35 by RNAi presented less NPCs than control RNAi embryos. This observation is in concordance with recent studies where depletion of Nup35 in Xenopus egg extracts prevented NPC and NE assembly in vitro (Hawryluk-Gara et al., 2008). Moreover, this study demonstrate that a fragment of human Nup35 containing aa 167–300 was sufficient to reconstitute the NPC and NE assembly in

extracts depleted of endogenous Nup35. Interestingly, the truncated Nup35 protein expressed in *tm2886* mutants lack aa 217–286, which overlaps with the human Nup35 fragment capable of reconstituting NPC and NE assembly. These data suggest that the central portions of human Nup35 and *C. elegans* NPP-19 have critical roles in NE reformation.

We also have demonstrated that the localization of Nup155 to the NE is regulated by Nup35 and that Nup107 localization to the nuclear periphery is independent of Nup35. This observation suggests that Nup35, together with Nup155, plays a role at the last step of NPC biogenesis, just downstream of the critical transmembrane nups POM121 and NDC1. In agreement with this idea, it has been shown that yeast Nup53p and vertebrate Nup35 interact with Ndc1p/NDC1 (Mansfeld et al., 2006; Uetz et al., 2000).

The inhibition of NPC assembly observed in embryos lacking Nup35 has severe implications in NE function, especially in the import of macromolecules inside the nucleus. We observed a defect in nuclear lamina assembly, probably due to a reduced import to the nucleus of lamin/LMN-1 after NE assembly. On the other hand, the recruitment of the transmembrane protein LEM-2 was not affected by the absence of Nup35. Accordingly with this last observation, we observed that the majority of chromatin in Nup35 RNAi embryos was enclosed by nuclear membranes, suggesting that membrane fusion is independent of Nup35. Consistent with this observation, previous studies have demonstrated that in vitro nuclear assembly of extracts immunodepleted of the Nup107-160 subcomplex resulted in chromatin enclosed by NEs that lack NPCs (Harel et al., 2003b; Walther et al., 2003a).

In summary, we have demonstrated that Nup35 is essential for NPC and NE assembly, providing the first mutational analysis of Nup35 in a metazoan organism. We propose that altered NE structure and function lead to severe chromosome segregation defects following perturbation of Nup35activity. However, a more direct involvement of Nup35 in mitotic spindle assembly may exist (Iouk et al., 2002) and deserves future study.

5. Conclusions

1. Mutantes *npp-19(tm2886)* expresan la proteína Nup35 truncada a la que le faltan aa 217–286 y como consecuencia muestran letalidad embriónica termosensible.
2. La expresión de Nup35-GFP es capaz de rescatar el fenotipo de letalidad embriónica en mutantes *tm2886*
3. Embriones *tm2886* presentan defectos de segregación cromosómica y defectos en la morfología nuclear
4. Depleción de Nup35 por RNAi provoca defectos en la asincronía de la división celular
5. El apropiado funcionamiento de la NE y el ensamblaje de la lámina nuclear depende de Nup35
6. El número de NPCs se ve reducido en NE que carecen de Nup35 por RNAi, demostrando que Nup35 es una nucleoporina esencial para el correcto ensamblaje del NPC.
7. Mutantes *npp-5(tm3039)* y *npp-5(ok1966)* son mutantes nulos para la proteína Nup107
8. El complejo Nup107-160 permanece estable en la ausencia de Nup107 en *C. elegans*
9. El importe nuclear de proteínas no se ve afectada por la ausencia de Nup107
10. El ensamblaje del NPC es independiente de Nup107
11. Nup133 depende de Nup107 para su correcta localización en los cinetocoros, pero no para su localización en los NPC
12. El apropiado ensamblaje de los cinetocoros y el reclutamiento de Aurora B depende de Nup107
13. El Spindle Assembly Checkpoint (SAC) se activa en la ausencia de Nup107
14. El componente del SAC Mad1 se localiza en la NE a través de su interacción con Nup107 en *C. elegans*
15. Nematodos *npp-5(tm3039)* envejecen más rápidamente que nematodos silvestre y muestran un envejecimiento acelerado en su morfología nuclear.

6. Materials and Methods

Nematode strains

The wild type strain was the C. elegans Bristol strain N2. *npp-19 (tm2886)* and *npp-5(tm3039)* strains were provided by Dr. Shohei Mitani at the Japanese National Bioresource Project and backcrossed to the wild type six times followed by self-fertilization to obtain the homozygous strain BN38 *npp-19(tm2886).* The balanced strain BN40 *npp-5(tm3039)* was obtained by crossing the already cleaned *npp-5(tm3039)* with the BN3 *vrk-1(ok1181)* strain*. npp-5(ok1966)* and *npp-15(ok1954)* were provided by the International *C. elegans* Gene Knockout Consortium and backcrossed to the wild type six times to obtain the homozygous strains BN28 *npp-5(ok1966)* and BN30 *npp-15(ok1954)* and the balanced strains BN85 *npp-5(ok1966)* and BN126 *npp-15(ok1954)* were obtained by crossing the BN28 and BN30 strains with BN40 and JK122 strains respectively.

BN7 *unc-119(ed3)* bqIs07[*unc-119(+); Ppie-1::LAP:: npp-19*], BN51 *unc-119(ed3)* bqIs51[*unc-119(+); Ppie-1::GFP::npp-5*] and XA3545 *qaIs3545*[$P_{pie\text{-}1}$*::gfp::him-10*] were obtained by microparticle bombardment (Praitis et al., 2001) of DP38 *unc-119(ed3)* using plasmids pDP#MM051 (Maduro and Pilgrim, 1995) and pPGLv.1 *npp-19* (this study), pUP1 (this study) or pDP#MM051 and pPAG27 respectively.

BN128 *bqEx128*[$P_{npp\text{-}2}$*::gfp::npp-2;* $P_{lmn\text{-}1}$*::mCherry::his-58*] was obtained by microinjection of plasmids pBN1 and pBN29 into N2. BN150 *bqSi150*[$P_{hsp\text{-}16.41}$*::gfp::C09G9.2a*] and BN168 bqSi168[$P_{hsp\text{-}16.41}$*::gfp::npp-15*] were obtained by MosSCI transformation (Frokjaer-Jensen et al., 2008) of EG4322 with plasmid pBN27 and pBN23, respectively.

Subsequently, BN7 was crossed with OD83 *gfp::lem-2; cherry::his-58* (Audhya et al., 2007) to generate BN14 *gfp::npp-19; cherry::his-58*, which was further crossed with BN38 to generate BN46 *npp-19 (tm2886); gfp::npp-19* and BN47 *npp-19(tm2886); gfp::npp-19; cherry::his-58*. Similarly, BN51 was crossed with OD57 *gfp::tba-2; cherry::his-58* (McNally et al., 2006) to generate BN68 *gfp::npp-5 cherry::his-58*, which was further crossed with BN38 to generate BN79 *npp-19(tm2886); gfp::npp-5 cherry::his-58*. BN78 *npp-19 (tm2886); gfp::lem-2; cherry::his-58* was obtained by crossing BN38 with OD83. BN13 *gfp::npp-8; cherry::his-58*, BN16 *yfp::lmn-1; cherry:: his-58*, and BN27 *gfp::pcn-1; cherry::his-58* were generated by crossing XA3546, XA3541 (Franz et al., 2005) and a GFP-

PCNA/PCN-1 expressing strain (Brauchle et al., 2003) with OD83, respectively. JH1327 *gfp::pie-1* was described previously (Reese et al., 2000).

BN40 was crossed with the following strains: PD4810 to generate BN58 *npp-5(tm3039); P_{lmn-1}::LMN-1::gfp*; TJ356 (Henderson and Johnson, 2001) to generate BN22 *npp-5(tm3039)/mIn1*; *zIs356*[*daf-16::gfp*]; BN68 to generate BN69 *npp-5(tm3039)/mIn1*; *bqIs51*[P_{pie-1}*::gfp::npp-5*]; *ltIs37*[P_{pie-1}*::mCherry::his-58*]; JH1327 (Reese et al., 2000) to generate BN73 *npp-5(tm3039)/mIn1*; *axIs*[P_{pie-1}*::gfp::pie-1*]; XA3501 (Askjaer et al., 2002) to generate BN106 *npp-5(tm3039)/mIn1*; *ruIs32*[P_{pie-1}*::gfp::his-58*] and BN107 *npp-5(tm3039)/mIn1[mIs14 dpy-10(e128)] II; ojIs1[unc-119(+) Ppie-1::GFP::tbb-2] V (?)*; XA3545 to generate BN114 *npp-5(tm3039)/mIn1*; *qaIs3545*[P_{pie-1}*::gfp::him-10*]; BN128 to generate BN133 *npp-5(tm3039)/mIn1*; *bqEx128*[P_{npp-2}*::gfp::npp-2; P_{lmn-1}::mCherry::his-58*]; OD27 (CGC) to generate BN153 *npp-5(tm3039)/mIn1*; *ltIs14*[P_{pie-1}*::gfp::air-2*]; OD8 (Cheeseman et al., 2004) to generate BN159 *npp-5(tm3039)/mIn1*; *ltIs4*[P_{pie-1}*::gfp::mis-12*]. BN107 was crossed with OD57 (McNally et al., 2006) to generate BN204 *npp-5(tm3039)/mIn1[mIs14 dpy-10(e128)] II; ltIs37[Ppie-1::mCherry::his-58; unc-119 (+)] IV; ojIs1[unc-119(+) Ppie-1::GFP::tbb-2] V (?).*

Similarly BN28 was crossed with PS3808 (Gupta and Sternberg, 2002) to generate BN59 *npp-5(ok1966)*; *syIs80*[P_{lin-11}*::nls::gfp::lacZ*]. RQ244 *mdf-1(gk2)* V; *jzIs1*[P_{pie-1}*::gfp:: mdf-1*]; *ltIs37*[P_{pie-1}*::mCherry::his-58*] and OD110 ltIs52[P_{pie-1}*::gfp::mdf-2*] *ltIs37*[P_{pie-1}*::mCherry::his-58*] were described (Essex et al., 2009; Yamamoto et al., 2008). For further details on strains refer to **Table 7**. All strains were cultured using standard *C. elegans* methods (Stiernagle, 2006).

Strain	Description	Genotype
BN7	Homozygous expression of GFP/LAP-Nup35.	unc-119(ed3) III; bqIs07[unc-119(+) pie-1::LAP::npp-19]
BN14	Expression of GFP/LAP-Nup35 and Cherry HisH2B.	unc-119(ed3) III; bqIs07[unc-119(+); Ppie-1::LAP::npp-19] ?; ltIs37[Ppie-1::mCherry::his-58; unc-119 (+)] IV
BN22	Balanced Nup107 deletion strain expressing GFP-DAF-16	npp-5(tm3039)/mIn1[mIs14 dpy-10(e128)] II, zIs356 IV
BN28	Homozygous Nup107 deletion; out-crossed with N2 six times	npp-5(ok1966) II

BN30	Balanced Nup133/npp-15 deletion strain; out-crossed with N2 six times	npp-15(ok1954) III/hT2[bli-4(e937) let-?(q782) qIs48](I;III).
BN38	npp-19/CeNup35 in-frame deletion; out-crossed with N2 six times	npp-19(tm2886) II
BN40	Balanced Nup107 deletion; out-crossed with N2 six times	npp-5(tm3039)/mIn1[mIs14 dpy-10(e128)] II
BN46	Homozygous Nup35 deletion strain expressing GFP/LAP Nup35	npp-19(tm2886) II; unc-119(ed3) or unc-119(+) III; bqIs07[unc-119(+); Ppie-1::LAP::npp-19] ?
BN47	Homozygous Nup35 deletion strain expressing GFP/LAP Nup35 and mCherry-HisH2B	npp-19(tm2886) II; unc-119(ed3) or unc-119(+) III; bqIs07[unc-119(+); Ppie-1::LAP::npp-19];ltIs37[Ppie-1::mCherry::his-58; unc-119 (+)] IV (?)
BN51	Expression of GFP::npp-5 from pie-1 promoter	unc-119(ed3); bqIs51[unc-119(+); Ppie-1::GFP::npp-5] IV (?)
BN58	Homozygous Nup107 deletion strain expressing GFP-LMN-1 from LMN-1 promoter	npp-5(ok1966) II, P(lmn-1)::GFP::lmn-1 X
BN59	Homozygous Nup107 deletion strain expressing NLS-GFP-lacZ from lin-11 promoter	npp-5(ok1966) II, unc-119(ed4); syIs80[unc-119(+) + pPGF11.13(lin-11::GFP)] III
BN68	Expression of GFP-Nup107 and mCherry-HisH2B	bqIs51[unc-119(+); Ppie-1::GFP::npp-5]; ltIs37[Ppie-1::mCherry::his-58; unc-119 (+)] IV (?)
BN69	Balanced Nup107 deletion strain expressing GFP-Nup107 and mCherry-HisH2B	npp-5(tm3039)/mIn1[mIs14 dpy-10(e128)] II, bqIs51[unc-119(+); Ppie-1::GFP::npp-5]; ltIs37[Ppie-1::mCherry::his-58; unc-119 (+)] IV (?)
BN73	Balanced Nup107 deletion strain expressing GFP-PIE-1	npp-5(tm3039)/mIn1[mIs14 dpy-10(e128)] II; axEx73 [Ppie-1::GFP::pie-1 + pRF4]
BN78	Homozygous Nup35 deletion strain expressing GFP-LEM-2 and mCherry-HisH2B	npp-19(tm2886) II; Ppie-1::gfp::lem-2; ltIs37[Ppie-1::mCherry::his-58; unc-119 (+)] IV
BN79	Homozygous Nup35 deletion strain expressing GFP-Nup107 and mCherry-HisH2B	npp-19(tm2886) II; Ppie-1::gfp::npp-5; ltIs37[Ppie-1::mCherry::his-58; unc-119 (+)] IV

BN85	Balanced Nup107 deletion; out-crossed with N2 six times	npp-5(ok1966)/mIn1[mIs14 dpy-10(e128)] II
BN106	Balanced Nup107 deletion strain expressing GFP-HisH2B	npp-5(tm3039)/mIn1[mIs14 dpy-10(e128)] II; unc-119(ed3) ruIs32[unc-119(+) Ppie-1::GFP::H2B] III
BN107	Balanced Nup107 deletion strain expressing GFP-beta-tub	npp-5(tm3039)/mIn1[mIs14 dpy-10(e128)] II; ojIs1[unc-119(+) Ppie-1::GFP::tbb-2] V (?)
BN114	Balanced Nup107 deletion strain expressing GFP-Nuf-2	npp-5(tm3039)/mIn1[mIs14 dpy-10(e128)] II; unc-119(ed3) qaIs3545[unc-119(+) pie-1::GFP::him-10] ?
BN126	Balanced Nup133 deletion; out-crossed with N2 six times	npp-15(ok1954)/qC1 dpy-19(e1259) glp-1(q339) III
BN128	Expression of GFP-Nup85 and mCherry-HisH2B	bqEx128[Pnpp-2::gfp::npp-2 Plmn-1::mCherry::his-58]
BN133	Balanced Nup107 deletion strain expressing GFP::Nup85 and mCherry-HisH2B	npp-5(tm3039)/mIn1[mIs14 dpy-10(e128)] II, bqEx128[Pnpp-2::gfp::npp-2 Plmn-1::mCherry::his-58]
BN150	Expression of GFP-Nup43	bqSi150[pBN27(unc-119(+) Phsp16.41::gfp::C09G9.2a)] II
BN153	Balanced Nup107 deletion strain expressing GFP-Aurora B	npp-5(tm3039)/mIn1[mIs14 dpy-10(e128)] II, ltIs14[pASM05: pie-1::GFP-TEV-STag::air-2 + unc-19(+)] IV
BN159	Balanced Nup107 deletion strain expressing GFP-MIS-12	npp-5(tm3039)/mIn1[mIs14 dpy-10(e128)] II, ltIs4[pIC32; pie-1/GFP-TEV-Stag::mis-12; unc-119(+)] ?
BN168	Expression of GFP-Nup133	bqSi168[pBN23(unc-119(+) Phsp16.41::gfp::npp-15)] II
BN204	Balanced Nup107 deletion strain expressing GFP-tbb-2 and mCherry-His-58.. Strain could potentially carry GFP-tba (from OD57) instead of or together with GFP-tbb-2	npp-5(tm3039)/mIn1[mIs14 dpy-10(e128)] II; ltIs37[Ppie-1::mCherry::his-58; unc-119 (+)] IV; ojIs1[unc-119(+) Ppie-1::GFP::tbb-2] V (?)
XA3545	Expression of GFP-Nuf2	unc-119(ed3) qaIs3545[unc-119(+) pie-1::GFP::him-10] ?

Table 7. Strains generated in this study

Plasmids and RNAi

Plasmid pGEX-GST-His for cloning and expression of N-terminally GST-tagged and C-terminally His-tagged fusion protein was generated by removal of a vrk-1-containing BamHI fragment of pGEX-VRK-1-His (Gorjanacz et al., 2007b). Full length and truncated npp-19 cDNAs were generated by RT-PCR using forward primer B179 and either B180 or B181 as reverse primer. PCR fragments were digested with BamHI and inserted into pGEX-GST-His. Plasmid pPGLv.1 *npp-19* was generated by Gateway cloning (Invitrogen) using a genomic *npp-19* sequence (Franz et al., 2005) and pPGLv.1 (Gorjanacz et al., 2007b).
Plasmid pQE30-Nup133(aa 739-1024) for expression of 6*His-tagged Nup133 antigen was generated by PCR amplification of *C. elegans* genomic DNA (primers B153+B154). Plasmid pUP1 for expression of GFP-Nup107 was made by insertion of *unc-119* derived from plasmid pDP#MM051 (Maduro and Pilgrim, 1995) into pPAG1 (Franz et al., 2005). Plasmid pPAG27 for expression of GFP-Nuf2/HIM-10 was constructed by replacing the *lmn-1* gene of plasmid pPAG4 (Galy et al., 2003) with a PCR-amplified *him-10* sequence (primers H556+H557). Plasmid pBN29 for expression of GFP-Nup85 was generated by cloning the *npp-2* gene (primers B069+B200+B071+B072) into plasmid pBN8, a derivative of pCFJ151 (Frokjaer-Jensen et al., 2008) containing a longer polylinker. pBN29 includes 1993 bp upstream of the start codon and 560 bp downstream of the stop codon as well as GFP inserted into a PCR-engineered *Bsr*GI site immediately after the start codon. Plasmids pBN23 and pBN27 for expression of GFP-Nup133 and GFP-Nup43 were generated by cloning *npp-15* (primers B236+B237) and C09G9.2a (primers B248+B249) into plasmid pBN16, respectively. Plasmid pBN16 for single-copy integration of heat shock-inducible transgenes into the *C. elegans* genome was made by insertion of the *hsp-16.41* promoter (primers B216+B232), a polylinker and the *unc-54* 3'UTR (B233+B217) into pBN8.
Plasmid pBN1 for expression of mCherry-HisH2B in somatic cells contains the *lmn-1* promoter (5088 bp) in front of a mCherry-*his-58* fusion gene and the *pie-1* 3'UTR (1822 bp).
Plasmids pGADT7-*npp-5* and pAD-*npp-19* encoding the yeast Gal4 activation domain fused to either *C. elegans* Nup107 or Nup35, were constructed by RT-PCR amplification with primers B364+B366 and primers H624+H633,

respectively. Plasmid pGBKT7-*mdf-1* encoding the yeast *GAL4* DNA binding domain fused to *C. elegans* Mad1 was constructed by PCR amplification of *mdf-1* cDNA from plasmid pACT-Ptac-GST (Watanabe et al., 2008) using primers B367+B368 into pGBKT7 (Clontech).

For primer sequences refer to Supplementary **Table 8**. All constructions were verified by sequencing.

RNAi constructs were described previously (Galy et al., 2003; Kamath et al., 2003). As negative control the empty pPD129.36 vector was used. RNAi experiments were performed by feeding at 20°C for ~36 h unless otherwise specified (Galy et al., 2003).

Primer	Description	Enzyme	Sequence	Plasmid
H363	*npp-5* f	NheI	GAGCTAGCATGACAGACTTGTTCGCTTCGGG	pUP1
H364	*npp-5* r	NheI	GAGCTAGCTTCGACTTTGAGATTGAGTTCTGC	pUP1
H439	*unc-119* f	XmaI	GACCCGGGACGGTATCGATAAGCTTCAG	pUP1
H440	*unc-119* r	XmaI	ATCCCCCGGGCTGCAGAATTCGT	pUP1
H556	*him-10* f	XbaI	TGCTCTAGAATGTCAAACGTTGTACTAATTGTGT	pPAG27
H557	*him-10* r	XbaI	TGCTCTAGATTTGAAAACGGAAAAACTCGAATCGT	pPAG27
H624	*npp-19* f	GW	ggggacaagtttgtacaaaaaagcaggct-TGTTCTCGCATCTTAACCAAAAT	pAD-npp-19
H633	*npp-19* f	GW	ggggaccactttgtacaagaaagctgggt-TAGTTGAGTCCGATCGTGTTCCA	pAD-npp-19
B069	*npp-2*$_{prom}$ f	XmaI	AGACCCGGGAAGAATTCTGGCACCA	pBN29
B200	*npp-2*$_{prom}$ r	BsrGI	ATCTGTACACATCTGAAAGAGATACTAATGTC-ATGTG	pBN29
B071	*npp-2*$_{AUG}$ f	BsrGI	ATGTGTACAGATGTCGCTCGAGAATTCGG	pBN29
B072	*npp-2*$_{3UTR}$ r	SpeI	GTGACTAGTTCTGACTGCGAACCAGACTCT	pBN29
B216	*hsp-16.41* f	NotI	ATGCGGCCGCCAAGCTTGCATGCCTGC	pBN16
B232	*hsp-16.41* r	MCS	TCCACGCGTTGCAGATCTTGAGCCGGCATC-CCCCGGGCATTTGTATAG	pBN16
B233	*unc-54* f	MCS	GCAACGCGTGGAGCTAGCGCATCGCGAAG-CTCCGCATCGGCCGCTGT	pBN16
B217	*unc-54* r	SpeI	ACGGCCGACTAGTAGGAAACA	pBN16
B153	*npp-15* ag f	BamHI	GAGGATCCATCTACGATTTCTACCTGTC	pQE30-Nup133 ag
B154	*npp-15* ag r	PstI	CTCTGCAGTGTCAGCAGGATACGAATTG	pQE30-Nup133 ag
B248	*npp-23* f	BglII	CAAGATCTGCCGTCGTAACAATCACTACGG	pBN27
B249	*npp-23* r	MluI	TCACGCGTTAAAATCTCCCGAAATTGGAATTTGG	pBN27
B236	*npp-15* f	NgoMIV	CAGCCGGCTCGGGACGAGATCTCGAACTA	pBN23
B237	*npp-15* r	NheI	CAGCTAGCTCAAGTCTCCATCATCGAATCA	pBN23
B364	*npp-5* r	ClaI	ATCGATTTCGACTTTGAGATTGAG	pGADT7-npp-5
B366	*npp-5* f	XmaI	CCCGGGCACAGACTTGTTCGCTTCG	pGADT7-npp-5
B367	*mdf-1* r	BamHI	GGATCCGTCCTCGTGTAAGACACT	pGBKT7-mdf-1
B368	*mdf-1* f	NcoI	CCATGGCCAATTACGATGAAGACATT	pGBKT7-mdf-1
B179	*npp-19* f	BamHI	caggatccATGTTCTCGCATCTTAACCA	pGEX-GST-His
B180	*npp-19* r	BamHI	caggatccGTTGAGTCCGATCGTGTTCCA	pGEX-GST-His
B181	*npp-19* r	BamHI	caggatccCAACAAAATCGACACTTGGCTTGG	pGEX-GST-His

Table 8. Primers used in this study

Western blot

Embryos were obtained by hypochlorite treatment (1N NaOH, 30% bleach solution), disrupted by boiling and vortexing in SDS sample buffer together with 0.5 μm diameter glass beads and separated by 10% SDS-PAGE. Proteins were transferred to Immobilon P membranes (Millipore), which were blocked with PBS containing 0.05% Tween-20 and 3% low-fat milk (PBST-M) and probed for 2 h at room temperature with antibodies diluted in PBST-M as described in **Table 9**. Next, membranes were washed with PBST for 1 h, incubated with peroxidase-conjugated secondary antibodies (Sigma-Aldrich, 1:5000–1:10,000) for 2 h at room temperature and developed with ECL Plus (GE Amersham).

Antibody	Western blot	Immuno-fluorescence	Description	Reference
Nup96 / NPP-10C	1:250	1:250	Rabbit polyclonal anti sera GBLC	Galy et al., 2003
Nup107 / NPP-5	1:100	1:100	Rabbit polyclonal affinity purified SG4839 (against peptide Nup107 aa12-25)	This study
Nup133 / NPP-15	1:25	1:10	Rabbit polyclonal affinity purified 62A (against recombinant Nup133 aa739-1024)	This study
ELYS / MEL-28	-	1:300	Rabbit polyclonal antiserum BUD3	Galy et al., 2006
Mad1	-	1:1000	Rabbit polyclonal	Watanabe et al., 2008
Nup35 / NPP-19	1:100	1:25	Rabbit polyclonal affinity purified from OWYL serum	Ródenas et al., 2009
Nup153 / NPP-7	1:300	-	Rabbit polyclonal antiserum BUB4	Galy et al., 2003
Nup155 / NPP-8	1:300	1:200	Rabbit polyclonal antisera BS08	Galy et al., 2003
Nup98 / NPP-10N	1:300	-	Rabbit polyclonal antiserum GBJQ	Galy et al., 2003
mAb414	1:250	-	Mouse monoclonal against FG nucleoporins	Covance MMS-120R
a-tubulin	1:1000	1:300	Mouse monoclonal DM1 alpha	Sigma T9026

Table 9. Antibodies used in this study. Antibodies utilized in this study and the concentrations used for Western blot and immunofluorescence analysis. References are included in manuscript reference list.

Production and purification of antibodies

Nup107 and Nup133 antibodies were raised in rabbits against a synthetic Nup107 peptide (aa 11-26) and recombinant Nup133 (aa 738-1023), respectively.

Nup133 antibodies were affinity purified from sera using an Immobilon-P (Millipore) membrane coated with the Nup133 antigen.

The Nup133 antigen was obtained by overexpresion of the antigen in BL21(DE3)pREP4 bacteria, then the bacteria were lysed with 8M Urea and the antigen was purified using Talon beads (Clontech), which were washed with lysis buffer and eluted six times with 1 ml of elution buffer (800 μL lysis buffer + 200 μL 1M Imidazole) . A total of 6ml of Nup133 antigen was recovered at a concentration of 0.35μg/μL. The antigen (200μL) was then coupled to an Immobilon P membrane (Millipore) of 50 cm^2, and then 300 μL of the antibodies were incubated with the membrane.

Bound antibodies were eluted with 1 ml 0.1 M glycine (pH 2.5) and immediately neutralized with 0.1 ml of 1 M Tris (pH 8.0).

For the Nup107 affinity purification we used 10 mg of the synthetic Nup107 peptide, which was coupled to an Affi-Gel 15 (BioRad) column. 2 ml of anti-Nup107 serum was incubated with Affi-Gel 15 beads O/N at 4 ^{0}C, and eluted twice with 1.5 ml of 0.1 M glycine (pH 2.5) and immediately neutralized with 100 μL of 1M Tris (pH 8.0).

Immunofluorescence

Gravid hermaphrodites were dissected in 3 μl M9 buffer (86 mM NaCl, 22 mM KH_2PO_4, 34 mM Na_2HPO4, 1 mM MgSO4) directly on poly-L-lysine–coated glass slides and covered with 12x12 mm coverslips. To crack the eggshells, slides were transferred immediately to metal plates on top of dry ice. After 15 min (or storage at -80°C) coverslips were flicked off and slides were placed in methanol for 15-18 min at -18°C. After rehydration for 30 min in PBS with 0.1% Tween 20 (PBST) and blocking for 30 min with 10% fetal calf serum in PBST (PBST-F) the embryos were incubated for 2 h with primary antibodies diluted in PBST-F as indicated in **Table 9**. Embryos were washed for 1 h in PBST followed by

incubation for 2 h with secondary antibodies diluted in PBST-F. Secondary antibodies were Alexa Fluor 546-conjugated goat anti-mouse antibodies (Invitrogen, 1:1000) and Alexa Fluor 633-conjugated goat anti-rabbit antibodies (Invitrogen, 1:1000). Embryos were washed again for 1 h in PBST and finally mounted with Mowiol containing 5 µg/ml Hoechst 33258. All steps were at room temperature. Confocal images were obtained with a Leica confocal SPE microscope equipped with a ACS APO 63x/1.3 objective and processed with ImageJ and Adobe Photoshop.

Live embryo imaging

Embryos were mounted in M9 buffer between a cover slip and a 2% agarose pad. Epifluorescence and transmitted light were recorded with a Leica Confocal Microscope TCS SP2 through a HCX PL APO 63×/ 1.4 objective. Images were captured using integrated Leica software and processed with ImageJ and Adobe Photoshop. The laser intensity was adjusted so that no effect on development was observed. Images were collected at 20 s intervals for a total of 20–40 min, except for **Fig. 52** and **Fig. 28B** where images were collected at 5 s and 8s intervals respectively. For extended recordings up to 14 h (**Fig. 46**), samples were sealed with VALAP and z-stacks were acquired at 15 min intervals.
For **Fig. 30** images were collected at 5 s intervals using a NIKON-A1R confocal microscope.
Fluorescent reporters driven by the *hsp-16.41* promoter were induce by a 32.7°C heat shock for 15 min followed by 5 h recovery at 20°C prior to observation.

Dextran microinjection

FITC-labeled 70 kD dextran (Sigma # FD70S) and TRITC-labeled 155 kD dextran (Sigma # T1287) were purified using Nanosep 10K centrifugal device (Nanosep #OD010C33) until a final concentration of 2 mg/mL in PBS. A 1:1 mixture of the two dextrans was injected into the gonads of N2 and BN40 animals, followed by incubation at 20°C for 5 h before dissection.

Transgenics generated by microparticle bombardment

Microparticle bombardment of *C. elegans* unc-119(ed3) hermaphrodites was

carried out using a home-made "gene gun" built at Ralf Schnabel lab at TU Braunschweig (http://www.ifg.tu-bs.de/Schnabel).
For each bombardment, 1 μl of 1–2 μg/l plasmid DNA was coupled to 0.6 mg of 1.0 μm microcarrier gold beads and bombarded onto a monolayer of 10,000 *unc-119(ed3)* L4 and adult hermaphrodites (a 75 μl pellet) placed on a 20 mm diameter lawn of OP50 on 60 mm NGM plates. Worms were allowed to recover for 0.5 to 2 hr after bombardment and were then transferred onto two 100 mm seeded Opti-gro plates and grown at 24 °C. Because *unc-119* mutants cannot form dauers, they die in the absence of food (Maduro and Pilgrim, 1995), making it easy to identify the non-Unc rescued transformants 7–14 days after bombardment. From each plate containing animals rescued for the *unc-119* mutation, individual transformed animals were cloned and their F1 progeny scored for presence of *unc-119* mutants. Homozygous stable lines were identified by the complete absence of *unc-119* mutant progeny over several generations.
To ensure that each line was the result of an independent transformation event, we retained only one transformed line from each Opti-gro plate.

Single copy integration transgenics generated by microinjection (MosSCI)
Transgenic worms were made by injection into EG4322 (ttTi5605 II; unc-119(ed3)) or EG5003 (unc-119(ed3) III; cxTi10882 IV) worms. The standard injection mix consisted of 50 ng/ml repair template, 50 ng/ml Mos1 transposase (either pJL44 ($P_{hsp-16-48}$::transposase) or pJL43.1 (P_{glh-2}::transposase)), 10 ng/ml pBN1 (P_{lmn-1}::mCherry::his-58), 5ng/ml pCFJ104 (P_{myo-3}::mCherry) and 1.25 ng/ml pCFJ90 (P_{myo-2}::mCherry). *unc-119* worms are severely paralyzed and egg-laying defective, so L1–L2 worms were manually distributed across a lawn of OP50, and very young adults were selected for injection. Injected worms were individually transferred to standard NGM plates and placed at 15 °C for a few hours to recover followed by incubation at 25 °C. Plates were scored for the number of phenotypically rescued F1 worms 3 d after injection.
For the heat-shock protocol, clonal populations of stable array-transmitting lines were picked from the F2 progeny. A population of ~500 young adults was heat-shocked for 1 h at 34 °C in a water bath and allowed to recover at 15 °C for several hours. Sets of 20 adult heat-shocked worms were transferred to 10 cm

NGM plates seeded with OP50 bacteria and propagated at 20 °C. When worms on these plates became starved, roughly a quarter of the plate was chunked to a fresh, seeded 10 cm NGM plate and placed at 25 °C. Two to five days later (but before starvation), these plates were visually screened for insertion events based on the presence of nonparalyzed, wild-type worms. Insertion strains were verified on a fluorescence dissection microscope by the lack of fluorescent mCherry coinjection markers and subsequently homozygosed.
For the direct insertion protocol, individual injected worms were allowed to exhaust the food source. Once starved, plates containing transgenic lines were screened for insertion events on a fluorescence dissection microscope based on wild-type movement but complete lack of fluorescent coinjection markers. Plates containing insertion events typically had a large proportion of non- fluorescent moving worms, although some plates only had a few.

Anoxia experiments

Ten gravid young hermaphrodites per condition were placed on a NGM plate for 1 h to lay embryos. The hermaphrodites were removed and plates were placed in an anaerobic jar (Schütt Labortechnik) that was flushed with nitrogen gas (O_2<0.1%). After 21 h at 20°C plates were removed from the jar and development was monitored for 4 d.

Yeast two-hybrid assay

Yeast strain AH109 (Clontech; *MATa, trp1-901, leu2-3, 112, ura3-52, his3-200, gal4Δ, gal80Δ, LYS2::GAL1*$_{UAS}$*-GAL1*$_{TATA}$*-HIS3, GAL2*$_{UAS}$*-GAL2*$_{TATA}$*-ADE2, URA3::MEL1*$_{TATA}$*-lacZ*) was transformed using the LiAc method and selected in the appropriated SC minimal medium. Transformants containing pGBKT7-*mdf-1* and either pGADT7-*npp-5* or pAD-*npp-19* were grown at 30°C to OD_{600} 0.5 in SC-Leu-Trp medium and spotted as 10-fold serial dilutions to detect the ability of growing on minimal medium plates lacking adenine and histidine. Growth was assayed after 3 days at 30°C. Combination of empty pGADT7 and pGBKT7 vectors were also transformed into AH109 with each construct to assess self-activation.

Life-span assay

One hundred WT and 100 homozygous BN40 *npp-5(tm3039)* L4 hermaphrodites were placed on NGM plates containing OP50 bacteria (20 animals per plate). Plates were counted for alive hermaphrodites every 24 hours and adult hermaphrodites were transferred to new plates every 48 hours to ensure separation of different generations.

Electron microscopy

C. elegans hermaphrodites fed bacteria expressing either control or *npp-19* dsRNA were cryo-immobilized using a Leica EM PACT high-pressure freezer (Leica, Vienna, Austria) and processed as described (Franz et al., 2005).

7. References

Ahmed, S., D.G. Brickner, W.H. Light, I. Cajigas, M. McDonough, A.B. Froyshteter, T. Volpe, and J.H. Brickner. 2010. DNA zip codes control an ancient mechanism for gene targeting to the nuclear periphery. *Nat Cell Biol*. 12:111-8.

Akey, C.W., and D.S. Goldfarb. 1989. Protein import through the nuclear pore complex is a multistep process. *J Cell Biol*. 109:971-82.

Akhtar, A., and S.M. Gasser. 2007. The nuclear envelope and transcriptional control. *Nat Rev Genet*. 8:507-17.

Alber, F., S. Dokudovskaya, L.M. Veenhoff, W. Zhang, J. Kipper, D. Devos, A. Suprapto, O. Karni-Schmidt, R. Williams, B.T. Chait, M.P. Rout, and A. Sali. 2007a. Determining the architectures of macromolecular assemblies. *Nature*. 450:683-94.

Alber, F., S. Dokudovskaya, L.M. Veenhoff, W. Zhang, J. Kipper, D. Devos, A. Suprapto, O. Karni-Schmidt, R. Williams, B.T. Chait, A. Sali, and M.P. Rout. 2007b. The molecular architecture of the nuclear pore complex. *Nature*. 450:695-701.

Anderson, D.J., and M.W. Hetzer. 2007. Nuclear envelope formation by chromatin-mediated reorganization of the endoplasmic reticulum. *Nat Cell Biol*. 9:1160-6.

Andres, V., and J.M. Gonzalez. 2009. Role of A-type lamins in signaling, transcription, and chromatin organization. *J Cell Biol*. 187:945-57.

Antonin, W., J. Ellenberg, and E. Dultz. 2008. Nuclear pore complex assembly through the cell cycle: regulation and membrane organization. *FEBS Lett*. 582:2004-16.

Antonin, W., C. Franz, U. Haselmann, C. Antony, and I.W. Mattaj. 2005. The integral membrane nucleoporin pom121 functionally links nuclear pore complex assembly and nuclear envelope formation. *Mol Cell*. 17:83-92.

Askjaer, P., V. Galy, E. Hannak, and I.W. Mattaj. 2002. Ran GTPase cycle and importins alpha and beta are essential for spindle formation and nuclear envelope assembly in living Caenorhabditis elegans embryos. *Mol Biol Cell*. 13:4355-70.

Audhya, A., A. Desai, and K. Oegema. 2007. A role for Rab5 in structuring the endoplasmic reticulum. *J Cell Biol*. 178:43-56.

Bai, S.W., J. Rouquette, M. Umeda, W. Faigle, D. Loew, S. Sazer, and V. Doye. 2004. The fission yeast Nup107-120 complex functionally interacts with the small GTPase Ran/Spi1 and is required for mRNA export, nuclear pore distribution, and proper cell division. *Mol Cell Biol*. 24:6379-92.

Bao, Z., Z. Zhao, T.J. Boyle, J.I. Murray, and R.H. Waterston. 2008. Control of cell cycle timing during C. elegans embryogenesis. *Dev Biol*. 318:65-72.

Beck, M., F. Forster, M. Ecke, J.M. Plitzko, F. Melchior, G. Gerisch, W. Baumeister, and O. Medalia. 2004. Nuclear pore complex structure and dynamics revealed by cryoelectron tomography. *Science*. 306:1387-90.

Beck, M., V. Lucic, F. Forster, W. Baumeister, and O. Medalia. 2007. Snapshots of nuclear pore complexes in action captured by cryo-electron tomography. *Nature*. 449:611-5.

Belgareh, N., G. Rabut, S.W. Bai, M. van Overbeek, J. Beaudouin, N. Daigle, O.V. Zatsepina, F. Pasteau, V. Labas, M. Fromont-Racine, J. Ellenberg, and V.

Doye. 2001. An evolutionarily conserved NPC subcomplex, which redistributes in part to kinetochores in mammalian cells. *J Cell Biol*. 154:1147-60.

Biggins, S., F.F. Severin, N. Bhalla, I. Sassoon, A.A. Hyman, and A.W. Murray. 1999. The conserved protein kinase Ipl1 regulates microtubule binding to kinetochores in budding yeast. *Genes Dev*. 13:532-44.

Boehmer, T., J. Enninga, S. Dales, G. Blobel, and H. Zhong. 2003. Depletion of a single nucleoporin, Nup107, prevents the assembly of a subset of nucleoporins into the nuclear pore complex. *Proc Natl Acad Sci U S A*. 100:981-5.

Boehmer, T., S. Jeudy, I.C. Berke, and T.U. Schwartz. 2008. Structural and functional studies of Nup107/Nup133 interaction and its implications for the architecture of the nuclear pore complex. *Mol Cell*. 30:721-31.

Brauchle, M., K. Baumer, and P. Gonczy. 2003. Differential activation of the DNA replication checkpoint contributes to asynchrony of cell division in C. elegans embryos. *Curr Biol*. 13:819-27.

Brickner, D.G., I. Cajigas, Y. Fondufe-Mittendorf, S. Ahmed, P.C. Lee, J. Widom, and J.H. Brickner. 2007. H2A.Z-mediated localization of genes at the nuclear periphery confers epigenetic memory of previous transcriptional state. *PLoS Biol*. 5:e81.

Brickner, J.H. 2009. Transcriptional memory at the nuclear periphery. *Curr Opin Cell Biol*. 21:127-33.

Brinkley, B.R., and E. Stubblefield. 1966. The fine structure of the kinetochore of a mammalian cell in vitro. *Chromosoma*. 19:28-43.

Brohawn, S.G., N.C. Leksa, E.D. Spear, K.R. Rajashankar, and T.U. Schwartz. 2008. Structural evidence for common ancestry of the nuclear pore complex and vesicle coats. *Science*. 322:1369-73.

Brohawn, S.G., and T.U. Schwartz. 2009. A lattice model of the nuclear pore complex. *Commun Integr Biol*. 2:205-7.

Brown, C.R., and P.A. Silver. 2007. Transcriptional regulation at the nuclear pore complex. *Curr Opin Genet Dev*. 17:100-6.

Burke, B., and J. Ellenberg. 2002. Remodelling the walls of the nucleus. *Nat Rev Mol Cell Biol*. 3:487-97.

Callan, H.G., and S.G. Tomlin. 1950. Experimental studies on amphibian oocyte nuclei. I. Investigation of the structure of the nuclear membrane by means of the electron microscope. *Proc R Soc Lond B Biol Sci*. 137:367-78.

Campbell, M.S., G.K. Chan, and T.J. Yen. 2001. Mitotic checkpoint proteins HsMAD1 and HsMAD2 are associated with nuclear pore complexes in interphase. *J Cell Sci*. 114:953-63.

Capelson, M., Y. Liang, R. Schulte, W. Mair, U. Wagner, and M.W. Hetzer. 2010. Chromatin-bound nuclear pore components regulate gene expression in higher eukaryotes. *Cell*. 140:372-83.

Carmena, M., S. Ruchaud, and W.C. Earnshaw. 2009. Making the Auroras glow: regulation of Aurora A and B kinase function by interacting proteins. *Curr Opin Cell Biol*. 21:796-805.

Casolari, J.M., C.R. Brown, S. Komili, J. West, H. Hieronymus, and P.A. Silver. 2004. Genome-wide localization of the nuclear transport machinery couples transcriptional status and nuclear organization. *Cell*. 117:427-39.

Chadrin, A., B. Hess, M. San Roman, X. Gatti, B. Lombard, D. Loew, Y. Barral, B. Palancade, and V. Doye. 2010. Pom33, a novel transmembrane nucleoporin required for proper nuclear pore complex distribution. *J Cell Biol*. 189:795-811.

Cheeseman, I.M., S. Anderson, M. Jwa, E.M. Green, J. Kang, J.R. Yates, 3rd, C.S. Chan, D.G. Drubin, and G. Barnes. 2002. Phospho-regulation of kinetochore-microtubule attachments by the Aurora kinase Ipl1p. *Cell*. 111:163-72.

Cheeseman, I.M., J.S. Chappie, E.M. Wilson-Kubalek, and A. Desai. 2006. The conserved KMN network constitutes the core microtubule-binding site of the kinetochore. *Cell*. 127:983-97.

Cheeseman, I.M., and A. Desai. 2008. Molecular architecture of the kinetochore-microtubule interface. *Nat Rev Mol Cell Biol*. 9:33-46.

Cheeseman, I.M., S. Niessen, S. Anderson, F. Hyndman, J.R. Yates, 3rd, K. Oegema, and A. Desai. 2004. A conserved protein network controls assembly of the outer kinetochore and its ability to sustain tension. *Genes Dev*. 18:2255-68.

Cohen, M., N. Feinstein, K.L. Wilson, and Y. Gruenbaum. 2003. Nuclear pore protein gp210 is essential for viability in HeLa cells and Caenorhabditis elegans. *Mol Biol Cell*. 14:4230-7.

Collas, P., and J.C. Courvalin. 2000. Sorting nuclear membrane proteins at mitosis. *Trends Cell Biol*. 10:5-8.

Cronshaw, J.M., A.N. Krutchinsky, W. Zhang, B.T. Chait, and M.J. Matunis. 2002. Proteomic analysis of the mammalian nuclear pore complex. *J Cell Biol*. 158:915-27.

D'Angelo, M.A., D.J. Anderson, E. Richard, and M.W. Hetzer. 2006. Nuclear pores form de novo from both sides of the nuclear envelope. *Science*. 312:440-3.

D'Angelo, M.A., and M.W. Hetzer. 2006. The role of the nuclear envelope in cellular organization. *Cell Mol Life Sci*. 63:316-32.

D'Angelo, M.A., and M.W. Hetzer. 2008. Structure, dynamics and function of nuclear pore complexes. *Trends Cell Biol*. 18:456-66.

D'Angelo, M.A., M. Raices, S.H. Panowski, and M.W. Hetzer. 2009. Age-dependent deterioration of nuclear pore complexes causes a loss of nuclear integrity in postmitotic cells. *Cell*. 136:284-95.

Daigle, N., J. Beaudouin, L. Hartnell, G. Imreh, E. Hallberg, J. Lippincott-Schwartz, and J. Ellenberg. 2001. Nuclear pore complexes form immobile networks and have a very low turnover in live mammalian cells. *J Cell Biol*. 154:71-84.

Dawson, T.R., M.D. Lazarus, M.W. Hetzer, and S.R. Wente. 2009. ER membrane-bending proteins are necessary for de novo nuclear pore formation. *J Cell Biol*. 184:659-75.

Debler, E.W., Y. Ma, H.S. Seo, K.C. Hsia, T.R. Noriega, G. Blobel, and A. Hoelz. 2008. A fence-like coat for the nuclear pore membrane. *Mol Cell*. 32:815-26.

DeLuca, J.G., B. Moree, J.M. Hickey, J.V. Kilmartin, and E.D. Salmon. 2002. hNuf2 inhibition blocks stable kinetochore-microtubule attachment and induces mitotic cell death in HeLa cells. *J Cell Biol*. 159:549-55.

Deppe, U., E. Schierenberg, T. Cole, C. Krieg, D. Schmitt, B. Yoder, and G. von Ehrenstein. 1978. Cell lineages of the embryo of the nematode Caenorhabditis elegans. *Proc Natl Acad Sci U S A*. 75:376-80.

Deyter, G.M., T. Furuta, Y. Kurasawa, and J.M. Schumacher. 2010. Caenorhabditis elegans cyclin B3 is required for multiple mitotic processes including alleviation of a spindle checkpoint-dependent block in anaphase chromosome segregation. *PLoS Genet*. 6:e1001218.

Ditchfield, C., V.L. Johnson, A. Tighe, R. Ellston, C. Haworth, T. Johnson, A. Mortlock, N. Keen, and S.S. Taylor. 2003. Aurora B couples chromosome alignment with anaphase by targeting BubR1, Mad2, and Cenp-E to kinetochores. *J Cell Biol*. 161:267-80.

Dong, Y., K.J. Vanden Beldt, X. Meng, A. Khodjakov, and B.F. McEwen. 2007. The outer plate in vertebrate kinetochores is a flexible network with multiple microtubule interactions. *Nat Cell Biol*. 9:516-22.

Doucet, C.M., J.A. Talamas, and M.W. Hetzer. 2010. Cell cycle-dependent differences in nuclear pore complex assembly in metazoa. *Cell*. 141:1030-41.

Doye, V., R. Wepf, and E.C. Hurt. 1994. A novel nuclear pore protein Nup133p with distinct roles in poly(A)+ RNA transport and nuclear pore distribution. *EMBO J*. 13:6062-75.

Drin, G., J.F. Casella, R. Gautier, T. Boehmer, T.U. Schwartz, and B. Antonny. 2007. A general amphipathic alpha-helical motif for sensing membrane curvature. *Nat Struct Mol Biol*. 14:138-46.

Dultz, E., and J. Ellenberg. 2010. Live imaging of single nuclear pores reveals unique assembly kinetics and mechanism in interphase. *J Cell Biol*. 191:15-22.

Earnshaw, W.C., and R.L. Bernat. 1991. Chromosomal passengers: toward an integrated view of mitosis. *Chromosoma*. 100:139-46.

Earnshaw, W.C., and B.R. Migeon. 1985. Three related centromere proteins are absent from the inactive centromere of a stable isodicentric chromosome. *Chromosoma*. 92:290-6.

Ellenberg, J., E.D. Siggia, J.E. Moreira, C.L. Smith, J.F. Presley, H.J. Worman, and J. Lippincott-Schwartz. 1997. Nuclear membrane dynamics and reassembly in living cells: targeting of an inner nuclear membrane protein in interphase and mitosis. *J Cell Biol*. 138:1193-206.

Encalada, S.E., J. Willis, R. Lyczak, and B. Bowerman. 2005. A spindle checkpoint functions during mitosis in the early Caenorhabditis elegans embryo. *Mol Biol Cell*. 16:1056-70.

Enninga, J., A. Levay, and B.M. Fontoura. 2003. Sec13 shuttles between the nucleus and the cytoplasm and stably interacts with Nup96 at the nuclear pore complex. *Mol Cell Biol*. 23:7271-84.

Essex, A., A. Dammermann, L. Lewellyn, K. Oegema, and A. Desai. 2009. Systematic analysis in Caenorhabditis elegans reveals that the spindle checkpoint is composed of two largely independent branches. *Mol Biol Cell*. 20:1252-67.

Fang, G., H. Yu, and M.W. Kirschner. 1998. Direct binding of CDC20 protein family members activates the anaphase-promoting complex in mitosis and G1. *Mol Cell*. 2:163-71.

Favreau, C., H.J. Worman, R.W. Wozniak, T. Frappier, and J.C. Courvalin. 1996. Cell cycle-dependent phosphorylation of nucleoporins and nuclear pore membrane protein Gp210. *Biochemistry*. 35:8035-44.

Fernandez, A.G., and F. Piano. 2006. MEL-28 is downstream of the Ran cycle and is required for nuclear-envelope function and chromatin maintenance. *Curr Biol*. 16:1757-63.

Finlan, L.E., D. Sproul, I. Thomson, S. Boyle, E. Kerr, P. Perry, B. Ylstra, J.R. Chubb, and W.A. Bickmore. 2008. Recruitment to the nuclear periphery can alter expression of genes in human cells. *PLoS Genet*. 4:e1000039.

Franz, C., P. Askjaer, W. Antonin, C.L. Iglesias, U. Haselmann, M. Schelder, A. de Marco, M. Wilm, C. Antony, and I.W. Mattaj. 2005. Nup155 regulates nuclear envelope and nuclear pore complex formation in nematodes and vertebrates. *EMBO J*. 24:3519-31.

Franz, C., R. Walczak, S. Yavuz, R. Santarella, M. Gentzel, P. Askjaer, V. Galy, M. Hetzer, I.W. Mattaj, and W. Antonin. 2007. MEL-28/ELYS is required for the recruitment of nucleoporins to chromatin and postmitotic nuclear pore complex assembly. *EMBO Rep*. 8:165-72.

Frey, S., and D. Gorlich. 2009. FG/FxFG as well as GLFG repeats form a selective permeability barrier with self-healing properties. *EMBO J*. 28:2554-67.

Frey, S., R.P. Richter, and D. Gorlich. 2006. FG-rich repeats of nuclear pore proteins form a three-dimensional meshwork with hydrogel-like properties. *Science*. 314:815-7.

Frokjaer-Jensen, C., M.W. Davis, C.E. Hopkins, B.J. Newman, J.M. Thummel, S.P. Olesen, M. Grunnet, and E.M. Jorgensen. 2008. Single-copy insertion of transgenes in Caenorhabditis elegans. *Nat Genet*. 40:1375-83.

Fujita, Y., T. Hayashi, T. Kiyomitsu, Y. Toyoda, A. Kokubu, C. Obuse, and M. Yanagida. 2007. Priming of centromere for CENP-A recruitment by human hMis18alpha, hMis18beta, and M18BP1. *Dev Cell*. 12:17-30.

Gall, J.G. 1967. Octagonal nuclear pores. *J Cell Biol*. 32:391-9.

Galy, V., P. Askjaer, C. Franz, C. Lopez-Iglesias, and I.W. Mattaj. 2006. MEL-28, a novel nuclear-envelope and kinetochore protein essential for zygotic nuclear-envelope assembly in C. elegans. *Curr Biol*. 16:1748-56.

Galy, V., I.W. Mattaj, and P. Askjaer. 2003. Caenorhabditis elegans nucleoporins Nup93 and Nup205 determine the limit of nuclear pore complex size exclusion in vivo. *Mol Biol Cell*. 14:5104-15.

Gillespie, P.J., G.A. Khoudoli, G. Stewart, J.R. Swedlow, and J.J. Blow. 2007. ELYS/MEL-28 chromatin association coordinates nuclear pore complex assembly and replication licensing. *Curr Biol*. 17:1657-62.

Glavy, J.S., A.N. Krutchinsky, I.M. Cristea, I.C. Berke, T. Boehmer, G. Blobel, and B.T. Chait. 2007. Cell-cycle-dependent phosphorylation of the nuclear pore Nup107-160 subcomplex. *Proc Natl Acad Sci U S A*. 104:3811-6.

Gonczy, P., C. Echeverri, K. Oegema, A. Coulson, S.J. Jones, R.R. Copley, J. Duperon, J. Oegema, M. Brehm, E. Cassin, E. Hannak, M. Kirkham, S. Pichler, K. Flohrs, A. Goessen, S. Leidel, A.M. Alleaume, C. Martin, N. Ozlu, P. Bork, and A.A. Hyman. 2000. Functional genomic analysis of cell division in C. elegans using RNAi of genes on chromosome III. *Nature*. 408:331-6.

Gorjanacz, M., A. Jaedicke, and I.W. Mattaj. 2007a. What can Caenorhabditis elegans tell us about the nuclear envelope? *FEBS Lett*. 581:2794-801.

Gorjanacz, M., E.P. Klerkx, V. Galy, R. Santarella, C. Lopez-Iglesias, P. Askjaer, and I.W. Mattaj. 2007b. Caenorhabditis elegans BAF-1 and its kinase VRK-1 participate directly in post-mitotic nuclear envelope assembly. *EMBO J*. 26:132-43.

Guelen, L., L. Pagie, E. Brasset, W. Meuleman, M.B. Faza, W. Talhout, B.H. Eussen, A. de Klein, L. Wessels, W. de Laat, and B. van Steensel. 2008. Domain organization of human chromosomes revealed by mapping of nuclear lamina interactions. *Nature*. 453:948-51.

Gupta, B.P., and P.W. Sternberg. 2002. Tissue-specific regulation of the LIM homeobox gene lin-11 during development of the Caenorhabditis elegans egg-laying system. *Dev Biol*. 247:102-15.

Haithcock, E., Y. Dayani, E. Neufeld, A.J. Zahand, N. Feinstein, A. Mattout, Y. Gruenbaum, and J. Liu. 2005. Age-related changes of nuclear architecture in Caenorhabditis elegans. *Proc Natl Acad Sci U S A*. 102:16690-5.

Hajeri, V.A., B.A. Little, M.L. Ladage, and P.A. Padilla. 2010. NPP-16/Nup50 function and CDK-1 inactivation are associated with anoxia-induced prophase arrest in Caenorhabditis elegans. *Mol Biol Cell*. 21:712-24.

Handa, N., M. Kukimoto-Niino, R. Akasaka, S. Kishishita, K. Murayama, T. Terada, M. Inoue, T. Kigawa, S. Kose, N. Imamoto, A. Tanaka, Y. Hayashizaki, M. Shirouzu, and S. Yokoyama. 2006. The crystal structure of mouse Nup35 reveals atypical RNP motifs and novel homodimerization of the RRM domain. *J Mol Biol*. 363:114-24.

Harel, A., R.C. Chan, A. Lachish-Zalait, E. Zimmerman, M. Elbaum, and D.J. Forbes. 2003a. Importin beta negatively regulates nuclear membrane fusion and nuclear pore complex assembly. *Mol Biol Cell*. 14:4387-96.

Harel, A., A.V. Orjalo, T. Vincent, A. Lachish-Zalait, S. Vasu, S. Shah, E. Zimmerman, M. Elbaum, and D.J. Forbes. 2003b. Removal of a single pore subcomplex results in vertebrate nuclei devoid of nuclear pores. *Mol Cell*. 11:853-64.

Hauf, S., R.W. Cole, S. LaTerra, C. Zimmer, G. Schnapp, R. Walter, A. Heckel, J. van Meel, C.L. Rieder, and J.M. Peters. 2003. The small molecule Hesperadin reveals a role for Aurora B in correcting kinetochore-microtubule attachment and in maintaining the spindle assembly checkpoint. *J Cell Biol*. 161:281-94.

Hawryluk-Gara, L.A., M. Platani, R. Santarella, R.W. Wozniak, and I.W. Mattaj. 2008. Nup53 is required for nuclear envelope and nuclear pore complex assembly. *Mol Biol Cell*. 19:1753-62.

Hawryluk-Gara, L.A., E.K. Shibuya, and R.W. Wozniak. 2005. Vertebrate Nup53 interacts with the nuclear lamina and is required for the assembly of a Nup93-containing complex. *Mol Biol Cell*. 16:2382-94.

Hayashi, T., Y. Fujita, O. Iwasaki, Y. Adachi, K. Takahashi, and M. Yanagida. 2004. Mis16 and Mis18 are required for CENP-A loading and histone deacetylation at centromeres. *Cell*. 118:715-29.

Heath, C.V., C.S. Copeland, D.C. Amberg, V. Del Priore, M. Snyder, and C.N. Cole. 1995. Nuclear pore complex clustering and nuclear accumulation of poly(A)+ RNA associated with mutation of the Saccharomyces cerevisiae RAT2/NUP120 gene. *J Cell Biol*. 131:1677-97.

Hediger, F., F.R. Neumann, G. Van Houwe, K. Dubrana, and S.M. Gasser. 2002. Live imaging of telomeres: yKu and Sir proteins define redundant telomere-anchoring pathways in yeast. *Curr Biol*. 12:2076-89.

Henderson, S.T., and T.E. Johnson. 2001. daf-16 integrates developmental and environmental inputs to mediate aging in the nematode Caenorhabditis elegans. *Curr Biol*. 11:1975-80.

Herndon, L.A., P.J. Schmeissner, J.M. Dudaronek, P.A. Brown, K.M. Listner, Y. Sakano, M.C. Paupard, D.H. Hall, and M. Driscoll. 2002. Stochastic and genetic factors influence tissue-specific decline in ageing C. elegans. *Nature*. 419:808-14.

Hetzer, M.W. 2010a. The nuclear envelope. *Cold Spring Harb Perspect Biol*. 2:a000539.

Hetzer, M.W. 2010b. The role of the nuclear pore complex in aging of post-mitotic cells. *Aging (Albany NY)*. 2:74-5.

Hetzer, M.W., T.C. Walther, and I.W. Mattaj. 2005. Pushing the envelope: structure, function, and dynamics of the nuclear periphery. *Annu Rev Cell Dev Biol*. 21:347-80.

Hetzer, M.W., and S.R. Wente. 2009. Border control at the nucleus: biogenesis and organization of the nuclear membrane and pore complexes. *Dev Cell*. 17:606-16.

Hoyt, M.A., L. Totis, and B.T. Roberts. 1991. S. cerevisiae genes required for cell cycle arrest in response to loss of microtubule function. *Cell*. 66:507-17.

Hsia, K.C., P. Stavropoulos, G. Blobel, and A. Hoelz. 2007. Architecture of a coat for the nuclear pore membrane. *Cell*. 131:1313-26.

Hwang, L.H., L.F. Lau, D.L. Smith, C.A. Mistrot, K.G. Hardwick, E.S. Hwang, A. Amon, and A.W. Murray. 1998. Budding yeast Cdc20: a target of the spindle checkpoint. *Science*. 279:1041-4.

Iouk, T., O. Kerscher, R.J. Scott, M.A. Basrai, and R.W. Wozniak. 2002. The yeast nuclear pore complex functionally interacts with components of the spindle assembly checkpoint. *J Cell Biol*. 159:807-19.

Joseph, J., S.H. Tan, T.S. Karpova, J.G. McNally, and M. Dasso. 2002. SUMO-1 targets RanGAP1 to kinetochores and mitotic spindles. *J Cell Biol*. 156:595-602.

Kalverda, B., H. Pickersgill, V.V. Shloma, and M. Fornerod. 2010. Nucleoporins directly stimulate expression of developmental and cell-cycle genes inside the nucleoplasm. *Cell*. 140:360-71.

Kalverda, B., M.D. Roling, and M. Fornerod. 2008. Chromatin organization in relation to the nuclear periphery. *FEBS Lett*. 582:2017-22.

Kamath, R.S., A.G. Fraser, Y. Dong, G. Poulin, R. Durbin, M. Gotta, A. Kanapin, N. Le Bot, S. Moreno, M. Sohrmann, D.P. Welchman, P. Zipperlen, and J. Ahringer. 2003. Systematic functional analysis of the Caenorhabditis elegans genome using RNAi. *Nature*. 421:231-7.

Kampmann, M., and G. Blobel. 2009. Three-dimensional structure and flexibility of a membrane-coating module of the nuclear pore complex. *Nat Struct Mol Biol*. 16:782-8.

Katsani, K.R., R.E. Karess, N. Dostatni, and V. Doye. 2008. In vivo dynamics of Drosophila nuclear envelope components. *Mol Biol Cell*. 19:3652-66.

Khadaroo, B., M.T. Teixeira, P. Luciano, N. Eckert-Boulet, S.M. Germann, M.N. Simon, I. Gallina, P. Abdallah, E. Gilson, V. Geli, and M. Lisby. 2009. The DNA damage response at eroded telomeres and tethering to the nuclear pore complex. *Nat Cell Biol*. 11:980-7.

Kohler, A., and E. Hurt. 2007. Exporting RNA from the nucleus to the cytoplasm. *Nat Rev Mol Cell Biol*. 8:761-73.

Kohler, A., and E. Hurt. 2010. Gene regulation by nucleoporins and links to cancer. *Mol Cell*. 38:6-15.

Kraemer, D., R.W. Wozniak, G. Blobel, and A. Radu. 1994. The human CAN protein, a putative oncogene product associated with myeloid leukemogenesis, is a nuclear pore complex protein that faces the cytoplasm. *Proc Natl Acad Sci U S A*. 91:1519-23.

Kuersten, S., M. Ohno, and I.W. Mattaj. 2001. Nucleocytoplasmic transport: Ran, beta and beyond. *Trends Cell Biol*. 11:497-503.

Kumaran, R.I., and D.L. Spector. 2008. A genetic locus targeted to the nuclear periphery in living cells maintains its transcriptional competence. *J Cell Biol*. 180:51-65.

Lampson, M.A., and I.M. Cheeseman. 2010. Sensing centromere tension: Aurora B and the regulation of kinetochore function. *Trends Cell Biol*.

Lampson, M.A., K. Renduchitala, A. Khodjakov, and T.M. Kapoor. 2004. Correcting improper chromosome-spindle attachments during cell division. *Nat Cell Biol*. 6:232-7.

Lange, A., R.E. Mills, C.J. Lange, M. Stewart, S.E. Devine, and A.H. Corbett. 2007. Classical nuclear localization signals: definition, function, and interaction with importin alpha. *J Biol Chem*. 282:5101-5.

Lee, K.K., D. Starr, M. Cohen, J. Liu, M. Han, K.L. Wilson, and Y. Gruenbaum. 2002. Lamin-dependent localization of UNC-84, a protein required for nuclear migration in Caenorhabditis elegans. *Mol Biol Cell*. 13:892-901.

Lee, S.H., H. Sterling, A. Burlingame, and F. McCormick. 2008. Tpr directly binds to Mad1 and Mad2 and is important for the Mad1-Mad2-mediated mitotic spindle checkpoint. *Genes Dev*. 22:2926-31.

Lenart, P., G. Rabut, N. Daigle, A.R. Hand, M. Terasaki, and J. Ellenberg. 2003. Nuclear envelope breakdown in starfish oocytes proceeds by partial NPC disassembly followed by a rapidly spreading fenestration of nuclear membranes. *J Cell Biol*. 160:1055-68.

Li, H.Y., and Y. Zheng. 2004. Phosphorylation of RCC1 in mitosis is essential for producing a high RanGTP concentration on chromosomes and for spindle assembly in mammalian cells. *Genes Dev*. 18:512-27.

Li, R., and A.W. Murray. 1991. Feedback control of mitosis in budding yeast. *Cell*. 66:519-31.

Lim, R.Y., and B. Fahrenkrog. 2006. The nuclear pore complex up close. *Curr Opin Cell Biol*. 18:342-7.

Lim, R.Y., B. Fahrenkrog, J. Koser, K. Schwarz-Herion, J. Deng, and U. Aebi. 2007. Nanomechanical basis of selective gating by the nuclear pore complex. *Science*. 318:640-3.

Lim, R.Y., N.P. Huang, J. Koser, J. Deng, K.H. Lau, K. Schwarz-Herion, B. Fahrenkrog, and U. Aebi. 2006. Flexible phenylalanine-glycine nucleoporins as entropic barriers to nucleocytoplasmic transport. *Proc Natl Acad Sci U S A*. 103:9512-7.

Loiodice, I., A. Alves, G. Rabut, M. Van Overbeek, J. Ellenberg, J.B. Sibarita, and V. Doye. 2004. The entire Nup107-160 complex, including three new members, is targeted as one entity to kinetochores in mitosis. *Mol Biol Cell*. 15:3333-44.

Luders, J., and T. Stearns. 2007. Microtubule-organizing centres: a re-evaluation. *Nat Rev Mol Cell Biol*. 8:161-7.

Lusk, C.P., D.D. Waller, T. Makhnevych, A. Dienemann, M. Whiteway, D.Y. Thomas, and R.W. Wozniak. 2007. Nup53p is a target of two mitotic kinases, Cdk1p and Hrr25p. *Traffic*. 8:647-60.

Lussi, Y.C., D.K. Shumaker, T. Shimi, and B. Fahrenkrog. 2010. The nucleoporin Nup153 affects spindle checkpoint activity due to an association with Mad1. *Nucleus*. 1:71-84.

Lutzmann, M., R. Kunze, A. Buerer, U. Aebi, and E. Hurt. 2002. Modular self-assembly of a Y-shaped multiprotein complex from seven nucleoporins. *Embo J*. 21:387-97.

Macaulay, C., and D.J. Forbes. 1996. Assembly of the nuclear pore: biochemically distinct steps revealed with NEM, GTP gamma S, and BAPTA. *J. Cell Biol.* 132:5-20.

Macaulay, C., E. Meier, and D.J. Forbes. 1995. Differential mitotic phosphorylation of proteins of the nuclear pore complex. *J Biol Chem*. 270:254-62.

Maddox, P.S., F. Hyndman, J. Monen, K. Oegema, and A. Desai. 2007. Functional genomics identifies a Myb domain-containing protein family required for assembly of CENP-A chromatin. *J Cell Biol*. 176:757-63.

Maduro, M., and D. Pilgrim. 1995. Identification and cloning of unc-119, a gene expressed in the Caenorhabditis elegans nervous system. *Genetics*. 141:977-88.

Malone, C.J., L. Misner, N. Le Bot, M.C. Tsai, J.M. Campbell, J. Ahringer, and J.G. White. 2003. The C. elegans hook protein, ZYG-12, mediates the essential attachment between the centrosome and nucleus. *Cell*. 115:825-36.

Mansfeld, J., S. Guttinger, L.A. Hawryluk-Gara, N. Pante, M. Mall, V. Galy, U. Haselmann, P. Muhlhausser, R.W. Wozniak, I.W. Mattaj, U. Kutay, and W. Antonin. 2006. The conserved transmembrane nucleoporin NDC1 is required for nuclear pore complex assembly in vertebrate cells. *Mol Cell*. 22:93-103.

Marelli, M., C.P. Lusk, H. Chan, J.D. Aitchison, and R.W. Wozniak. 2001. A link between the synthesis of nucleoporins and the biogenesis of the nuclear envelope. *J Cell Biol*. 153:709-24.

Maresca, T.J., and E.D. Salmon. 2009. Intrakinetochore stretch is associated with changes in kinetochore phosphorylation and spindle assembly checkpoint activity. *J Cell Biol*. 184:373-81.

Maresca, T.J., and E.D. Salmon. 2010. Welcome to a new kind of tension: translating kinetochore mechanics into a wait-anaphase signal. *J Cell Sci*. 123:825-35.

Maul, G.G., H.M. Maul, J.E. Scogna, M.W. Lieberman, G.S. Stein, B.Y.-L. Hsu, and T.W. Borun. 1972. TIME SEQUENCE OF NUCLEAR PORE FORMATION IN PHYTOHEMAGGLUTININ-STIMULATED LYMPHOCYTES AND IN HELA CELLS DURING THE CELL CYCLE. *J. Cell Biol.* 55:433-447.

McCleland, M.L., R.D. Gardner, M.J. Kallio, J.R. Daum, G.J. Gorbsky, D.J. Burke, and P.T. Stukenberg. 2003. The highly conserved Ndc80 complex is required for kinetochore assembly, chromosome congression, and spindle checkpoint activity. *Genes Dev*. 17:101-14.

McEwen, B.F., Y. Dong, and K.J. VandenBeldt. 2007. Using electron microscopy to understand functional mechanisms of chromosome alignment on the mitotic spindle. *Methods Cell Biol*. 79:259-93.

McNally, K., A. Audhya, K. Oegema, and F.J. McNally. 2006. Katanin controls mitotic and meiotic spindle length. *J Cell Biol*. 175:881-91.

Mekhail, K., and D. Moazed. 2010. The nuclear envelope in genome organization, expression and stability. *Nat Rev Mol Cell Biol*. 11:317-28.

Mishra, R.K., P. Chakraborty, A. Arnaoutov, B.M. Fontoura, and M. Dasso. 2010. The Nup107-160 complex and gamma-TuRC regulate microtubule polymerization at kinetochores. *Nat Cell Biol*. 12:164-9.

Mitchell, J.M., J. Mansfeld, J. Capitanio, U. Kutay, and R.W. Wozniak. 2010. Pom121 links two essential subcomplexes of the nuclear pore complex core to the membrane. *J Cell Biol*. 191:505-21.

Nachury, M.V., and K. Weis. 1999. The direction of transport through the nuclear pore can be inverted. *Proc Natl Acad Sci U S A*. 96:9622-7.

Nagai, S., K. Dubrana, M. Tsai-Pflugfelder, M.B. Davidson, T.M. Roberts, G.W. Brown, E. Varela, F. Hediger, S.M. Gasser, and N.J. Krogan. 2008. Functional targeting of DNA damage to a nuclear pore-associated SUMO-dependent ubiquitin ligase. *Science*. 322:597-602.

Nystul, T.G., J.P. Goldmark, P.A. Padilla, and M.B. Roth. 2003. Suspended animation in C. elegans requires the spindle checkpoint. *Science*. 302:1038-41.

Onischenko, E.A., N.V. Gubanova, E.V. Kiseleva, and E. Hallberg. 2005. Cdk1 and okadaic acid-sensitive phosphatases control assembly of nuclear pore complexes in Drosophila embryos. *Mol Biol Cell*. 16:5152-62.

Orjalo, A.V., A. Arnaoutov, Z. Shen, Y. Boyarchuk, S.G. Zeitlin, B. Fontoura, S. Briggs, M. Dasso, and D.J. Forbes. 2006. The Nup107-160 nucleoporin complex is required for correct bipolar spindle assembly. *Mol Biol Cell*. 17:3806-18.

Osmani, A.H., J. Davies, H.L. Liu, A. Nile, and S.A. Osmani. 2006. Systematic deletion and mitotic localization of the nuclear pore complex proteins of Aspergillus nidulans. *Mol Biol Cell*. 17:4946-61.

Oza, P., S.L. Jaspersen, A. Miele, J. Dekker, and C.L. Peterson. 2009. Mechanisms that regulate localization of a DNA double-strand break to the nuclear periphery. *Genes Dev*. 23:912-27.

Oza, P., and C.L. Peterson. 2010. Opening the DNA repair toolbox: localization of DNA double strand breaks to the nuclear periphery. *Cell Cycle*. 9:43-9.

Padmakumar, V.C., S. Abraham, S. Braune, A.A. Noegel, B. Tunggal, I. Karakesisoglou, and E. Korenbaum. 2004. Enaptin, a giant actin-binding protein, is an element of the nuclear membrane and the actin cytoskeleton. *Exp Cell Res*. 295:330-9.

Palancade, B., X. Liu, M. Garcia-Rubio, A. Aguilera, X. Zhao, and V. Doye. 2007. Nucleoporins prevent DNA damage accumulation by modulating Ulp1-dependent sumoylation processes. *Mol Biol Cell*. 18:2912-23.

Palmer, D.K., K. O'Day, H.L. Trong, H. Charbonneau, and R.L. Margolis. 1991. Purification of the centromere-specific protein CENP-A and demonstration that it is a distinctive histone. *Proc Natl Acad Sci U S A*. 88:3734-8.

Pinsky, B.A., C. Kung, K.M. Shokat, and S. Biggins. 2006. The Ipl1-Aurora protein kinase activates the spindle checkpoint by creating unattached kinetochores. *Nat Cell Biol*. 8:78-83.

Platani, M., R. Santarella-Mellwig, M. Posch, R. Walczak, J.R. Swedlow, and I.W. Mattaj. 2009. The Nup107-160 nucleoporin complex promotes mitotic events via control of the localization state of the chromosome passenger complex. *Mol Biol Cell*. 20:5260-75.

Praitis, V., E. Casey, D. Collar, and J. Austin. 2001. Creation of low-copy integrated transgenic lines in Caenorhabditis elegans. *Genetics*. 157:1217-26.

Pyrpasopoulou, A., J. Meier, C. Maison, G. Simos, and S.D. Georgatos. 1996. The lamin B receptor (LBR) provides essential chromatin docking sites at the nuclear envelope. *EMBO J*. 15:7108-19.

Rabut, G., V. Doye, and J. Ellenberg. 2004. Mapping the dynamic organization of the nuclear pore complex inside single living cells. *Nat Cell Biol*. 6:1114-21.

Rasala, B.A., A.V. Orjalo, Z. Shen, S. Briggs, and D.J. Forbes. 2006. ELYS is a dual nucleoporin/kinetochore protein required for nuclear pore assembly and proper cell division. *Proc Natl Acad Sci U S A*. 103:17801-6.

Rasala, B.A., C. Ramos, A. Harel, and D.J. Forbes. 2008. Capture of AT-rich Chromatin by ELYS Recruits POM121 and NDC1 to Initiate Nuclear Pore Assembly. *Mol Biol Cell*. 19:3982-96.

Reddy, K.L., J.M. Zullo, E. Bertolino, and H. Singh. 2008. Transcriptional repression mediated by repositioning of genes to the nuclear lamina. *Nature*. 452:243-7.

Reese, K.J., M.A. Dunn, J.A. Waddle, and G. Seydoux. 2000. Asymmetric segregation of PIE-1 in C. elegans is mediated by two complementary mechanisms that act through separate PIE-1 protein domains. *Mol Cell*. 6:445-55.

Rodenas, E., E.P. Klerkx, C. Ayuso, A. Audhya, and P. Askjaer. 2009. Early embryonic requirement for nucleoporin Nup35/NPP-19 in nuclear assembly. *Dev Biol*. 327:399-409.

Rout, M.P., J.D. Aitchison, A. Suprapto, K. Hjertaas, Y. Zhao, and B.T. Chait. 2000. The yeast nuclear pore complex: composition, architecture, and transport mechanism. *J Cell Biol*. 148:635-51.

Ruchaud, S., M. Carmena, and W.C. Earnshaw. 2007. Chromosomal passengers: conducting cell division. *Nat Rev Mol Cell Biol*. 8:798-812.

Ryan, K.J., J.M. McCaffery, and S.R. Wente. 2003. The Ran GTPase cycle is required for yeast nuclear pore complex assembly. *J Cell Biol*. 160:1041-53.

Salina, D., P. Enarson, J.B. Rattner, and B. Burke. 2003. Nup358 integrates nuclear envelope breakdown with kinetochore assembly. *J Cell Biol*. 162:991-1001.

Sasagawa, S., A. Yamamoto, T. Ichimura, S. Omata, and T. Horigome. 1999. In vitro nuclear assembly with affinity-purified nuclear envelope precursor vesicle fractions, PV1 and PV2. *Eur J Cell Biol*. 78:593-600.

Scaffidi, P., and T. Misteli. 2006. Lamin A-dependent nuclear defects in human aging. *Science*. 312:1059-63.

Schirmer, E.C., and L. Gerace. 2002. Organellar proteomics: the prizes and pitfalls of opening the nuclear envelope. *Genome Biol*. 3:REVIEWS1008.

Schwartz, T.U. 2005. Modularity within the architecture of the nuclear pore complex. *Curr Opin Struct Biol*. 15:221-6.

Scott, R.J., C.P. Lusk, D.J. Dilworth, J.D. Aitchison, and R.W. Wozniak. 2005. Interactions between Mad1p and the nuclear transport machinery in the yeast Saccharomyces cerevisiae. *Mol Biol Cell*. 16:4362-74.

Seo, H.S., Y. Ma, E.W. Debler, D. Wacker, S. Kutik, G. Blobel, and A. Hoelz. 2009. Structural and functional analysis of Nup120 suggests ring formation of the Nup84 complex. *Proc Natl Acad Sci U S A*. 106:14281-6.

Siniossoglou, S., C. Wimmer, M. Rieger, V. Doye, H. Tekotte, C. Weise, S. Emig, A. Segref, and E.C. Hurt. 1996. A novel complex of nucleoporins, which includes Sec13p and a Sec13p homolog, is essential for normal nuclear pores. *Cell*. 84:265-75.

Starr, D.A., and M. Han. 2002. Role of ANC-1 in tethering nuclei to the actin cytoskeleton. *Science*. 298:406-9.

Starr, D.A., G.J. Hermann, C.J. Malone, W. Fixsen, J.R. Priess, H.R. Horvitz, and M. Han. 2001. unc-83 encodes a novel component of the nuclear envelope and is essential for proper nuclear migration. *Development*. 128:5039-50.

Stemmann, O., H. Zou, S.A. Gerber, S.P. Gygi, and M.W. Kirschner. 2001. Dual inhibition of sister chromatid separation at metaphase. *Cell*. 107:715-26.

Stewart, M. 2007. Molecular mechanism of the nuclear protein import cycle. *Nat Rev Mol Cell Biol*. 8:195-208.

Stiernagle, T. 2006. Maintenance of C. elegans. *WormBook*:1-11.

Sullivan, K.F., M. Hechenberger, and K. Masri. 1994. Human CENP-A contains a histone H3 related histone fold domain that is required for targeting to the centromere. *J Cell Biol*. 127:581-92.

Suntharalingam, M., and S.R. Wente. 2003. Peering through the pore: nuclear pore complex structure, assembly, and function. *Dev Cell*. 4:775-89.

Tan-Wong, S.M., H.D. Wijayatilake, and N.J. Proudfoot. 2009. Gene loops function to maintain transcriptional memory through interaction with the nuclear pore complex. *Genes Dev*. 23:2610-24.

Tanaka, T.U. 2010. Kinetochore-microtubule interactions: steps towards bi-orientation. *EMBO J*. 29:4070-82.

Towbin, B.D., P. Meister, and S.M. Gasser. 2009. The nuclear envelope--a scaffold for silencing? *Curr Opin Genet Dev*. 19:180-6.

Uchida, K.S., K. Takagaki, K. Kumada, Y. Hirayama, T. Noda, and T. Hirota. 2009. Kinetochore stretching inactivates the spindle assembly checkpoint. *J Cell Biol*. 184:383-90.

Uetz, P., L. Giot, G. Cagney, T.A. Mansfield, R.S. Judson, J.R. Knight, D. Lockshon, V. Narayan, M. Srinivasan, P. Pochart, A. Qureshi-Emili, Y. Li, B. Godwin, D. Conover, T. Kalbfleisch, G. Vijayadamodar, M. Yang, M. Johnston, S. Fields, and J.M. Rothberg. 2000. A comprehensive analysis of protein-protein interactions in Saccharomyces cerevisiae. *Nature*. 403:623-7.

Vader, G., C.W. Cruijsen, T. van Harn, M.J. Vromans, R.H. Medema, and S.M. Lens. 2007. The chromosomal passenger complex controls spindle checkpoint function independent from its role in correcting microtubule kinetochore interactions. *Mol Biol Cell*. 18:4553-64.

Vader, G., A.F. Maia, and S.M. Lens. 2008. The chromosomal passenger complex and the spindle assembly checkpoint: kinetochore-microtubule error correction and beyond. *Cell Div*. 3:10.

van Steensel, B. 2011. Chromatin: constructing the big picture. *EMBO J*. 30:1885-95.

van Zon, W., and R.M. Wolthuis. 2010. Cyclin A and Nek2A: APC/C-Cdc20 substrates invisible to the mitotic spindle checkpoint. *Biochem Soc Trans*. 38:72-7.

Vaquerizas, J.M., R. Suyama, J. Kind, K. Miura, N.M. Luscombe, and A. Akhtar. 2010. Nuclear pore proteins nup153 and megator define transcriptionally active regions in the Drosophila genome. *PLoS Genet*. 6:e1000846.

Vigers, G.P., and M.J. Lohka. 1991. A distinct vesicle population targets membranes and pore complexes to the nuclear envelope in Xenopus eggs. *J Cell Biol*. 112:545-56.

Walther, T.C., A. Alves, H. Pickersgill, I. Loiodice, M. Hetzer, V. Galy, B.B. Hulsmann, T. Kocher, M. Wilm, T. Allen, I.W. Mattaj, and V. Doye. 2003a. The conserved Nup107-160 complex is critical for nuclear pore complex assembly. *Cell*. 113:195-206.

Walther, T.C., P. Askjaer, M. Gentzel, A. Habermann, G. Griffiths, M. Wilm, I.W. Mattaj, and M. Hetzer. 2003b. RanGTP mediates nuclear pore complex assembly. *Nature*. 424:689-94.

Wan, X., R.P. O'Quinn, H.L. Pierce, A.P. Joglekar, W.E. Gall, J.G. DeLuca, C.W. Carroll, S.T. Liu, T.J. Yen, B.F. McEwen, P.T. Stukenberg, A. Desai, and E.D. Salmon. 2009. Protein architecture of the human kinetochore microtubule attachment site. *Cell*. 137:672-84.

Wang, H.W., S. Long, C. Ciferri, S. Westermann, D. Drubin, G. Barnes, and E. Nogales. 2008. Architecture and flexibility of the yeast Ndc80 kinetochore complex. *J Mol Biol*. 383:894-903.

Watanabe, S., T.G. Yamamoto, and R. Kitagawa. 2008. Spindle assembly checkpoint gene mdf-1 regulates germ cell proliferation in response to nutrition signals in C. elegans. *EMBO J*. 27:1085-96.

Wei, R.R., J. Al-Bassam, and S.C. Harrison. 2007. The Ndc80/HEC1 complex is a contact point for kinetochore-microtubule attachment. *Nat Struct Mol Biol*. 14:54-9.

Wei, R.R., J.R. Schnell, N.A. Larsen, P.K. Sorger, J.J. Chou, and S.C. Harrison. 2006. Structure of a central component of the yeast kinetochore: the Spc24p/Spc25p globular domain. *Structure*. 14:1003-9.

Wente, S.R., and M.P. Rout. 2010. The nuclear pore complex and nuclear transport. *Cold Spring Harb Perspect Biol*. 2:a000562.

Wiese, C., and Y. Zheng. 2006. Microtubule nucleation: gamma-tubulin and beyond. *J Cell Sci*. 119:4143-53.

Wilson, K.L., and J. Newport. 1988. A trypsin-sensitive receptor on membrane vesicles is required for nuclear envelope formation in vitro. *J Cell Biol*. 107:57-68.

WormAtlas, Altun, Z.F., Herndon, L.A., Crocker, C., Lints, R. and Hall, D.H. (ed.s) 2002-2010. http://www.wormatlas.org

Wu, J., M.J. Matunis, D. Kraemer, G. Blobel, and E. Coutavas. 1995. Nup358, a cytoplasmically exposed nucleoporin with peptide repeats, Ran-GTP binding sites, zinc fingers, a cyclophilin A homologous domain, and a leucine-rich region. *J Biol Chem*. 270:14209-13.

Xu, D., A. Farmer, and Y.M. Chook. 2010. Recognition of nuclear targeting signals by Karyopherin-beta proteins. *Curr Opin Struct Biol*. 20:782-90.

Xu, S., and M.A. Powers. 2009. Nuclear pore proteins and cancer. *Semin Cell Dev Biol*. 20:620-30.

Yamamoto, T.G., S. Watanabe, A. Essex, and R. Kitagawa. 2008. SPDL-1 functions as a kinetochore receptor for MDF-1 in Caenorhabditis elegans. *J Cell Biol*. 183:187-94.

Yang, L., T. Guan, and L. Gerace. 1997. Integral membrane proteins of the nuclear envelope are dispersed throughout the endoplasmic reticulum during mitosis. *J Cell Biol*. 137:1199-210.

Yang, Q., M.P. Rout, and C.W. Akey. 1998. Three-dimensional architecture of the isolated yeast nuclear pore complex: functional and evolutionary implications. *Mol Cell*. 1:223-34.

Zuccolo, M., A. Alves, V. Galy, S. Bolhy, E. Formstecher, V. Racine, J.B. Sibarita, T. Fukagawa, R. Shiekhattar, T. Yen, and V. Doye. 2007. The human Nup107-160 nuclear pore subcomplex contributes to proper kinetochore functions. *EMBO J*. 26:1853-64.